Doctoral Thesis

Contributions to reliability assessment of engineering structures with special consideration of the seismic safety of an arch dam

submitted in satisfaction of the requirements for the degree of
Doctor of Science in Civil Engineering
of the TU Wien, Faculty of Civil Engineering

Dissertation

Beiträge zur Zuverlässigkeitsbeurteilung von Baukonstruktionen unter besonderer Berücksichtigung der Erdbebensicherheit einer Gewölbestaumauer

ausgeführt zum Zwecke der Erlangung des akademischen Grades eines
Doktors der technischen Wissenschaften
eingereicht an der Technischen Universität Wien, Fakultät für Bauingenieurwesen

von

Dipl.-Ing. **Christian Gasser**, BSc
Matr.Nr.: 00716180

Betreuer: Univ.Prof. Dipl.-Ing. Dr.techn. **Christian Bucher**
Institut für Hochbau und Technologie
Technische Universität Wien
Karlsplatz 13/206-3, 1040 Wien, Österreich

Gutachter: Univ.Prof. Dipl.-Ing. Dr.techn **Christoph Adam**
Institut für Grundlagen der Technischen Wissenschaften
Universität Innsbruck
Technikerstraße 13, 6020 Innsbruck, Österreich

Gutachter: Prof. Dr. Eng. **Dimitar Kisliakov**
Faculty of Hydraulic Engineering
University of Architecture, Civil Engineering and Geodesy
Hristo Smirnenski Blvd. 1, 1164 Sofia, Bulgarien

Wien, im Dezember 2018

Vorwort

Diese Dissertation entstand im Rahmen meiner Tätigkeit als Universitätsassistent am nunmehrigen Forschungsbereich Strukturdynamik und Risikobewertung von Tragwerken an der Technischen Universität Wien.

Mein Betreuer, Prof. Christian Bucher, gab mir die Möglichkeit, meinen Interessen und meiner Neugierde frei zu folgen. Von dieser Freiheit konnte ich sehr profitieren. Dafür bedanke mich bei Prof. Bucher, und ebenso dafür, dass er sich immer viel Zeit genommen hat, wenn ich Fragen hatte.

Ich bedanke mich herzlich bei Prof. Christoph Adam, der diese Arbeit sorgfältig begutachtet hat und wertvolle Vorschläge zur Verbesserung des Manuskripts einbrachte. Ich besuchte seine exzellenten Vorlesungen über Mechanik und Baudynamik an der Universität Innsbruck und verfasste bei ihm und seinem damaligen Assistenten Dr. Alexander Tributsch meine Diplomarbeit über dynamische Strukturidentifikation. In diesem Sinne verdanke ich ihm wichtige Grundlagen zu dieser Dissertation.

Ein großer Dank gilt auch dem Gutachter Prof. Dimitar Kisliakov. Ihm verdanke ich wesentliche Kenntnisse über Staumauern, insbesondere über deren Erdbebensicherheit. Ich erwarb diese Kenntnisse im Rahmen seiner Vorlesung an der TU Wien, welche wohl zu oft durch meine neugierigen Fragen unterbrochen wurde.

Ich bedanke mich bei Dr. Markus Goldgruber für gelungene fachliche Zusammenarbeit, und bei Josef Beiglböck für wertvolle Hilfe bei "High Performance Computing".

Für gute Zusammenarbeit und ein angenehmes Miteinander bedanke ich mich bei meinen Kollegen: insbesondere bei Prof. Rudolf Heuer, sowie bei Dr. Piotr Borejko, Dr. Franz Bamer, Dr. Peter Rosko, Katrin Zierler, Daniel Trauner, Dr. Abbas Kazemi Amiri, Paul Steiner, Tsuyoshi Kouta und bei allen Tutoren. Gleiches gilt für die beiden Damen im Sekretariat Caroline Schneider und Martina Gausterer.

Bei meinen guten Freunden Dr. Georg Brandstetter und Dr. Klaus Hackl vom Forschungsbereich Stahlbau bedanke ich mich für viele heitere, interessante und fachlich nützliche Unterhaltungen.

Mein ganz besonderer Dank gilt meinen Eltern Jakob Gasser und Filomena Pöll Gasser. Auf ihre Unterstützung konnte ich stets zählen und ich verdanke ihnen viel.

Kurzfassung

Die Sicherheit von Bauwerken hängt von Einwirkungen und Widerständen ab, welche dem Zufall unterliegen. Berechnungsingenieure tragen diesen Zufälligkeiten üblicherweise mittels Sicherheitsfaktoren Rechnung. Obwohl sich diese Vorgehensweise in der Praxis bewährt hat, ist sie eher ungeeignet für den Entwurf eines Bauwerks gemäß einer vorgegebenen Zuverlässigkeit im Sinne einer Schadens- oder Versagenswahrscheinlichkeit bezogen auf einen Zeitraum. Das liegt daran, dass das Zusammenspiel aller Einwirkungen und Widerstände bei einem realen Bauwerk viel komplizierter ist als jegliche Situation, die von einem allgemeinen Normenwerk genau abgedeckt werden kann. Jeder Bauingenieur, der schon einmal (z.B. von einem Laien) gefragt wurde, unter welcher Last eine Brücke mit Lastbeschränkung denn nun wirklich einstürtzt, wird dies leicht nachvollziehen können.

Dem Ziel, eine genaue Aussage über die Versagenswahrscheinlichkeit (bzw. über die exakte maximale Tragfähigkeit) treffen zu können, kommt man näher, indem man eine probabilistische Berechnung vornimmt. Dabei gehen die Wahrscheinlichkeitsverteilungen der Einwirkungen und Widerstände direkt in die Tragwerksberechnungen ein. Dadurch, dass Tragwerksberechnungen heute vorwiegend mit numerischen Methoden durchgeführt werden, erfolgt auch die eigentliche probabilistische Analyse numerisch. Das entsprechende Verfahren heißt Monte-Carlo-Simulation (MCS). Dabei wird eine Stichprobe mit unterschiedlichen Parametersätzen untersucht. Die Verteilung der resultierenden Antwortgrößen, insbesondere die Anzahl der Grenzzustandsüberschreitungen, gibt Aufschluss über Schadens- und Versagenswahrscheinlichkeiten bzw. über die exakte Traglast.

Diese Dissertation beginnt mit einer Darstellung der Zuverlässigkeitstheorie. Es werden die Hintergründe des semiprobabilistischen Sicherheitskonzepts an einem einfachen Beispiel erläutert. Darauf aufbauend erfolgt der Übergang auf immer allgemeinere und kompliziertere Systeme, wobei auf die sich daraus ergebenden Einschränkungen eingegangen wird. Dies führt schließlich zur MCS, welche die universalste Methode der Zuverlässigkeitsberechnung darstellt.

Das Thema des darauffolgenden Abschnitts ist die Abschätzung sehr kleiner Versagenswahrscheinlichkeiten. Hierbei stößt die herkömmliche MCS bisweilen an Grenzen, da die hohe Anzahl an erforderlichen Simulationen den Berechnungsaufwand unerschwinglich macht. Diesem Unstand kann man in vielen Fällen mittels *Asymptotic Sampling* entgegentreten. Das Zuverlässigkeitsproblem, d.h. die multivariate Verteilungsfunktion und die Grenzzustandsbedingung, wird dabei zunächst in den Standardnormalraum transformiert. Dann werden Monte-Carlo-Schätzungen für die Versagenswahrscheinlichkeiten einiger künstlich gestreckter (skalierter) Systeme durchgeführt. Der Berechnungsaufwand ist hierfür wesentlich geringer, weil die Versagenswahrscheinlichkeiten höher sind. Die Versagenswahrscheinlichkeit des Originalsystems ergibt sich dann aus Extrapolation der Ergebnisse für die gestreckten Systeme. Dabei werden gewisse asymptotische Eigenschaften im Standardnormalraum genutzt, welche in dieser Arbeit detailliert erklärt werden.

Es werden Verfahren zur Optimierung der Asymptotic-Sampling-Methode präsentiert. Insbesondere wird ein Verfahren entwickelt, das im Falle einer sehr hohen Anzahl an Zufallsvariablen verbesserte Ergebnisse liefert. Zudem werden Empfehlungen für die optimale Anzahl von Skalierungsstufen und Einzelauswertungen gegeben. Darüber hinaus wird die Methode erweitert, sodass sie Überschreitungswahrscheinlichkeiten für eine Bandbreite von Werten der Antwortgrößen ergibt. Anhand von Beispielen werden die Vorzüge der (weiter-)entwickelten Methoden aufgezeigt.

Im nächsten Abschnitt wird die Erdbebensicherheit einer Gewölberstaumauer untersucht. Die dabei auftretenden Herausforderungen ergeben sich nicht nur aus der Erweiterung um den komplizierten Lastfall Erdbeben, sondern auch aus der Anwendung auf ein Finite-Element-Modell eines realistischen Bauwerks. Es werden vier Schadensszenarien sowie das Versagen der Staumauer untersucht. Da Versagen als Folge von sukzessiver Betonschädigung eintritt, ist hierfür die Anwendung eines speziellen Materialmodells für den Beton erforderlich.

Im Zentrum der Untersuchung der Schadensszenarien und des Versagens steht die Entwicklung jeweiliger Fragilitätskurven, welche die Auftrittswahrscheinlichkeiten als Funktionen der Bebenintensität angeben. Da auch hierzu MCSs zum Einsatz kommen (und zwar in Verbindung mit einem aufwändigen nichtlinearen Finite-Element-Modell) ist man wieder an einer Reduktion des Berechnungsaufwands interessiert. Hierzu werden zwei Ansätze erfolgreich getestet und weiterentwickelt, welche von einer Lognormalverteilung der Fragilitätskurven ausgehen.

Schließlich werden die Fragilitätskurven mit dem seismischen Risiko von drei ausgewählten Standorten kombiniert. Dabei kann insbesondere gezeigt werden, dass genaue Untersuchungen für schwächere Erdbeben entbehrlich sind und eine MCS für eine einzelne Intensitätsstufe nicht zu brauchbaren Ergebnissen führt.

Abstract

The safety of structures depends on loads and resistances which both eventually have to be considered as random by nature. The conventional approach to handle uncertainties in engineering is to use safety factors. Although this approach has proven its worth in practice, it is rather inappropriate for designing a real structure such as to match a target reliability level, in the sense of a damage/failure probability referring to a given period of time. This is because, in a real situation, the interaction of all kinds of resistances and prospective loads is much more complicated than any situation that can be covered by a general framework of design rules. These considerations will be easy to understand for any civil engineer who has ever been asked, e.g. by a non-expert person, under which load a bridge provided with a load limitation is eventually going to collapse.

To get one step closer to the aim of predicting the exact failure probability (respectively, the exact bearing capacity), one may adopt a (full) probabilistic analysis. Hereby, the probability distributions of loads and resistances enter the structural calculations directly. Since, nowadays, structural calculations are primarily performed by numerical methods, also the actual probabilistic analysis is performed numerically. The appropriate method is Monte-Carlo simulation (MCS). Thereby, a sample with different parameter sets is analysed. The distributions of the resulting response quantities - especially the number of limit state exceedances - give information about the damage and failure probabilities, respectively about the exact bearing capacity.

This thesis starts with a presentation of reliability theory. The background of the semiprobabilistic safety concept is explained using a simple example. Based in this, transition takes places to more and more general and complicated systems, whereas the resulting limitations are elaborated. This leads to MCS, which is the most universal method of reliability calculation.

The topic of the subsequent chapter is the estimation of small failure probabilities. In that case, conventional MCS may become unaffordable since the high number of necessary simulation runs increases the computational effort substantially. The problem may be addressed by the asymptotic sampling technique. Thereby, first, the reliability problem, i.e. the multivariate probability distribution and the limit state condition, is transformed to standard normal space. Then, some MCS estimates are performed for the failure probabilities of some artificially stretched (scaled) systems. The computational effort is thereby much smaller because the failure probabilities are higher. The failure probability of the original system is obtained by extrapolation of the results of the stretched systems. This can be accomplished by exploiting some asymptotic properties in standard normal space, which are explained in detail in this work.

Strategies to optimize the asymptotic sampling technique are presented. In particular, a method is developed that yields better results in cases where the number of random variables is very high. Furthermore, recommendations concerning the optimal number of scale levels and simulation runs are provided. Moreover, the technique is extend such that it yields exceedance probabilities for a range of values of the response quantities. By means of several examples, the advantages of the methods developed or refined are shown.

In the next chapter, the seismic safety of an arch dam is analysed. The associated challenges arise not only from the extension to the complicated earthquake load case, but also from the fact that a finite element model of a realistic structure is analysed. Four damage mechanisms as well

as failure of the dam are analysed. Since failure occurs as a consequence of progressive concrete deterioration, the implementation of a special material model for concrete is necessary.

At the centre of the analyses of damage and failure is the development of fragility curves, which indicate the occurrence probabilities as functions of the seismic intensity. Since this is accomplished by means of MCSs (involving, furthermore, a complex nonlinear finite element model), one is particularly interested in a reduction of the computational effort. In this regard, two approaches are successfully tested and refined, which are based on the assumption of a lognormal distribution of the fragility curves.

Finally, the fragility curves are combined with the seismic risk of three selected locations. As a result of that it can be shown that an additional investigation of smaller earthquakes in greater detail is expendable, and that MCS for a single intensity level is inappropriate for seismic safety analysis.

Contents

Chapter 1

Motivation

The most basic duty of a structural engineer is to design and to build structures that are safe. This might seem an obvious requirement. In practice however, the engineer will face challenges and difficulties, just like any other practitioner. Even the engineer with the best training and the highest experience will inevitably be constrained to make decisions in situations where she/he is in doubt about the specific situation. The doubts may arise from the incompleteness of informations, e.g. about the bearing capacity of the ground underneath the structure, as well as from the fact that all properties of materials and structures on one hand, and all phenomena which act on the structure on the other hand, are random, to a greater or lesser degree.

Furthermore, one has to consider that the safety of a structure does not depend only on the structural engineer, but on the work of many other people. At this point, as a trivial fact, natural fallibility of human beings will readily come to one's mind. However, the special circumstances and requirements of a construction site cause that deviations from the plan will effectively occur quite regularly. This specific nature of a construction process, which maybe distinguishes it considerably from other production processes, arises from the fact that mostly unique products (prototypes) are built in a given environment.

An aspect of growing importance is ageing of civil structures. Especially in Europe and in the United States, a considerable part of the infrastructure is older than several decades. Time, or more specifically, long lasting environmental actions cause deterioration of structures, e.g. in the form of corrosion. As a consequence, the risk of malfunction and failure increases with time. Especially, design errors and careless construction may develop fatal consequences as temporal effects are exacerbating the situation. Hence, it is increasingly important to conduct inspections, maintenance works or even replacement of the structure. Omission or inadequate implementation of these measures may lead to a substantially worsened condition, which requires even more expensive repair afterwards, (partial) operational interruption, or, in the worst case, lead to collapse (fig. 1.1).

Next to the duty to build safe structures, the engineer faces additional economic, ecological and aesthetic necessities and objectives in her/his practical work. As for economic efficiency, it is logical that a saving in material will go with cost saving, in general. However it should be noted that, in civil engineering, the objective to save material has become less important since, nowadays, building materials are cheap compared to workforce. In contrast, saving material is of outstanding importance in other engineering fields, like aircraft construction, whereby the objective is not primarily to save material costs but to reduce the weight of the product. In modern civil engineering, on the other hand, economic safety can be greatly associated with an optimal maintenance strategy. Costs for inspections and maintenance works should be minimized, downtimes possibly avoided and reconstruction delayed as long as possible while keeping the structure safe.

Nevertheless, material saving in civil engineering has a major impact on climate protection. In particular the cement production is known to be a major source of carbon dioxide emission.

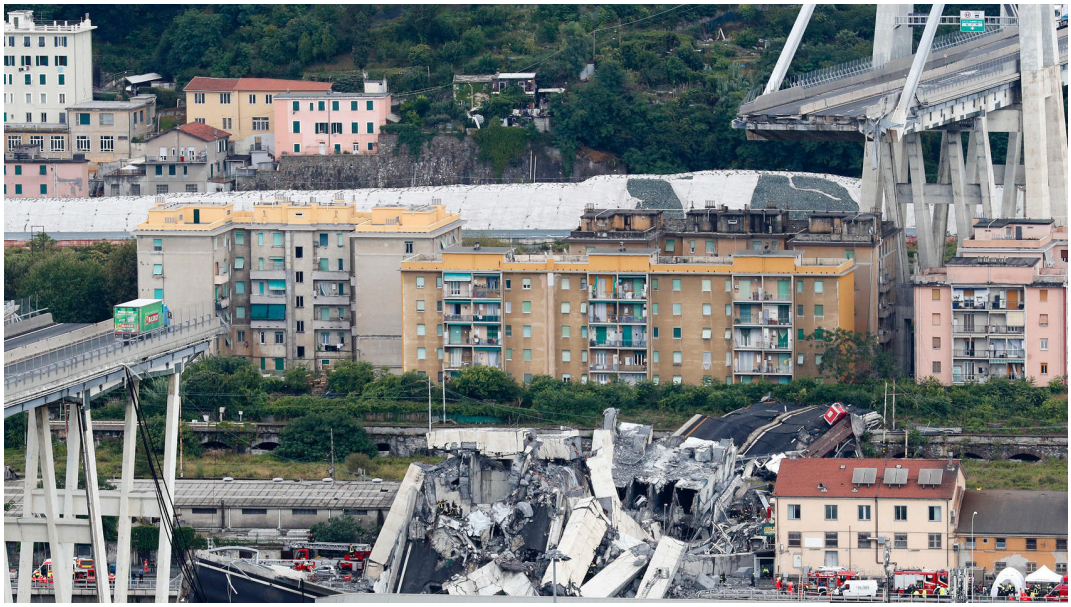

Fig. 1.1: On the 14th of August 2018 the motorway bridge "Ponte Morandi" in Genoa, Italy, collapsed (from http://press24.net)

In addition to that, material consumption is associated with aesthetic aspects. While, in general, a generous usage of material makes a structure more robust, a massive design compromises elegance and beauty.

So, engineers finds themselves constantly in between conflicting objectives. Next to their education, they rely on experience and on their ingenious mind whenever facing situations of doubt and uncertainty.

Nevertheless, it must be the ambition of a modern society to provide a formal framework for rational treatment of uncertainties, at least as basis for decisions. Attempts to formalize uncertainty treatment date back to the establishment of structural engineering as a scientific discipline. Traditionally, safety factors are being used. Nowadays, design in civil engineering is regulated by detailed (national) codes.

The Eurocodes are based on the *semi-probabilistic safety concept* with *partial safety factors*. The idea thereby is to perform calculations using conservative estimates of actions and resistances by considering their variabilities. Specifically, for material properties the 5% fractile, and for actions the 95% fractile is adopted, in general. These values are referred to as *characteristic values*. Additionally, they are modified by safety factors, whereby, in general, each load is increased by multiplication with an individual (*partial*) safety factor and each resistance quantity is decreased by division. This is done to take account of the different variances of the variables and to take account for inaccuracy in modelling. Different loadings are then combined to load cases - again using factors, which take account of the probability of coincident occurrence of different actions. Finally, it must be made sure that resulting *design values* of actions do not exceed design values of resistances.

There are considerable differences in the variabilities of different resistances and loads. One need only think of the fact that material properties scatter much more for inhomogeneous materials like concrete or soil than for the homogeneous material steel. The semi-probabilistic safety concept takes account of this circumstance since it is (widely) based on fractiles and partial safety factors.

However, the verification is eventually based on discrete values - the characteristic values -, omitting the actual probability distributions of the parameters. Although this procedure has shown to be a convenient way for practical design purposes, as a matter of fact, it fails to yield a numerical estimate for the safety of the structure, or, in other words, for the failure probability.

By contrast, a numerical estimate requires full mathematical consideration of the probability distributions of the uncertain parameters - thus, theoretically, of all parameters. The probability distributions enter directly the limit state calculations, which may be given as analytic equations or be performed by numerical procedures, such as the finite element method. Approaches of this kind are referred to as *(full) probabilistic methods/calculations/analyses*. Obviously, the outcome is still a failure probability *estimate*, since nobody can be absolutely sure about the probability distributions itself and, furthermore, no model can ever represent reality perfectly.

As an example, imagine that during a construction process, samples of the concrete used are tested for compressive strength. However, the testing machine is defective. Then, one will obtain wrong statistics about the samples, primarily a biased mean value. Consequently, the error will also be present in any probabilistic calculation regarding limit states. Moreover, the consequences of such a systematic error will not be quantifiable anyhow. Thus, in such a case, the indication of confidence intervals for probability estimates seems pointless.

On the other hand, if one was able to perfectly determine the compressive strength of all the concrete used for a building, and to do so in every point of the building and even for every point in its life time, there would be no doubt about this parameter and any stochastic consideration of it would be obsolete.

Anyway, reality, and especially engineering needs, will be somewhere in between. The benefit of full probabilistic calculations is that all available informations can be integrated. Only they are able to yield an estimate for the probability of exceeding a limit state. Hence, they can be deployed when the task is to optimize a system, e.g. in terms of material consumption or costs, while matching a defined target safety level.

Furthermore, full probabilistic calculations are particularly suitable in cases involving uncertainties of aleatoric type. An uncertainty is defined as aleatoric if it originates from a random physical process and is thus not reducible by more elaborate testing or investigation. Wind actions and earthquake excitations can clearly be put into this category. They are contrasted by the epistemic uncertainties, which are somehow subjective, originate from incomplete knowledge and can be reasonable reduced by humans. This category has already been illustrated above in the example of the concrete strength testing.

The Eurocode leaves it up to the user to adopt full probabilistic calculations instead of the semi-probabilistic safety concept. Because of the increased effort, full probabilistic calculations are rather performed for some special structures and in cases where the verification cannot be accomplished otherwise.

Moreover, referring to codes, one has to be aware that the safety factors required in the semi-probabilistic safety concept have to be determined somehow. This can be made on the basis of calibration to a long experience of building tradition. Alternatively, the calibration may be done on the basis of statistical evaluation of experimental data. In fact, this needs to be carried out within the framework of probabilistic reliability theory.

This thesis is dedicated to full probabilistic methods. It is far away from being a comprehensive manual of the topic where a beginner could look up an explanation of interest. After the introduction, the focus is rather on selected methods and applications.

Chapter 2 constitutes a general introduction to probability concepts and reliability analysis methods. In section 2.1 some distribution functions are presented that are widely used in

engineering. In particular, the transformation of (normally distributed) variables to the standard normal distribution is explained. This transformation is a pivotal concept in reliability theory since some (classical) methods are based on it. Section 2.2 is about the basics of reliability theory. The semi-probabilistic safety concept is illustrated by means of a simple example. Proceeding from that, more complicated and more general cases are introduced, where the previous probabilistic concepts do not hold anymore exactly. So, alternative calculation methods (and their respective limitations) are presented. Eventually, the Monte-Carlo simulation is presented, which is the most versatile method. It is also used in the subsequent chapters.

Chapter 3 is dedicated to the estimation of small (failure) probabilities by means of Monte-Carlo simulation. Section 3.1 outlines the computational difficulties associated with the estimation of small failure probabilities. Section 3.2 describes an algorithm to efficiently address these difficulties: asymptotic sampling. In section 3.3 various strategies to optimize the algorithm are proposed. The validation is done in section 3.4 by means of numerical examples. In section 3.5 a modified asymptotic sampling strategy is shown and tested.

Chapter 4 covers the probabilistic seismic analysis of an arch dam. The solution strategies required for that task differ considerably from the ones discussed in the previous chapters. This is because, here, a realistic structure is analysed, and particularly because a very complicated load case - seismic action - is involved. The peculiarities of probabilistic *seismic* analysis are outlined in section 4.1. Section 4.2 is an introduction to seismic analysis of dams, where also the state of the art is presented. In section 4.3 the model of the arch dam, which is studied in this thesis, is described in detail. Section 4.4 describes the seismic modelling. In section 4.5 the parameters that are considered as random variables are described. In section 4.6 four realistic damage mechanisms are identified. Besides, failure is assumed to occur if cracking is so extensive and widespread that equilibrium does not subsist anymore. Therefore, an appropriate damage material model has to be implemented for the concrete. Section 4.7 is about sampling methods - they have to be modified entirely in the case of seismic action. In section 4.8 the results are presented as structure-specific fragility curves for the damage mechanisms, respectively for failure. In section 4.9 the fragility curves are combined with the location-referred seismic hazard. That way, interesting findings about the damage/failure risk distribution over the range of seismic intensities are obtained, and conclusions for Monte-Carlo analysis can be drawn.

It is important to realize that full probabilistic methods build upon models of the physical reality - just as conventional safety assessment methods. This means that it is of utmost importance that the engineer is first of all able to understand the problem and to translate it into a physically appropriate model. This need existed also here in the modelling of the dam example. As a consequence, this work deals also with a number of other engineering disciplines, such as dam engineering, dynamics of structures, earthquake engineering, and material modelling.

Chapter 2

Introduction

"The safety, respectively the reliability, of a structure is endangered on one hand by the dispersions in loads and capacities, and, on the other hand, by errors in design, construction and usage - hence, by human error. Human error may hardly be captured by any safety concept, but has rather to be excluded as far as possible by appropriate measures, such as by checking the static analysis, quality checks in the construction process and by appropriate maintenance. Only the stochasticity of the input variables may be reasonably treated by probabilistic methods - provided that the uncertainties are quantified." [Zilch and Zehetmaier, 2006]

For that purpose, statistics are made for the material properties and loads of interest. These observations are then translated to stochastic distributions, amenable to mathematical treatment. In practical design, the determination of the statistics of the used materials and the expected loads is mostly too expensive. Instead, the engineer refers to safety factors in codes, which are calibrated according to the variabilities of the specific materials, respectively loading situations.

2.1 Stochastic distributions [1]

A *random variable* or *random quantity* is a property of an event that assumes random values. One can also say that a random variable is a function of chance. As an example, take the compressive strength f_c of a test specimen made of concrete. This random variable [2] $X(= f_c)$ attains different values x_i. The entirety of all possible values is referred to as *(basic) population*. The results of the testings, say the values of the random variables, can be arranged in a number of classes, and for each class, the *relative frequency* can be determined. The relative frequency indicates how often a sample has fallen into a certain class. The result can be represented in a *histogram*, see fig. 2.1. If the frequencies are summed up from the left side, one obtains the *cumulative frequency* of the sample. The cumulative frequency describes the frequency of all sample values smaller than or equal to x.

The larger the size of a sample, the more accurate the classification can be done and the more reliable statements can be made about the probability distribution of the random variable. For an increasing number of tested specimens, the (discrete) distribution of the histogram, respectively of the cumulative frequency, approaches the (continuous) *probability density function* (PDF) [3] $f_X(x)$, respectively the *cumulative distribution function* (CDF) $F_X(x)$. The two functions are interconnected by the relation [Zilch and Zehetmaier, 2006]

$$F_X(x_i) = \int_{-\infty}^{x_i} f_X(x)dx \quad , \quad 0 \leq F_X(x_i) \leq 1 \tag{2.1}$$

[1] To some extend, this section follows [Zilch and Zehetmaier, 2006, Feix and Walkner, 2010, Schneider, 1997].

[2] **Notation**: Capital letters (e.g. X) are used for random variables, i.e. for the property itself (e.g. compressive strength); the realizations of the properties are lowercase (e.g. x). Greek letters represent quantities of the basic population (e.g. μ_X for mean value)

[3] The total area under any PDF curve equals 1.

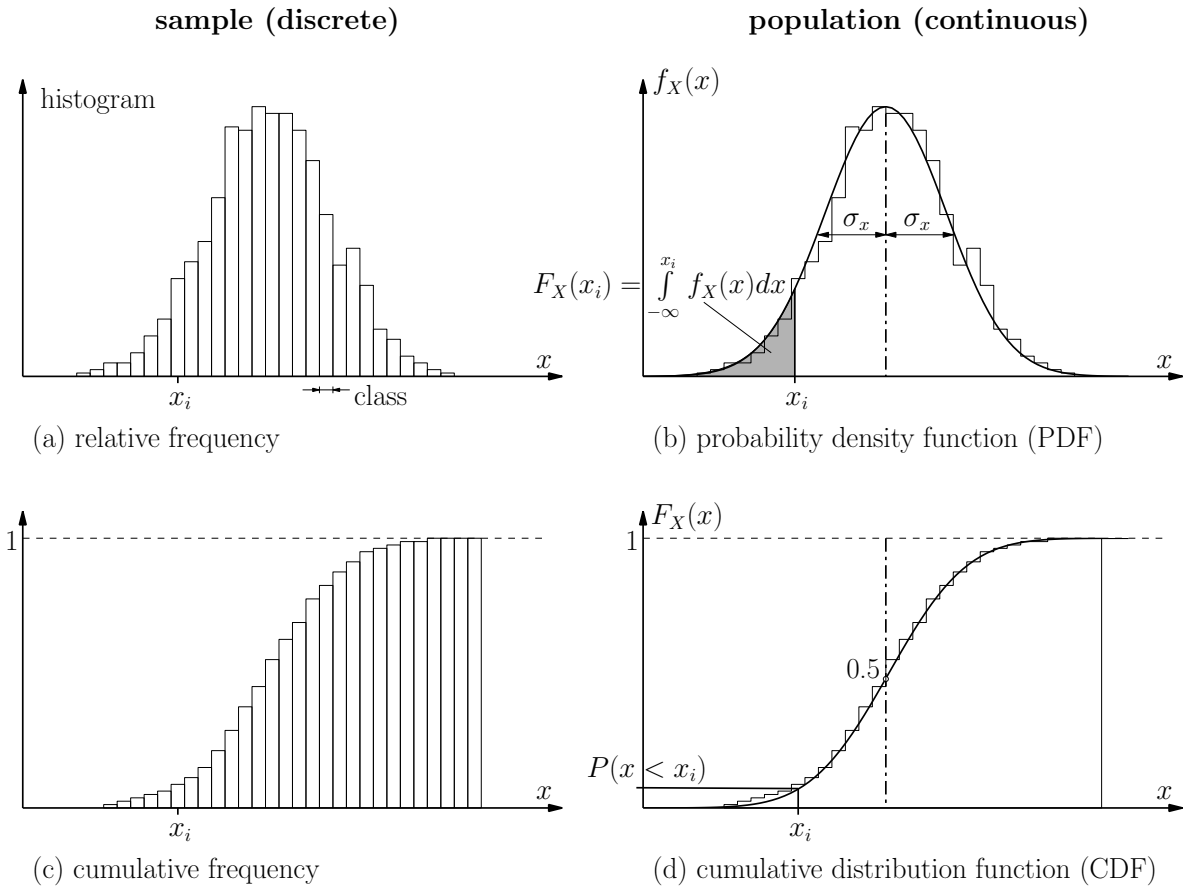

Fig. 2.1: Relative frequency, probability density function, cumulative frequency, cumulative distribution function, from [Zilch and Zehetmaier, 2006] with modifications

Here, $F_X(x_i)$ describes the probability P that the value of the property of interest is smaller or equal x_i. It is equal to the area under the respective PDF in the interval $(-\infty, x_i]$ [Zilch and Zehetmaier, 2006],

$$F_X(x_i) = P(x \leq x_i) = \int_{-\infty}^{x_i} f_X(x)dx \tag{2.2}$$

Important properties of a PDF are (cf. [Zilch and Zehetmaier, 2006]):

$$\mu_X = \int_{-\infty}^{\infty} x \cdot f_X(x)dx = \mathbf{E}[X] \quad \text{mean value} \tag{2.3}$$

$$\sigma_X^2 = \int_{-\infty}^{\infty} (x - \mu_X)^2 \cdot f_X(x)dx \quad \text{variance} \tag{2.4}$$

$$\sigma_X = \sqrt{\sigma_X^2} \quad \text{standard deviation} \tag{2.5}$$

$$V_X = \frac{\sigma_X}{\mu_X} \quad \text{coefficient of variation} \tag{2.6}$$

The mean value μ_X is equal to the expected value of the random variable, $\mathbf{E}[X]$. For symmetric density functions, it is equal to the median. The variance and the standard deviation describe the dispersion of the values around the mean value. The smaller the variance, the higher is the probability that a random variable of a sample assumes a value near the mean value.

The coefficient of variation corresponds to the standard deviation divided by the mean value. By this standardization it becomes a more expressive measure of the dispersion of a PDF. The coefficient of variation is only meaningful for measurement series with only positive (or only negative) values.

There is a multitude of PDFs to describe the stochasticity of quantities. In science and engineering, the normal distribution, the lognormal distribution and the uniform distribution are widely used. Additionally, there exist special distributions for extreme events, i.e. for the distribution of the peaks of a time history.

2.1.1 Normal distribution and standard normal distribution

Many random variables in science and engineering can be described best by the normal distribution. Moreover, not only single random variables are often normally distributed. The central limit theorem states that also the distribution of a random quantity that is composed by the sum of n arbitrary (but positive) random variables tends toward the normal distribution for growing n.

The PDF of the normal distribution is given by:

$$f_X(x) = \frac{1}{\sigma_X\sqrt{2\pi}} e^{-(x-\mu_X)^2/2\sigma_X^2} \quad \text{for} \quad -\infty < x < \infty \tag{2.7}$$

The cumulative distribution function (CDF) is given by:

$$F_X(x) = \frac{1}{\sigma_X\sqrt{2\pi}} \int_{-\infty}^{x} e^{-(x-\mu_X)^2/2\sigma_X^2} dt \quad \text{for} \quad -\infty < x < \infty \tag{2.8}$$

Any normally distributed random variable X characterized by the parameters μ_X and σ_X may be transformed to a random variable U such that mean value and standard deviation assume the values $\mu_U = 0$ respectively $\sigma_U = 1$, see fig. 2.2. This special kind of normal distribution is called *standard* normal distribution. The linear transformation, respectively, the substitution, is performed as follows:

$$\frac{u-\mu_U}{\sigma_U} = \frac{x-\mu_X}{\sigma_X} \quad \text{with} \quad \mu_U = 0 \quad \text{and} \quad \sigma_U = 1 \quad \Rightarrow \quad u = \frac{x-\mu_X}{\sigma_X} \tag{2.9}$$

The PDF of the standard normal distribution is given by:

$$f_U(u) = \varphi_U(u) = \frac{1}{\sqrt{2\pi}} e^{-\frac{1}{2}u^2} \quad \text{for} \quad -\infty < u < \infty \tag{2.10}$$

and the CDF is given by:

$$F_U(u) = \Phi_U(u) = \frac{1}{\sqrt{2\pi}} \int_{-\infty}^{u} e^{-\frac{1}{2}t^2} dt \quad \text{for} \quad -\infty < u < \infty \tag{2.11}$$

Frequently, one is interested in a value that is not exceeded with a predefined probability p. Such a value x_p is called *p-fractile* [Feix and Walkner, 2010]:

$$p = P_X(X \le x_p) = F_X(x_p) = P_U(U \le u_p) = \Phi_U(u_p) \tag{2.12}$$

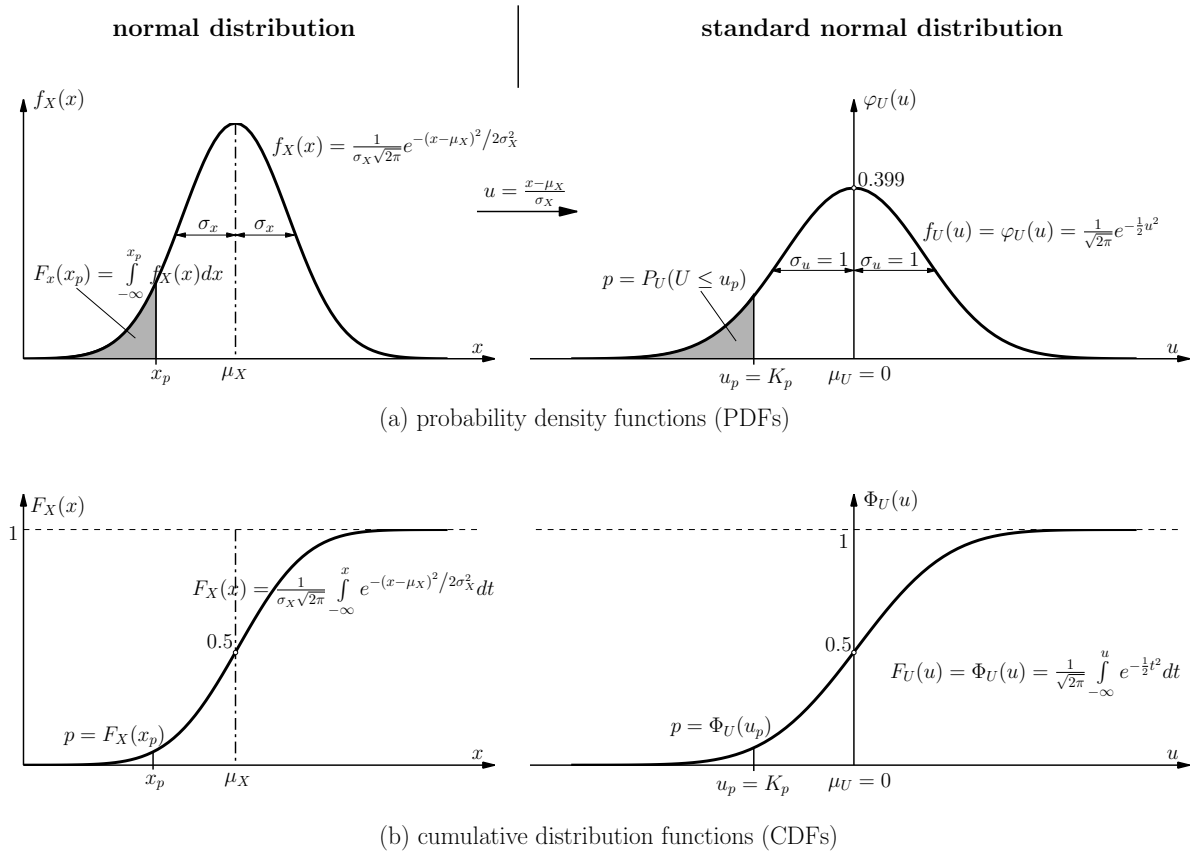

(a) probability density functions (PDFs)

(b) cumulative distribution functions (CDFs)

Fig. 2.2: Normal distribution and standard normal distribution; from [Feix and Walkner, 2010] with modifications

In the Eurocodes, e.g., characteristic material properties, such as the characteristic concrete compressive strength f_{ck}, are defined as 5%-fractiles.

The relation between the fractiles of the normal distribution and the fractiles of the standard normal distribution follows from equation (2.9) [Feix and Walkner, 2010]:

$$x_p = \mu_x + u_p \sigma_x \tag{2.13}$$

where u_p is also called *fractile factor* K_p. For the 5% fractile, respectively for the 95% fractile it assumes the values $K_{0.05}$ = -1.645, respectively $K_{0.95}$ = 1.645.

2.1.2 Other probability distributions

Additionally to the normal distribution, there are some more distribution types commonly used in civil engineering. Some important ones are shown in fig. 2.3.

One should be aware of the fact that, in practice, it is not sufficient to know which type of distribution fits best a quantity of interest. Moreover, obviously, also the distribution parameters have to be identified. Especially in cases where little data are available, or where informations are not given by numbers but rather by expert opinions, it might be convenient just to define a lower limit and an upper limit, and to assume equal probability of all the values between them. This approach leads to the uniform distribution, see fig. 2.3 (b).

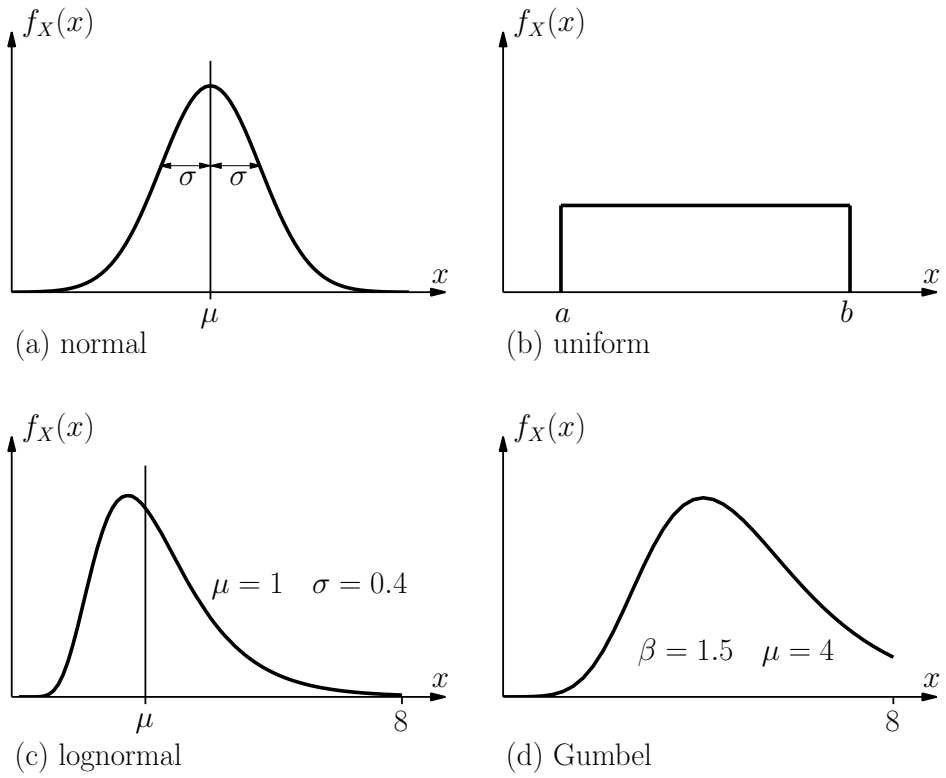

Fig. 2.3: Some types of probability distributions, shown as probability density functions (PDFs)

A number of phenomena follow a distribution whose logarithm is normally distributed, see fig. 2.3 (c). In fact, yield strength and and tensile strength of steel are rather lognormally distributed. It is a asymmetric distribution, defined just for positive values. Indeed, the fact that the domain of definition is positive, is mostly a clear advantage since, physically, resistance parameters and many other parameters cannot be negative. The significance of this distribution originates also from the fact that the product of random variables that take only positive values approaches a lognormal distribution. Theoretically, this is justified by considering the central limit theorem in the log domain.

For loads that are characterized by a high variability in time, such as traffic and wind loads, asymmetric extreme value distributions are commonly applied, see fig. 2.3 (d), which shows a Gumbel extreme value distribution defined by parameters β and μ. For these distributions, only the extreme values in defined time intervals are gathered, see fig. 2.4. Specifically for traffic and wind, the load quantities indicated in codes do not constitute characteristic values of the population, but rather characteristic values of relative extremes. Usually a Gumbel distribution as assumed for the maximum values.

2.2 Basics of reliability theory

Consider the very simple case of a beam that is loaded by a single force F in the middle, see fig. 2.5. In the following, the limit state is analysed at which the acting bending moment equals

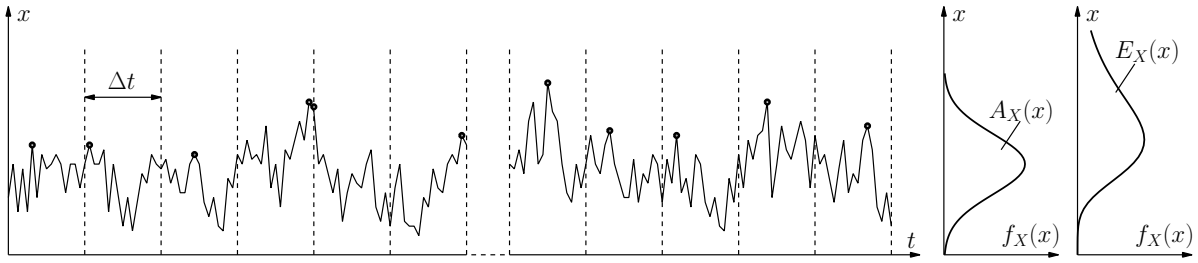

Fig. 2.4: A random process with the (normal) distribution of all value, $A_X(x)$, and the (Gumbel) distribution of the maximum values, $E_X(x)$, from [Zilch and Zehetmaier, 2006] with modifications

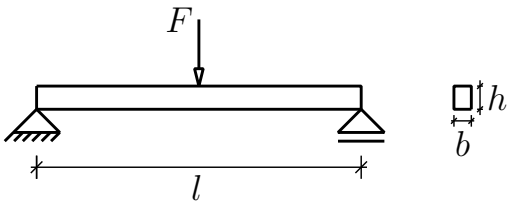

Fig. 2.5: Beam subjected to single load at midspan

the resisting bending moment [4]. The maximum bending moment occurs in the middle of the beam,

$$\frac{F}{2}\frac{l}{2} = \frac{Fl}{4} := E \tag{2.14}$$

For the verification, the acting moment is interpreted as the *effect of action* E, whereby the action is constituted here only by the single force F.

By defining the limit state as initiation of yielding, the resisting bending moment is equal to

$$W_{el} f_y = \frac{bh^2}{6} f_y := R \tag{2.15}$$

where W_{el} is the elastic section modulus and f_y is the yield strength of the material. This resisting bending moment is interpreted as the *resistance* R.

Failure is given by

$$E > R \tag{2.16}$$

or one can write it as a function:

$$G = R - E \quad , \quad \text{failure: } G < 0 \tag{2.17}$$

The limit state is described by

$$G = R - E = 0 \tag{2.18}$$

which is called *limit state equation*.

[4] This means that the verification is done at the level of the cross section. Naturally, the verification could also be done in terms of stresses, by comparing the maximum acting stress with the (resisting) yield strength of the material.

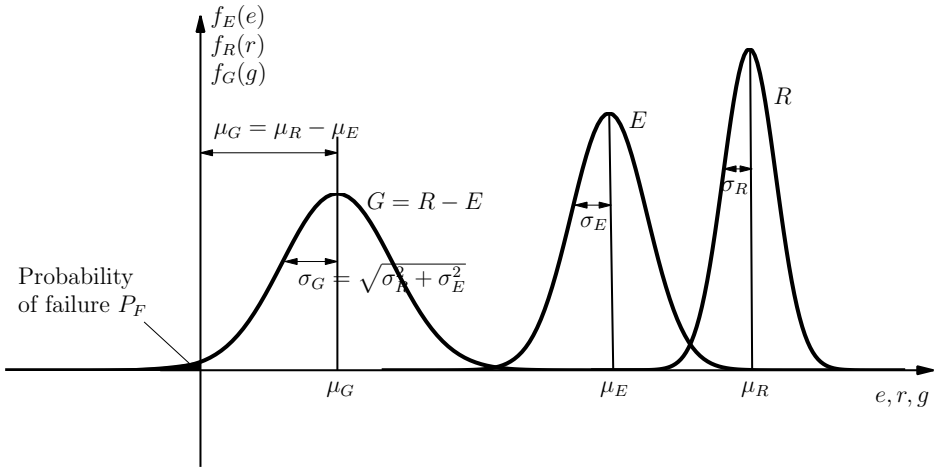

Fig. 2.6: PDFs of: effect of action E, resistance R and state function G

In a hypothetical deterministic case it is quite easy do design a safe structure. One only has to select such a combination of the basic variables (F, l, b, h, f_y) that $E < R$.

Imagine now that the force F and the yield strength f_y are uncertain parameters. Consequently, also the effect of action E and the resistance R are random variables, or, in other words, functions of chance. It is assumed that these quantities can be described by two independent normal distributions - characterized by (μ_E, σ_E), respectively (μ_R, σ_R), see fig. 2.6. Since both PDFs are not limited, there is always an overlapping of the respective curves. Of course this is not just a theoretical or academic problem. Rather it reflects reality where there is always a chance that the effects of actions are greater than the resistances. Hence, strictly speaking, *safety* cannot be guaranteed. The overlapping increases as the mean values come closer together and, also, as the variances of the PDFs increase. [5]

Although the size of the overlapping area is obviously an apparent indicator for the failure probability, numerically it does not correspond to the failure probability. For that purpose, it is most straightforward (and more convenient in anticipation of subsequent more difficult examples) to work with the state function G, which is now a random variable as well. In the present case, where both variables E and R are normally distributed, also G (which is a linear combination of these variables) is normally distributed. It can be represented in the same diagram, see fig. 2.6. Its mean value is

$$\mu_G = \mu_R - \mu_E \tag{2.19}$$

Its standard deviation is

$$\sigma_G = \sqrt{\sigma_R^2 + \sigma_E^2} \tag{2.20}$$

[5] This is a typical situation encountered in ageing structures, where resistances decrease due to fatigue and environmental attacks in general. Also, the uncertainties of the resistance parameters increase with time, and furthermore, there is often a rise in loads due to more traffic and heavier vehicles.
Time-variant reliability problems are not addressed in this work. General information and reviews about the topic are given in [Frangopol and Soliman, 2016, Frangopol and Maute, 2003, Biondini and Frangopol, 2016], applications can be found in [Bucher and Frangopol, 2006] (optimization of lifetime maintenance; silane application), [Sudret et al., 2005] (durability of cooling towers), [Wang et al., 2013] (seismic safety of arch dams with ageing effects), [Dolen et al., 2003] (concrete deterioration at dams), [Strauss et al., 2008] (use of monitoring extreme data; Bayesian updating), [Barone et al., 2014] (maintenance of bridges; cost optimization).

The failure probability P_F can clearly be identified in fig. 2.6 as the area under the curve of the PDF of G in the negative range,

$$P_F = \int_{-\infty}^{0} f_G(g)dg \tag{2.21}$$

where g is the value (realization) of the random variable G. Remember that, for any PDF,

$$P_F = \int_{-\infty}^{\infty} f_X(x)dx = 1 \tag{2.22}$$

2.2.1 The semi-probabilistic safety concept [6]

Within the framework of the reliability theory, the basic aim of the designer is to select the basic variables, i.e. material strength parameters and cross section values [7], such that the overlapping is sufficiently small, say, the failure probability does not exceed a defined acceptable value. In the Eurocodes and many other codes, this is assured by adoption of the semi-probabilistic safety concept.

The concept is shown in fig. 2.7. As in fig. 2.6, it is assumed that the system can be described by two normally distributed independent random variables, E and R, and that failure occurs if the realization of E is greater than the realization of R. The PDF of the resulting state function G is shown in the central diagram. The diagram on the bottom shows the transformation of the state function G to the standard normal distribution $\varphi_U(u)$ by means of

$$u = \frac{g - \mu_G}{\sigma_G} \tag{2.23}$$

The advantage of this is that, for the standard normal distribution, the integral values - and hence the failure probabilities - can be retrieved from integral tables or from many computer programs. The possibility to avoid tedious integration is particularly useful in case of many random variables (as will be explained later). The upper bound of integration is obtained by setting g equal to 0 in equation (2.23). Its absolute value is called *reliability index* β [Hasofer and Lind, 1974].

$$\beta = \frac{\mu_G}{\sigma_G} \tag{2.24}$$

Using the standard normal distribution, the probability of failure can then be calculated as

$$P_F = \int_{-\infty}^{-\beta} \varphi_U(u)du = \Phi_U(-\beta) \tag{2.25}$$

Usually, the index U is omitted,

$$P_F = \Phi(-\beta) \tag{2.26}$$

In this equation, $\Phi(.)$ is the standardized normal distribution function. Conversely, the reliability index β is obtained by

[6] To some extend, this subsection follows [Zilch and Zehetmaier, 2006, Feix and Walkner, 2010, Schneider, 1997].

[7] Of course, loads are as well parameters subjected to high variability, however their values can hardly be influenced by the designer.

$$\beta = \Phi^{-1}(1 - P_F) \tag{2.27}$$

Table 2.1 shows the values of β for some values of P_F.

Tab. 2.1: Relation between β and P_F; from [EN1990, 2013]

P_F	10^{-1}	10^{-2}	10^{-3}	10^{-4}	10^{-5}	10^{-6}	10^{-7}
β	1.28	2.32	3.09	3.72	4.27	4.75	5.20

In the following it will be shown how partial safety factors may be calculated for given PDFs of the variables and a prescribed reliability level, cf. [EN1990, 2013, Feix and Walkner, 2010]. The idea of designing by means of partial safety factors is to find a design point $E_d = R_d$ which, in reality, will not be reached with a defined probability. The partial safety factors γ_E and γ_R should be greater than 1. They refer to the nominal safety zone and hence to the characteristic values E_k and R_k, see fig. 2.7. Consequently the design point is obtained by

$$E_d = \gamma_E E_k \stackrel{!}{=} R_d = \frac{R_k}{\gamma_R} \tag{2.28}$$

However, the starting point is the central safety zone, i.e. the distance between the mean resistance and the mean effect of action:

$$\mu_G = \mu_R - \mu_E \tag{2.29}$$

With equation (2.24):

$$\mu_R - \mu_E = \beta\sigma_G \tag{2.30}$$

and equation (2.20) [Hasofer and Lind, 1974]:

$$\mu_R - \mu_E = \beta\sqrt{\sigma_R^2 + \sigma_E^2} \tag{2.31}$$

The right side is now split in a part for E and a part for R.

$$= \beta\frac{\sigma_R^2 + \sigma_E^2}{\sqrt{\sigma_R^2 + \sigma_E^2}} = \beta\frac{\sigma_R^2 + \sigma_E^2}{\sigma_G} \tag{2.32}$$

$$= \beta \underbrace{\frac{\sigma_R}{\sigma_G}}_{\alpha_R}\sigma_R + \beta \underbrace{\frac{\sigma_E}{\sigma_G}}_{\alpha_E}\sigma_E \quad , \quad \alpha_{R,E} \quad \text{being weighting factors} \tag{2.33}$$

$$\mu_R - \mu_E = \beta\alpha_R\sigma_R + \beta\alpha_E\sigma_E \tag{2.34}$$

$$\underbrace{\mu_R - \beta\alpha_R\sigma_R}_{R_d} = \underbrace{\mu_E + \beta\alpha_E\sigma_E}_{E_d} \tag{2.35}$$

Finally, the partial safety factors are obtained with equations (2.28) and (2.35):

$$\gamma_E = \frac{E_d}{E_k} = \frac{\mu_E + \beta\alpha_E\sigma_E}{\mu_E + K_{p,E}\sigma_E} \quad \text{and} \quad \gamma_R = \frac{R_k}{R_d} = \frac{\mu_R + K_{p,R}\sigma_R}{\mu_R - \beta\alpha_R\sigma_R} \tag{2.36}$$

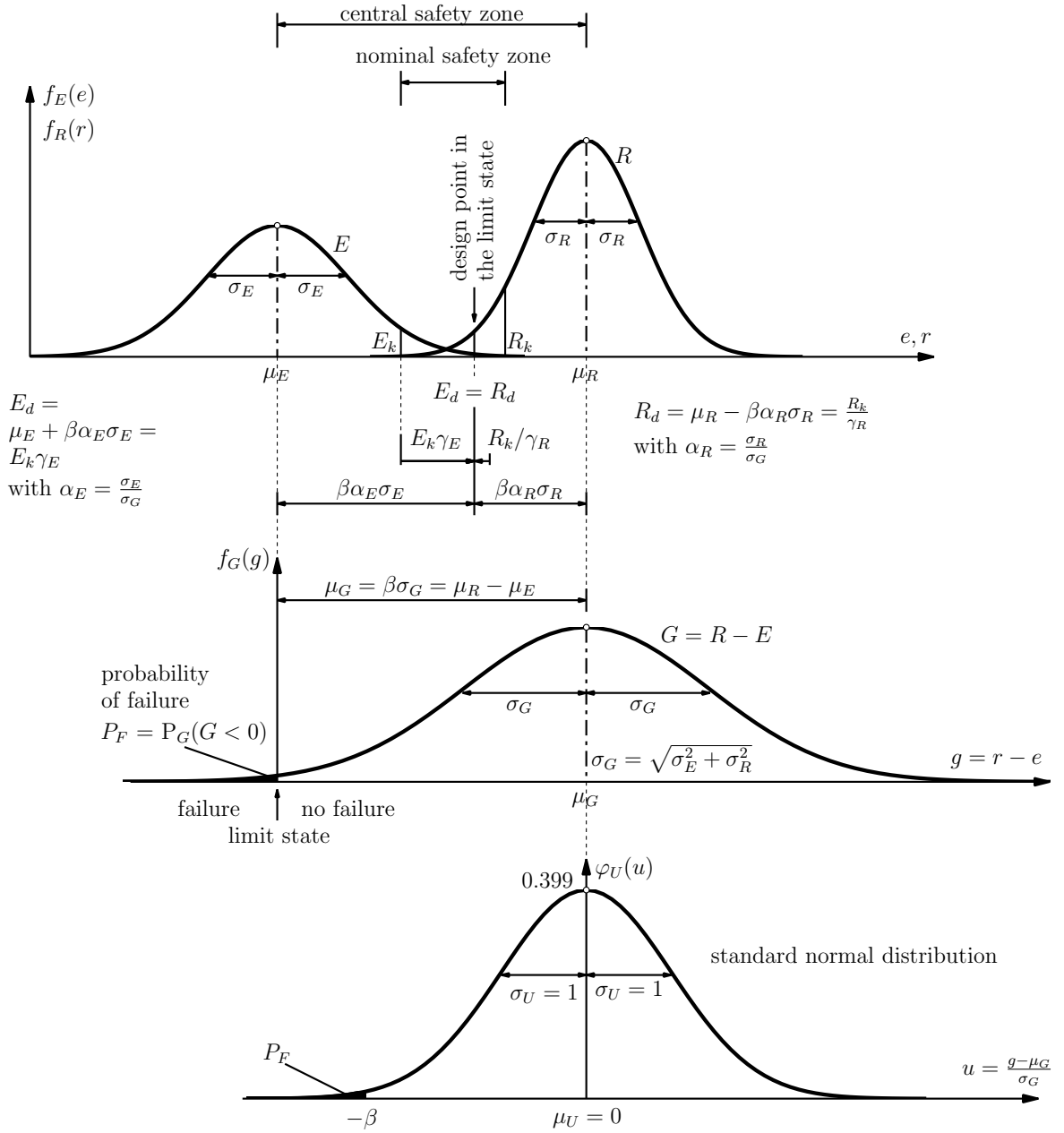

Fig. 2.7: The semi-probabilistic safety concept. Upper diagram: PDF of effect of action E and PDF of resistance R. Central diagram: PDF of state function G. Bottom diagram: PDF of state function G transformed to standard normal space; not true to scale; from [Feix and Walkner, 2010] with modifications

Apparently, the partial safety factors depend on the mean values and standard deviations of the PDFs of E and R - from which the reliability index β and the weighting factors α_E and α_R follow from - as well as from the defined fractiles.

Example

Consider the beam example shown in fig. 2.5. The maximum acting moment and the maximum resisting moment are now given as (primary) random variables. In order to stay with the notation of equation (2.18), we refer to effect of action E and resistance R.

Effect of action E	Resistance R
$\mu_E = 80$ Nm	$\mu_R = 200$ Nm
$\sigma_E = 25$ Nm	$\sigma_R = 20$ Nm
$V_E = \frac{\sigma_E}{\mu_E} = 0.3125$	$V_R = \frac{\sigma_R}{\mu_R} = 0.1$

In the following, the failure probability is calculated first. Then the partial safety factors γ_E and γ_R are searched for which are to be applied to the two given PDFs so that exactly that failure probability is attained.

Mean value and standard deviation of the state function $G = R - E$ are obtained by equations (2.19) and (2.20):

$$\mu_G = \mu_R - \mu_E = 200 - 80 = 120 \text{ Nm} \tag{2.37}$$

$$\sigma_G = \sqrt{\sigma_R^2 + \sigma_E^2} = \sqrt{20^2 + 25^2} = 32.0156 \text{ Nm} \tag{2.38}$$

Then the reliability index β and the failure probability can be calculated:

$$\beta = \frac{\mu_G}{\sigma_G} = \frac{120}{32.0156} = 3.748 \quad \Rightarrow \quad P_F = \Phi(-\beta) = 8.9125 \cdot 10^{-5} \tag{2.39}$$

Then the characteristic values are calculated. R_k shall be defined as 5% fractile and E_k as 95% fractile:

$E_k = \mu_E + K_{p,E}\, \sigma_E =$	$R_k = \mu_R + K_{p,R}\, \sigma_R =$
$= 80 + 1{,}645 \cdot 25 = 121.125$ Nm	$= 200$ - $1{,}645 \cdot 20 = 167.1$ Nm

Then the weighting factors α_E and α_R, the design values E_d and R_d and finally the partial safety factors are calculated:

$\alpha_E = \frac{\sigma_E}{\sigma_G} = \frac{25}{32.0156} = 0.7809$	$\alpha_R = \frac{\sigma_R}{\sigma_G} = \frac{20}{32.0156} = 0.6247$
$E_d = \mu_E + \beta\alpha_E\sigma_E =$	$R_d = \mu_R - \beta\alpha_R\sigma_R =$
$= 80 + 3.748 \cdot 0.7809 \cdot 25 = 153.17$ Nm	$= 200 - 3.748 \cdot 0.6247 \cdot 20 = 153.17$ Nm
$\gamma_E = \frac{E_d}{E_k} = \frac{153.17}{121.125} = 1.2646$	$\gamma_R = \frac{R_k}{R_d} = \frac{167.1}{153.17} = 1.0909$

In practice, it is up to the engineer to design a structure such that the target safety level is achieved, in compliance with the safety factors. This is accomplished by selection of appropriate

materials with sufficient strengths as well as by appropriate dimensioning of the structural components.

At this point it is absolutely legit to ask: Why do we need (partial) safety factors if they are eventually deduced from a failure probability? Why don't we determine the design point based on a target safety level directly? The answer is that the calculation of failure probabilities is straightforward just in very simple cases. In a real-life situation, the exact determination of failure probabilities is hardly a reasonable task for a practitioner. This is why engineers rather resort to safety factors to take account of the uncertainties (approximately). The subsection 2.2.2 addresses the problem in detail.

2.2.2 Generalizations

In the example given above, the state function $G = R - E$ is a linear expression of two normally distributed random variables. The limit state equation is $G = R - E = 0$. As already stated above - given this case - the reliability index β can simply be calculated by dividing the mean value μ_G by the standard deviation σ_G [Hasofer and Lind, 1974],

$$\beta = \frac{\mu_G}{\sigma_G} \tag{2.40}$$

The same equation holds exactly also in cases where the state function G is a linear combination of more than two random variables, as long as they are each normally distributed:

$$G = c_0 + c_1 X_1 + c_2 X_2, \ldots, c_n X_n \tag{2.41}$$

In this case, β can be calculated as follows (cf. e.g. [Ditlevsen and Madsen, 2007]):

With equation (2.3):

$$\mu_G = \mathbf{E}[G] = c_0 + c_1 \mathbf{E}[X_1] + c_2 \mathbf{E}[X_2], \ldots, c_n \mathbf{E}[X_n] \tag{2.42}$$

and

$$\sigma_G = \sqrt{c_1^2 \sigma_1^2 + c_2^2 \sigma_2^2, \ldots, c_n^2 \sigma_n^2} \tag{2.43}$$

$$\rightarrow \beta = \frac{\mu_G}{\sigma_G} \tag{2.44}$$

Furthermore, equation (2.40) can be used as an approximation in cases where the state function G is a linear combination of not normally distributed random variables. This is due to the central limit theorem, which states that the a linear combination of any independent positive distributions asymptotically approximates the normal distribution as their number increases.

However, the limit state is often nonlinear and, furthermore, in modern engineering practice it is rarely available as an explicit equation. In these cases, things become more complicated.

As starting point for the illustration the respective difficulties and solution strategies consider fig. 2.8. In the e-r-plane, the limit state separates the safe region from the failure region. The vertical axis indicates the probability density of the random variables E and R. In principle, the diagram shows a similar situation as the one shown in fig. 2.6, however the distributions are now shown as *joint* PDF. It can clearly be seen that the peak of this distribution lies in the safe zone, while a minor part lies beyond the limit state. This resembles a real situation, where a structure will usually be "safe". Additionally, it is pointed out that the random variables may be correlated.

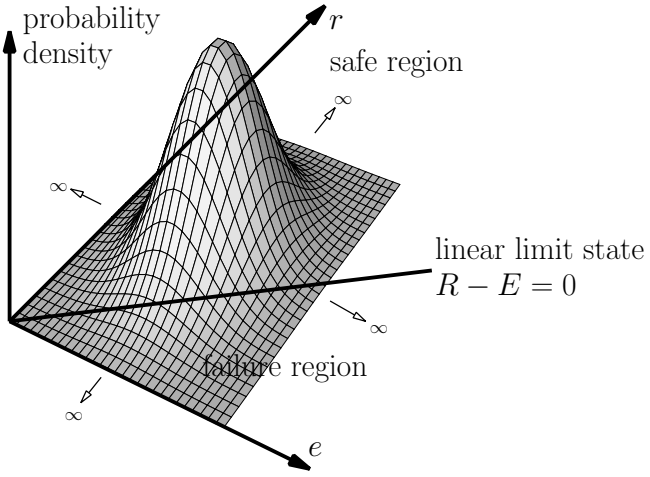

Fig. 2.8: Joint PDF of two normally distributed variables with linear limit state

The problem may be transformed to the standard normal space, as can be seen in fig. 2.9 [Zilch and Zehetmaier, 2006]:

$$\tilde{e} = \frac{e - \mu_E}{\sigma_E} \tag{2.45}$$

$$\tilde{r} = \frac{r - \mu_R}{\sigma_R} \tag{2.46}$$

$f_E(e)$ and $f_R(r)$ are now (uncorrelated) standard normal distributions. The peak of the joint PDF is in the origin; curves of identical probability appear as concentric circles around the origin, in the projection. The transformation changes the position of the limit state, however, it is still linear.[8] The design point is the point on the limit state with the shortest distance to the origin - and at the same time the most probable point on the limit state. The distance between the origin and the design point is again β. The coordinates of the design point correspond to the value of β scaled by the weighting factor of the respective variable.

Typically, the limit state equation will comprehend more than two random variables. The limit state is then characterized by a hypersurface, which separates the failure region from the safe region. Anyway, in standard normal space, the distance to the origin corresponds always to the reliability index β, which can be converted to the failure probability straightforwardly.

While high-dimensional problems (i.e. problems involving many random variables) do not pose any difficulty to the approach, things get more complicated when the limit state is nonlinear, see fig. 2.10. Then, in standard normal space, see fig. 2.11, the proportionality of the exact failure probability to the distance to any distinct point of the limit state does not hold anymore. Of course, however, one can still identify the point of the limit state with the shortest distance to the origin, i.e. the point of maximum value of the PDF, and use this distance as an approximation for β. This procedure corresponds to a linearization of the limit state in the design point. As this is equivalent to a first-order Taylor series approximation, it is called First-Order Reliability Method (FORM). A better approximation of the limit state in the design point may be achieved

[8] In principle, the transformation to the standard normal space is feasible for all kinds of reliability problems, i.e. also for non-normal and correlated distributions as well as for nonlinear limit state equations. In these cases, Rosenblatt's or Nataf's transformation is adopted, see [Nataf, 1962, Ditlevsen and Madsen, 2007, Papaioannou et al., 2015]. There exist, however, many theoretical PDFs which cannot be represented exactly by such transformations [Schuëller et al., 2004].

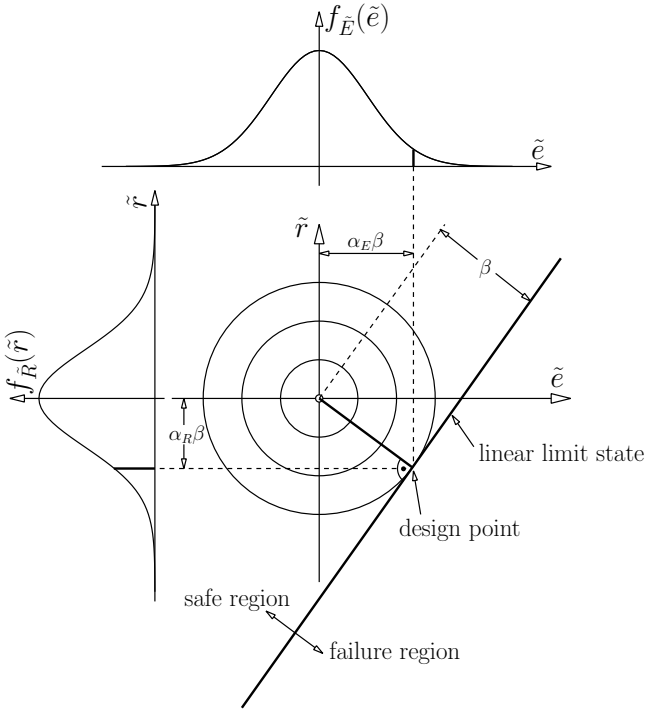

Fig. 2.9: Joint PDF in standard normal space (projections) with linear limit state; from [Zilch and Zehetmaier, 2006] with modifications

by a curved approximation (Second Order Reliability Method, SORM). For further information, the reader is referred to [Bucher, 2009b, Ditlevsen and Madsen, 2007].

There is naturally the possibility to calculate the integral analytically. It should be remembered that, basically, it is all about integrating over a (multidimensional) solid section confined by a (nonlinear) (hyper)surface.

However the main problem is, as stated above, that the limit state is often not given as an analytic function. In modern engineering, design commonly relies on numerical computations, especially on the finite element method (FEM). This means that, in general, a specific set of input quantities is converted to a set of output quantities by numerical procedures. These output quantities (e.g. stresses) can then be compared with respective admissible values (e.g. strength values). So, the method dispenses with any analytic expression of the output quantity in terms of the basic variables. Hence, for a reliability problem such as illustrated in fig. 2.10, there would be no confinement available for the multidimensional integral.

As an approximation, one may try to find the design point. Since the design point is characterized as the one point on the limit state associated with the maximum value of the PDF, this can be thought of as an optimization problem. The approach requires repeated evaluation of the numerical model and calculation of gradients, whereby one tries to get closer to the (global) maximum in each step. Subsequently, the unknown limit state is approximated by a linear (FORM) or curved (SORM) function in the design point. It should be noted that especially the calculation of the gradients respective to the basic variables is not straightforward and, furthermore, computationally very expensive if the number of basic variables is high. In general, this kind of reliability calculation is reserved to highly specialized companies and institutions.

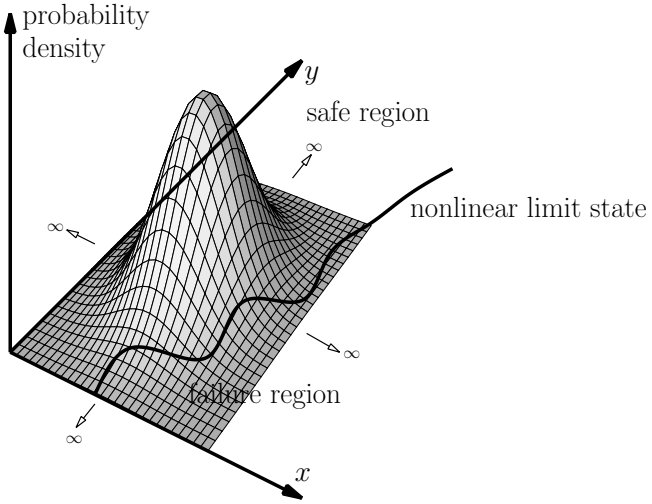

Fig. 2.10: Joint PDF of two normally distributed variables with nonlinear limit state

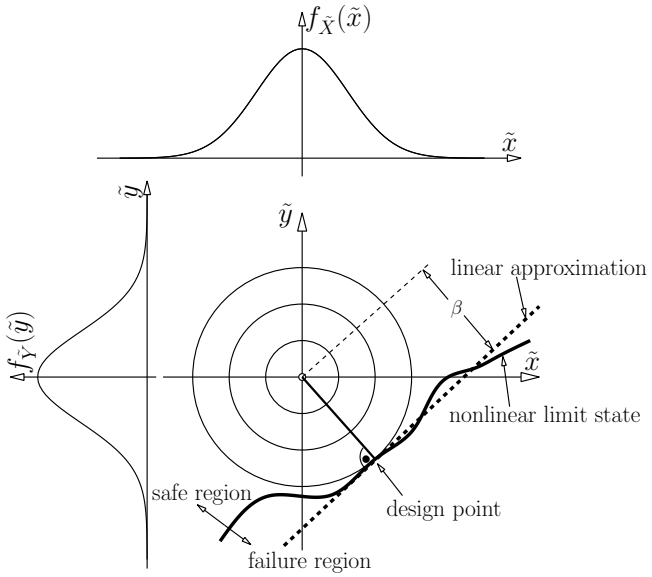

Fig. 2.11: Joint PDF in standard normal space (projections) with nonlinear limit state and linearization in the design point; from [Zilch and Zehetmaier, 2006] with modifications

As a conclusion, it can be stated that the rigorous solution [9] of a general reliability problem is hardly achievable. However, it must be stated that, in practice, it is even difficult to find an approximate solution (FORM and SORM). This comes especially due to the fact that engineering calculations are nowadays performed numerically rather than analytically with explicit limit state equations.

It is therefore comprehensible that for (everyday) engineering practice another design method is necessary. Indeed, this is the limit state design with (partial) safety factors, which has been presented before. In case of a (known) linear limit state equation and normal random variables, this safety concept is - in theory [10] - suitable for the designing structures such as to match a defined reliability level exactly. The relations between the failure probability (respectively the reliability index β) and the safety factors γ_E and γ_R and weighting factors α_E and α_R are shown in fig. 2.7 and fig. 2.9. In all other cases the application of safety factors constitutes an approximation for the target reliability level.

The determination of safety factors provided in codes is done either by empirical methods or by calibration with the results of fully probabilistic analyses. "Empirical" here means that the safety factors are based in expert opinion and long construction experience [EN1990, 2013]. In general, high safety factors are provided for quantities with (empirically) high dispersion. For example, safety factors for the strength of concrete are higher than the ones for the strength of steel because there is higher uncertainty about the strength of concrete than of steel. Alternatively (or complementarily), safety factors may be calibrated by comparison with fully probabilistic analyses, i.e. by the solution (respectively the approximation) of the reliability integral.

This necessity immediately leads back to the need to find a method by which one can evaluate the reliability integral. The desire to solve the integral does not only arise for calibration of respective appropriate safety factors, which are to be used for everyday calculations, but also for special applications, and moreover, for academic reasons.

A straightforward method to evaluate arbitrary integrals is Monte Carlo simulation (MCS). Thereby, the integral is evaluated by repeated random sampling. The failure probability is then expressed as

$$P_F = \frac{n_{fail}}{n_{eval}} \tag{2.47}$$

[9] By the term *rigorous solution* the solution of the reliability integral for given PDFs of the basic variables and given limit state equation is understood.

[10] In fact, all of the above presented "exact" methods actually require that the PDFs of all random variables are exactly known. Strictly speaking, only in that special case, the calculated failure probability is the "true" one. However, the idea of exact knowledge of the distribution of a random variable implicates some conceptional contradiction: The more knowledge one gains about a property of part of a system the smaller becomes the uncertainty about it. Mathematically speaking, the variance decreases. In principle, the examination of the property could continually be improved and, furthermore, the examination could also be refined in space (and in time), i.e. the properties of ever smaller parts could be examined. The distinction between epistemic and aleatoric uncertainties would be vanishing (see also [Kiureghian and Ditlevsen, 2009]). The overlapping as shown in fig. 2.6 would become smaller and smaller. In the limit case eventually, one would not attain perfect knowledge about the parameters' PDFs, but perfect knowledge about the system itself. Hence it would be possible to make a deterministic assertion about the safety of the system - the failure probability would be either 0 or 1.
For that reason, *in a realistic situation*, one should correctly speak of *failure probability based on the knowledge and the assumptions of the analyst.*

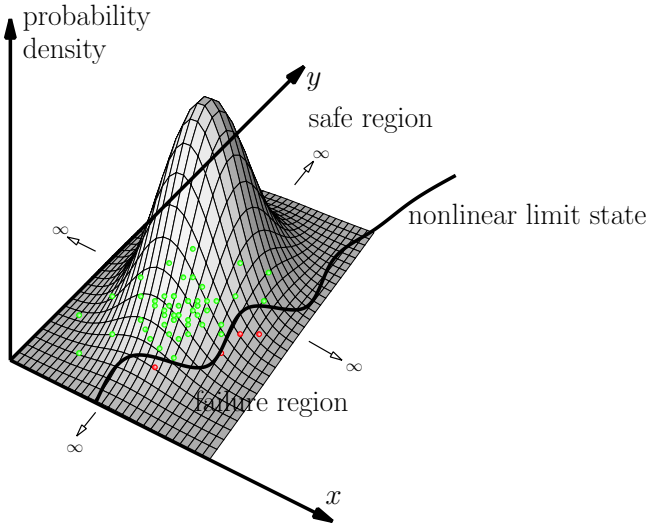

Fig. 2.12: Joint PDF of two normally distributed variables with nonlinear limit state and MCS samples. Red dots: failed samples.

Here n_{eval} is the number of evaluations of the state function G and n_{fail} is the number of evaluations that resulted in failure. The method is conceptually shown in fig. 2.12 and in fig. 2.13 [11].

The high versatility of MCS comes from the fact that it is independent of the dimension of the problem. However, the major drawback is that the method becomes evermore expensive as the failure probability to estimate becomes smaller. The reason is that then a very high number of simulation runs [12] is required to obtain a representative number of results in the failure region. This might become computationally prohibitive if already a single evaluation of the model is expensive.

There are basically two methods to reduce the computational effort:

- The use of a metamodel. Hereby, a (small) number of simulation runs are performed with the original model (with alternating parameter sets). The responses can be used as support points for a response surface, i.e. for an *analytical* expression for exactly these response quantities. Substituting the real model by the easy to evaluate metamodel - which might be, e.g. a polynomial expression - makes it possible to explore also very unlikely regions of the variable space with reasonable computational effort. The reader is referred to [Bucher and Bourgund, 1990, Bucher and Most, 2008, Bucher, 2018, Sudret et al., 2017].

- The other option is to adopt the original model but to modify the sampling in such a way to explore the failure region by a reduced number of simulation runs. [13]

The next chapter is entirely dedicated to the latter kind of evaluation strategies. Since it was published in form of two articles [Gasser and Bucher, 2018, Gasser and Bucher, 2017a] (only minor modifications were made here), some concepts will be repeated.

[11] It should be noted that integral calculation by means on MCS does not require any transformation of the basic variables.

[12] Throughout this thesis, by the term (*simulation*) *run*, the evaluation of a *single* state function or finite element model is understood.

[13] Also combinations of both approaches are possible.

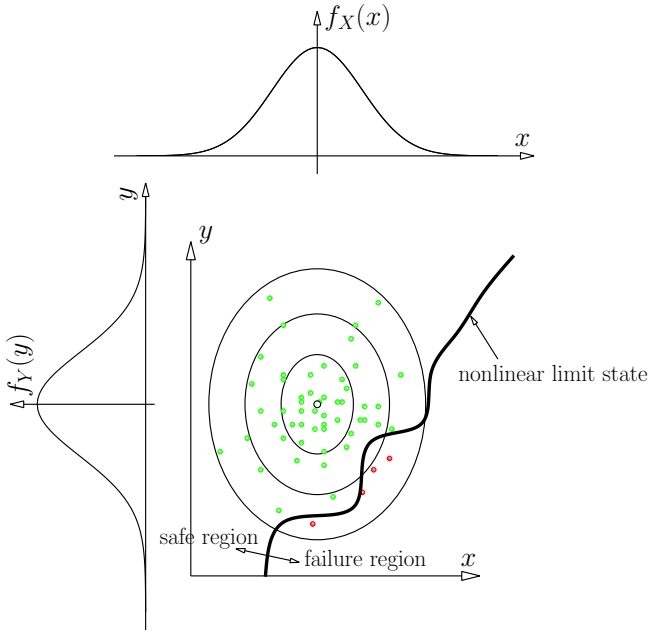

Fig. 2.13: Joint PDF (projections) with nonlinear limit state and MCS samples. Red dots: failed samples.

Chapter 3

Asymptotic sampling

3.1 Estimation of small failure probabilities [1]

The safety of structures depends on resistances and loads, which both eventually have to be considered as random by nature. All parameters which influence the resistance of the structure (cross-section values and material properties) as well as all kinds of loads acting on the structure can be considered as random variables described by their respective probability density functions. In this way, one obtains a multidimensional joint probability density function (cf. [Bucher, 2009b]):

$$f_{X_1,...,X_n}(x_1, ..., x_n) \tag{3.1}$$

in which X_i are the random variables and n is the dimension. Failure is typically denoted in terms of a scalar state function $G(.)$ attaining negative values. The failure probability P_F can then be expressed as an integral, bounded by the limit state function (cf. [Bucher, 2009b]):

$$P_F = \int \cdots \int_{G(x_1,...,x_n)\leq 0} f_{X_1,...,X_n}(x_1, ..., x_n) dx_1, ..., dx_n \tag{3.2}$$

The challenge in calculating this integral lies in evaluating the limit state function, which for nonlinear systems usually requires an incremental/iterative numerical approach [Bucher, 2009b]. Since usually just a very small region contributes to the value of the integral, it is difficult to place integration points for numerical integration procedures appropriately [Bucher, 2009b]. This is particularly true for high-dimensional integrals.

One method to overcome this difficulty is Monte Carlo simulation (MCS). Thereby, the integral is evaluated by repeated random sampling. The failure probability is then expressed as

$$P_F = \frac{n_{fail}}{n_{eval}} \tag{3.3}$$

Here n_{eval} is the number of evaluations of the state function G and n_{fail} is the number of evaluations which resulted in a failure.

The (generalized) reliability index β is defined by (cf. [Ditlevsen and Madsen, 2007])

$$\beta = \Phi^{-1}(1 - P_F) \tag{3.4}$$

In this equation, $\Phi^{-1}(.)$ is the inverse standardized normal distribution function. In the following, it will be assumed that the random variables X_i are independent and identically distributed (i.i.d.) normal variables with zero mean and standard deviation σ. Not normally distributed variables and possible correlations among them may be introduced using marginal transformations and

[1] Sections 3.1 - 3.4 have been published as [Gasser and Bucher, 2018]. The text here contains just minor modifications.

joint probability density function models such as the Nataf-model [Nataf, 1962, Liu and Der Kiureghian, 1986, Bucher, 2009b].

The major advantage of MCS for integral calculation lies in its independence of the dimension. This means that the efficiency of the method is not impaired by the number of variables the state function G depends on. However, since a representative number of failures is needed, the number of function evaluations becomes prohibitively large when small failure probabilities are to be calculated. For example, to calculate a failure probability of the order of 10^{-5}, the number of evaluations should be larger than 10^6. Hence, one can easily imagine, that MCS becomes impracticable when a complicated finite element model is to be analysed.

Different strategies have been developed to reduce the number of necessary function/model evaluations. Importance sampling methods [Bucher, 2009b] aim at obtaining more failures by shifting the sampling to the small region in $n-$dimensional space that actually contributes significantly to the failure probability. An alternative approach is to express the failure probability as a product of larger conditional probabilities by introducing intermediate failure levels. Thereby, the samples are drifted closer to the failure space in each level. This method is known as subset simulation [Au and Beck, 2001]. Recently, another method, called asymptotic sampling (AS), has been presented in [Bucher, 2009a].

3.2 Concept of asymptotic sampling

Similarly to the previously mentioned approaches, AS aims at obtaining a representative number of failures out of a moderate number of function evaluations. However, the method relies on a certain asymptotic property of the failure probability in the $n-$dimensional i.i.d. normal space.

AS exploits the asymptotic behaviour of the failure probability expressed in terms of the reliability index β when changing the standard deviation of the basic random variables. If the original standard normally distributed random variables are replaced by variables with non-unit standard deviations $\sigma = \frac{1}{f}$, then the computed reliability index will depend on the choice of f. As a first simple case, consider a linear function of the basic random variables X_k, say [Bucher, 2013]

$$G(\boldsymbol{X}) = \sum_{k=1}^{N} a_k X_k \tag{3.5}$$

with arbitrary real-valued coefficients a_k. The random variable $Y = G(\boldsymbol{X})$ will then be normally distributed with a zero mean and a variance [Bucher, 2013]

$$\sigma_Y^2 = \sum_{k=1}^{N} a_k^2 \tag{3.6}$$

The distribution function $F_Y(\xi)$ of this variable will therefore be given by [Bucher, 2013]

$$F_Y(\xi) = \Phi\left(\frac{\xi}{\sigma_Y}\right) = \Phi\left(\xi / \sqrt{\sum_{k=1}^{N} a_k^2}\right) \tag{3.7}$$

Upon changing the standard deviation of all basic variables from unity to a value of $1/f$, the standard deviation of Y changes by the same amount. Thus, the distribution function changes to [Bucher, 2013]

$$F_Y(\xi) = \Phi\left(\xi f / \sqrt{\sum_{k=1}^{N} a_k^2}\right) \tag{3.8}$$

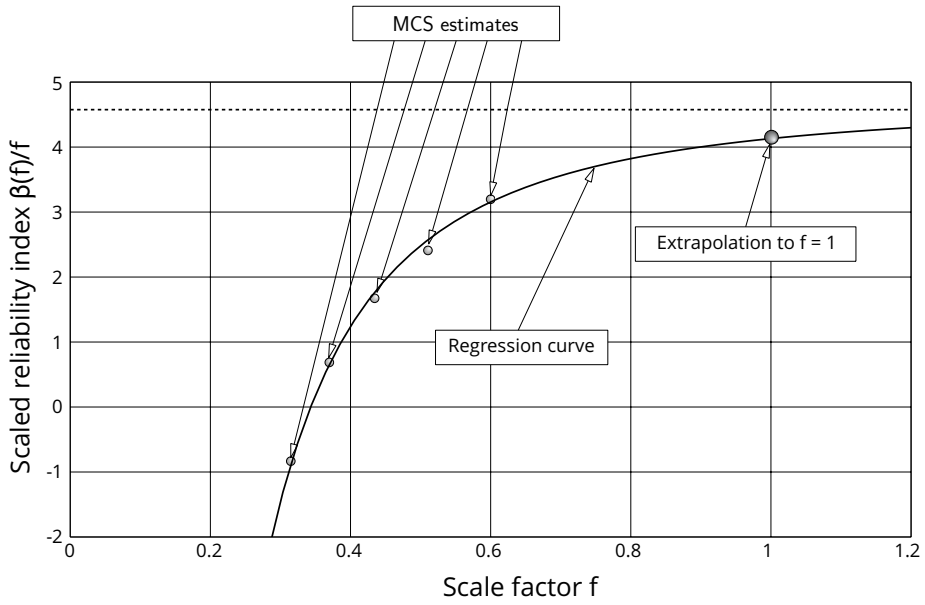

Fig. 3.1: Basic concept of asymptotic sampling (AS)

from which the generalized reliability index (with respect to scale factor f) is immediately found as (cf. [Bucher, 2013])

$$\beta(f) = \frac{\xi f}{\sqrt{\sum_{k=1}^{N} a_k^2}} \quad \rightarrow \quad \frac{\beta(f)}{f} = \frac{\xi}{\sqrt{\sum_{k=1}^{N} a_k^2}} = \text{const.} \qquad \text{(for fixed } \xi\text{)} \tag{3.9}$$

This means that for a linear function of normally distributed variables, the expression $\beta(f)/f$ is invariant with respect to the choice of f. Geometrically, β is the minimum distance of the origin from the limit state surface $G(\boldsymbol{X}) = 0$.

Equation (3.9) is not true for the general, i.e. nonlinear, case. There is, however, an asymptotic property which ensures similar behaviour for many nonlinear cases. Equation (15b) of [Breitung, 1984] states that the reliability index asymptotically converges to the minimum distance of the origin from the limit surface as $\beta \rightarrow \infty$. Hence the above relation holds asymptotically as f approaches infinity [Bucher, 2013]:

$$\lim_{f \rightarrow \infty} \frac{\beta(f)}{f} = \text{const.} \tag{3.10}$$

This asymptotic property is exploited to construct a regression model which allows to determine the reliability index for extremely small failure probabilities. Figure 3.1 shows this concept. By increasing the standard deviation of the basic variables, a representative number of failure events can be obtained out of a moderate number of simulation runs. The scaled reliability indices obtained in that way are used as support points for the regression. The reliability index of the original system, i.e. $\beta(f = 1)$, is then obtained by extrapolation.

For the fitting process the functional dependence is chosen as

$$\frac{\beta(f)}{f} = A + \frac{B}{f^C} \tag{3.11}$$

Assuming C to be positive, this approach ensures asymptotic convergence to a constant value (here to A) as $f \to \infty$ (which is equivalent to $\sigma \to 0$). Thus, the asymptotic property given in equation (3.10) is satisfied. Of course, any other approach maintaining the asymptotic behaviour could be chosen as well. The coefficients A, B and C can be determined from a regression analysis, typically by a least-squares fitting [Bucher, 2009a].

3.3 Optimizing the algorithm

In [Bucher, 2009a] it has been shown that AS is independent of the dimensionality. However, accuracy of the approach depends on several other factors, namely:

- accuracy of support points
- number of support points
- collocation of support points
- regression parameters
- particular geometrical shape of the limit state surface.

Obviously, the geometrical shape of the limit state surface of a specific problem in standard normal space cannot be influenced by the analyst. Thus, a substantial part of this chapter focuses on strategies to increase the accuracy of the support points. Furthermore, advices concerning number and collocation of the support points are given. As compared to the original paper on AS [Bucher, 2009a], the regression function is augmented by an additional parameter, C (see equation (3.11)), which ensures general applicability of the approach, independently of the shape of the limit state.

3.3.1 Low-discrepancy sampling

The accuracy of the support points is primarily determined by the number of sample evaluations they are based on. This is evident, since the support points are basically MCS estimates for scaled systems. Anyway, in general, low-discrepancy sampling methods can be applied in order to populate the variable space more uniformly and, as a result, get support points which are more stable. There are several low-discrepancy sampling methods, such as Latin Hypercube sampling [Olsson et al., 2003], Halton Sequences [Halton, 1960, Wang and Hichernell, 2000] or Good lattice point (GLP) sets [Fang and Wang, 1994]. Here, Sobol sequences are applied, using an algorithm as discussed in [Bratley and Fox, 1988, Hong and Hickernell, 2003].

As an example consider the function

$$G(X) = t - 10 \cdot (X/2.8)^2 \tag{3.12}$$

Here, X is a standard normally distributed variable. As the function depends on just one variable, it is suitable for showing the advantages of applying low-discrepancy sampling. The parameter t could be a threshold parameter (representing, e.g., an acceptable deflection), and is chosen as $t = 30$. As a consequence, G could be interpreted as safety margin, which indicates the difference between a sample evaluation and the threshold t. Note that equation (3.12) constitutes a state function, cf. equations (2.17) and (3.5), however it is nonlinear. Failure is indicated be negative function values.

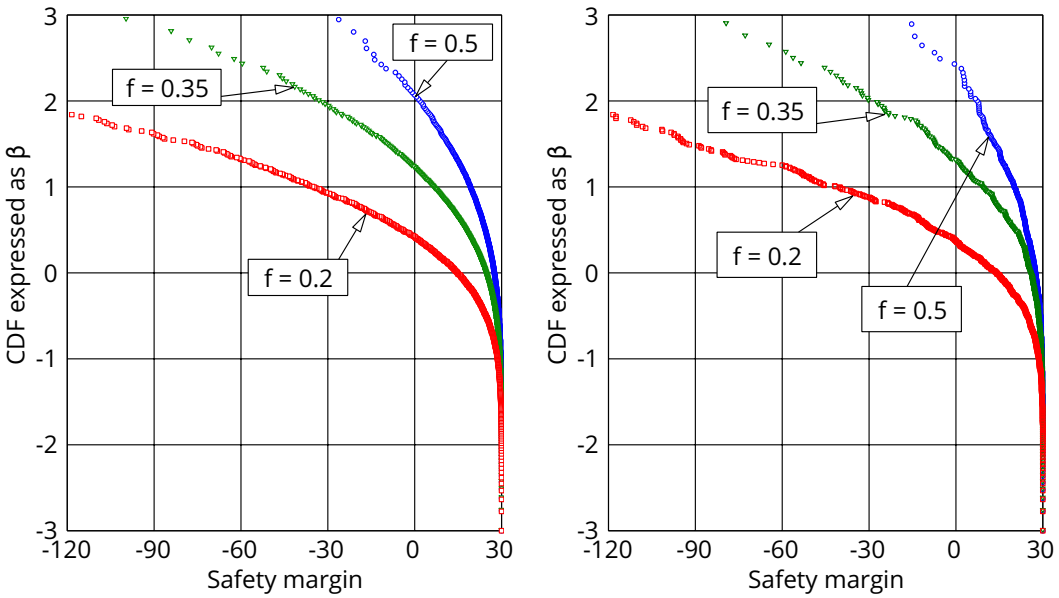

Fig. 3.2: CDFs created with (left) and without (right) Sobol sequences

In order to obtain three support points, three different scale factors f (0.5, 0.35 and 0.2) are adopted. For every scale factor f, several hundreds of samples are evaluated. More specifically, the number of evaluations is 500, 350 and 200 for scale factors 0.5, 0.35 and 0.2, respectively. An explanation regarding the number of sample evaluations follows in subsection 3.3.3.

The outcomes of the simulations are represented as cumulative distribution functions (CDFs) $F_X(x)$ expressed as the reliability index, $\beta = \Phi^{-1}(F_X(x))$, see fig. 3.2. In the case of the left picture, the samples have been generated with Sobol sequences. Because of that, the CDF in the left diagram has a very even distribution. In a second experiment, the samples are purely random. Hence, the respective results in the right diagram are more scattered.

As mentioned before, the failure probability of the system can be estimated by a regression and extrapolation technique based on the support points. In the present case, the positions of the three support points can be deduced from the diagrams in fig. 3.2, namely from the values of β at safety margin = 0. Obviously, these values of β are a measure of how many failures occurred for the respective scale level f. It is clear, that the support points deduced from the left picture will be more reliable, since the number of failures of an experiment based on Sobol sequences is, in general, statistically more stable.

This fact can be seen in fig. 3.3. It shows the support points corresponding to the experiment just described, executed 20 times. Again, the diagram on the left side shows the case where the input samples have been generated by Sobol sequences. As a result, the support points at all three scale levels lie close together. This means that they are relatively stable and, hence, also the extrapolated reliability index will be more accurate.

On the other hand, the right diagram shows the support points for the experiments without applying Sobol sequences. As expected, the support points at all three scaling levels feature a high variability. Obviously, as a consequence, also the extrapolated reliability index will be affected.

Unfortunately, low-discrepancy sampling methods such as Sobol sequences (and, hence, also the so called Quasi-Monte Carlo sampling methods, QMCS) are hardly applicable in high-dimensional problems. Dai and Wang [Dai and Wang, 2004] have tested different low-discrepancy sampling methods in the context of structural reliability. It is stated that the efficiency of all of them

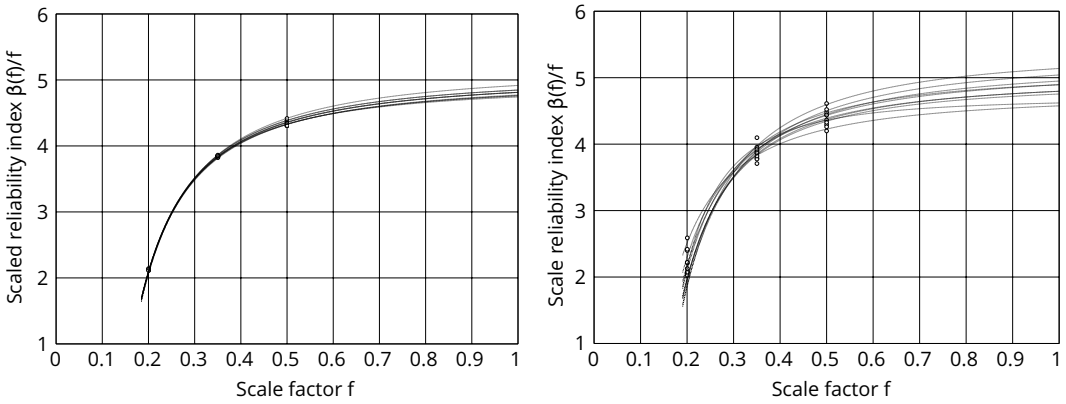

Fig. 3.3: Support points and regression curves created with (left) and without (right) Sobol sequences

decreases rapidly as the number of dimensions increases. Sobol and Asotsky [Sobol and Asotsky, 2003] have demonstrated that the efficiency of QMCS methods also highly depends on whether the input variables are equally important and on whether there is a strong interaction between them. In [Kucherenko et al., 2011] functions are classified into three types:

- Type A: Functions with not equally important variables
- Type B: Functions with equally important variables and with dominant low order terms (this means that there is little interaction between the variables)
- Type C: Functions with equally important variables and with dominant interaction terms.

It is stated that for type C functions the "effective dimension" (see [Caflisch et al., 1997]) is equal or nearly equal to the nominal dimension. For this type of functions, QMCS would lose its advantage over MCS in high dimensions. By studying their expected discrepancies, it is stated that, in general, QMCS methods outperform MCS up to some threshold value of N^*,

$$N^* \approx exp(n) \tag{3.13}$$

in which N^* is the number of samples and n is the (effective) dimension of the problem. According to this equation, for a problem depending on twelve variables, the required number of samples should be at least around 160.000 to gain any benefit from the application of low-discrepancy sequences. That would mean that even for problems of moderate dimensionality (for instance, $n = 12$), QMCS offers no practical advantage over MCS.

To verify this statement, a single-degree-of-freedom (SDOF) oscillator excited by a random force was studied by the author. In case of a random excitation, the excitation force at every time step constitutes a single variable. It can be assumed that all variables have similar importance and that the response depends throughout on multiple variables, i.e. on the excitation in some time before the considered response. Thus, such an example represents a high-dimensional problem belonging to type C. It was found that the relationship stated in equation (3.13) holds for that example.

There may be, however, situations in which the effective number of variables can be reduced. This is possible if the state function G does not depend on a large number of variables at all, or if the dependence is very weak except for a small number of variables. Such a situation can in principle be detected by a preliminary sensitivity analysis. In the context of reliability analysis,

there is frequently a situation in which only one specific combination of the basis variables is most likely to lead to failure. This is closely related to cases in which the First-Order Reliability Method (FORM) yields highly accurate estimates for the failure probability. In these cases, one specific linear combination of basic variables (i.e. the design point) provides the most relevant contributions to the failure probability. Introducing multiples of this specific combination as a new variable and transforming the remaining variables such that orthogonality is maintained (e.g. using a Gram-Schmidt scheme) can lead to substantial improvement of QMCS methods by reducing the effective dimensionality of the problem.

By way of illustration, a simple high-dimensional example is considered, i.e. the equivalent stiffness k^* of a series system consisting of n springs with individual stiffnesses k_i , $i = 1 \dots n$. The equivalent stiffness of the spring assembly is given by the relation

$$k^* = \frac{1}{\sum_{i=1}^{n} \frac{1}{k_i}} \tag{3.14}$$

Assume k_i, $i = 1 \dots n$, to be i.i.d. random variables with a lognormal distribution with a mean value of 1 and a standard deviation of 0.1. The probability of having an equivalent stiffness larger than a given threshold K_n is computed for different values of n. Herein K_n is defined implicitly such that $P[k^* > K_n] = 1.35 \cdot 10^{-3}$ or, equivalently, a reliability index $\beta = 3$. MCS is compared to QMCS, in which both methods use 3000 samples. For each value of n, 500 repetitions of samplings were carried out and the mean values and standard deviations of the reliability indices were estimated using a fixed value of K_n. The results are shown in fig. 3.4. The label "MCS" refers to Monte Carlo simulation (mere random samples), "QMCS" refers to Quasi-Monte Carlo simulation (Sobol sequences). The comparison of these two results clearly shows that QMCS loses its advantage as the number of variables increases and approaches MCS.

Additionally, this figure contains results labelled "QMCS/T". These results were obtained using a linear variable transformation such that the most important linear combination of variables k_i (as obtained e.g. from FORM, or even from simple linear regression analysis on a small number of MCS samples) is introduced as a new variable, and all the others are transformed accordingly using a Gram-Schmidt orthogonalization scheme. This concept basically introduces a rotation of the coordinate system, and in its effect it is quite similar to line sampling ([Pradlwarter et al., 2007, de Angelis et al., 2015]). In this way, the effective dimension of the problem is substantially reduced such that QMCS/T performs much better than standard QMCS.

However, in order to avoid the necessity to detect the most important direction in the standard normal space, an alternative approach is sought for, which is presented in the next subsection.

3.3.2 Stabilizing the CDF

Dynamical systems excited by random forces are a subject of high interest in structural reliability. In the previous subsection it has been explained that for such systems, low-discrepancy sampling methods are not applicable in a straightforward way. However, for AS it would be highly desirable to have support points as stable as when obtained using Sobol sequences (see fig. 3.3, left).

For this purpose a new approach was tested. In order to get a similar effect as when using Sobol sequences, the CDFs corresponding to the example specified by equation (3.12) are stabilized by regression curves (see fig. 3.5). This means that the reliability index β is determined by the regression function, instead of the CDF itself. That way, random local deviations of the CDF can be avoided and the support points derived thereby are statistically much more stable.

There is another advantage of the stabilizing technique. Imagine, for a (relatively high) scale factor f, the MCS yields just one or two failures. Normally, this estimate should be rejected,

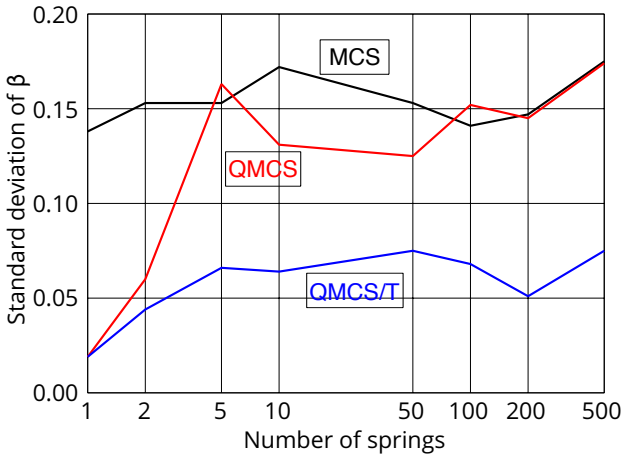

Fig. 3.4: Standard deviation of β for series spring system

because a reliability index β based on just one or two failures cannot be considered very reliable. But if β is based on the proposed regression function, it is much more reliable and it can be used as a support point. Hence, this stabilizing approach is particularly useful for the support point based on the highest scale factor f. As for the other support points, they are usually based on a more representative number of failures and, hence, can be considered more reliable anyway.

The regression function chosen is:

$$\beta = A \ln[B(Safety\ margin) + C] + D \tag{3.15}$$

The logarithmic approach guarantees monotonicity. The four coefficients A, B, C and D enable the regression curve to be flexible enough to retrace the regression points. The coefficients have to be determined by an optimization algorithm. Here, the nonlinear optimization algorithm CONMIN [Vanderplaats and Moses, 1973] implemented in the software package slangTNG [Bucher and Wolff, 2013] is used.

It is pointed out that the stabilizing approach is intended to be used for problems for which low-discrepancy sampling can hardly be applied effectually, namely for systems with a high effective dimensionality. This is certainly the case for systems excited by a force which consists of a series of random variables in time domain. For other systems, the effective number of random variables may be determined by performing a sensitivity analysis. However, it is recommended to generate the samples by Sobol sequences (or an other low-discrepancy sampling technique) anyway. Even though these techniques may loose their strengths compared to mere random sampling in high dimensions, they at least do not perform worse than mere random sampling, as can be seen in fig. 3.4.

3.3.3 Number of sample evaluations and support points

Just as is traditional MCS, a higher number of sample evaluations will result in a higher number of failures, making the scaled reliability indices $\beta(f)$ more reliable. As a result, also the support points will be more stable. Obviously, more evaluations need more computation time. So, this is a tradeoff between accuracy and efficiency. However, it was observed that the accuracy of the resulting failure probability depends primarily on the accuracy of the support point for

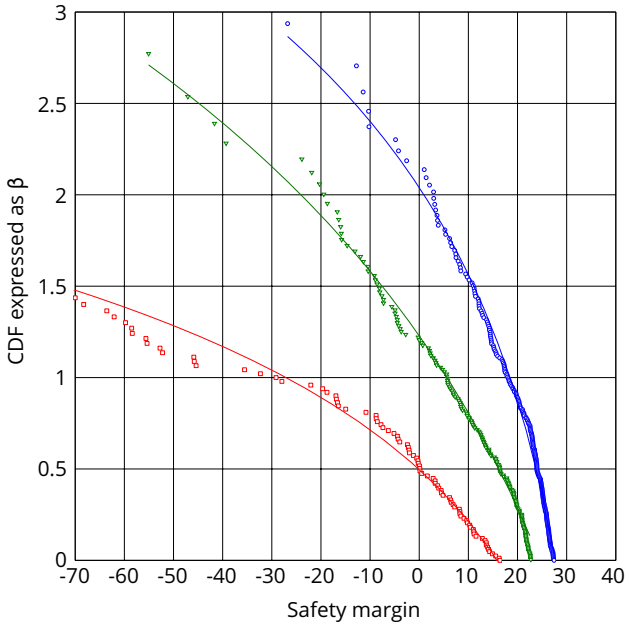

Fig. 3.5: CDFs with stabilizing regression curves

the highest scale factor. This means that it is worth spending more computation effort for the simulation with the highest scale factor. Hence, an adaptive number of evaluations is proposed:

$$n_{sim} = n_{init} f \tag{3.16}$$

Thus, the number of evaluations decreases as the scale factor f decreases. The initial number of evaluations (n_{init}) will actually never be executed, unless there would be a simulation with scale factor $f = 1$.

Of course, the appropriate number of evaluations depends essentially on the complexity of the model as well as on the available computational power. However, as a minimum, it is suggested to choose n_{init} such that the number of evaluations for the highest scale factor f is in the order of 1000. The estimates for the lower scale factors will then rely on some hundreds of single evaluations.

In general, the number of support points should be at least three, when using equation (3.11) for the regression. Four or more support points can help making the regression more stable, but the computation effort increases. For the spacing between the support points, 0.10 or 0.15 may be a good choice (this means that f is reduced by 0.10 or 0.15 each time). However, if one support point has been found to lie in the negative range of $\beta(f)/f$, no more support points should be added by reducing the scale factor f, cf. fig. 3.1. Instead, an additional support point can be chosen between the existing ones.

These suggestions are based on extensive testings carried out by the author. It was found that the optimal number of sample evaluations and support points as well as the collocation of the support points very much depend on the specific problem. Clear general (or also problem-specific) rules for optimal choices could not be identified. Hence, it was decided to present the empirical findings here in the form of general, but rather "loose" suggestions.

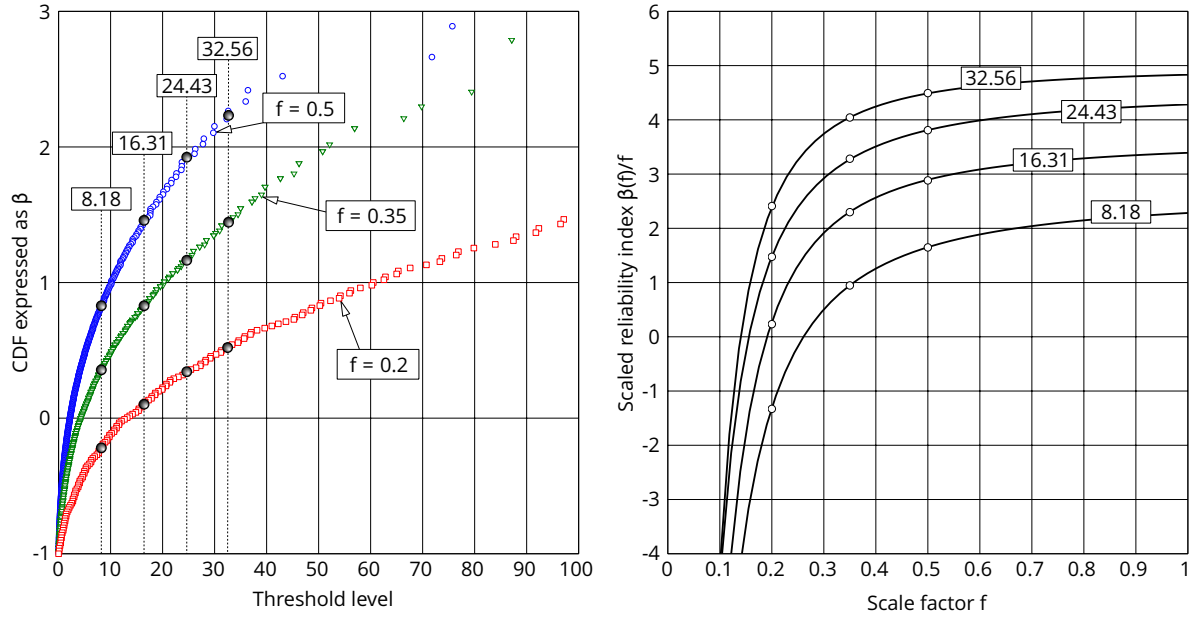

Fig. 3.6: Basic procedure for estimation of threshold exceedance probabilities

3.3.4 Probability of exceedance as function of threshold level

In the previous subsections, the probability of a specific failure state, which can be indicated by a certain scalar value, was studied. Such a failure state could be, for instance, a certain deflection that must not be exceeded. However, it might be more interesting and instructive to determine the probability of exceedance as a function of a threshold level. Having that information, one could not just indicate the probability of exceeding a certain deflection level, but express the probability of exceedance over a whole range of deflection levels.

In fact, AS can also be used to gain this type of information without any additional computational effort for simulation. For that purpose, the state function is slightly modified such that it does not simply indicate failure when being negative, but it indicates the performance over a range of threshold values. Equation (3.12), e.g., could be modified to

$$Y(X) = 10 \cdot (X/2.8)^2 \tag{3.17}$$

where Y could indicate a deflection directly (instead of the corresponding safety margin).

The general procedure is shown in fig. 3.6. From the CDFs of the simulations, multiple sets of support points (for four threshold levels, in this case) are deduced. Then, from each set of support points, the reliability index for the respective threshold level is extrapolated using equation (3.11).

The results can then be represented in a diagram with the threshold level on the x-axis and the probability of exceedance on the y-axis, as shown in fig. 3.7 for 100 different threshold levels. Figure 3.8 shows also the results obtained without applying Sobol sequences. Since this problem has a theoretical solution, that one can serve as a reference. It is evident that the accuracy of the results can be increased significantly when generating the samples by Sobol sequences.

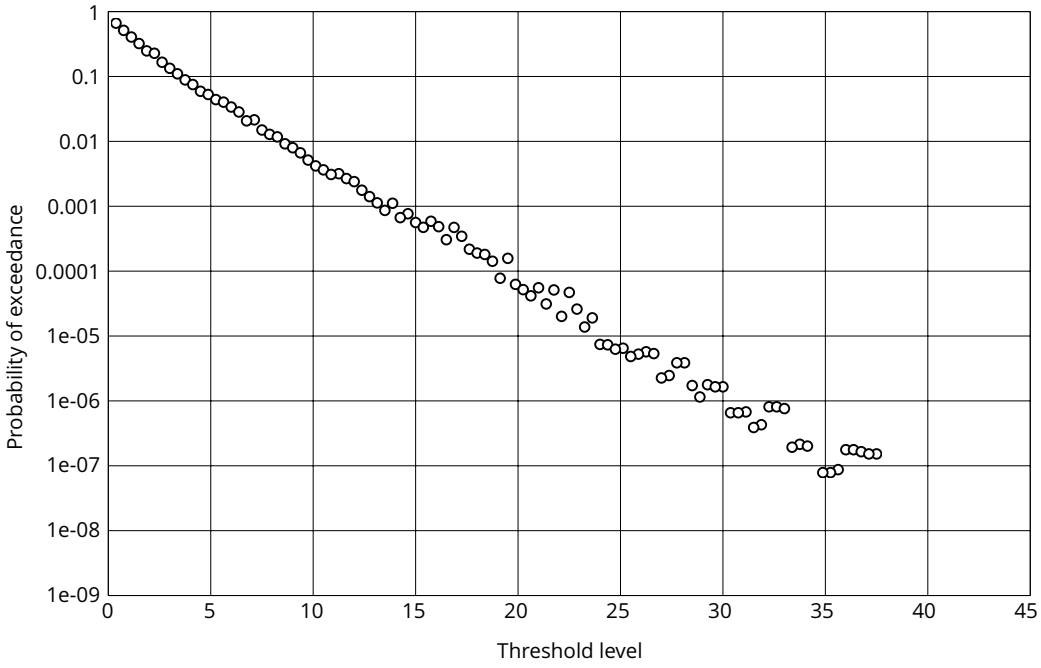

Fig. 3.7: Example for representation of exceedance probabilities of different threshold levels

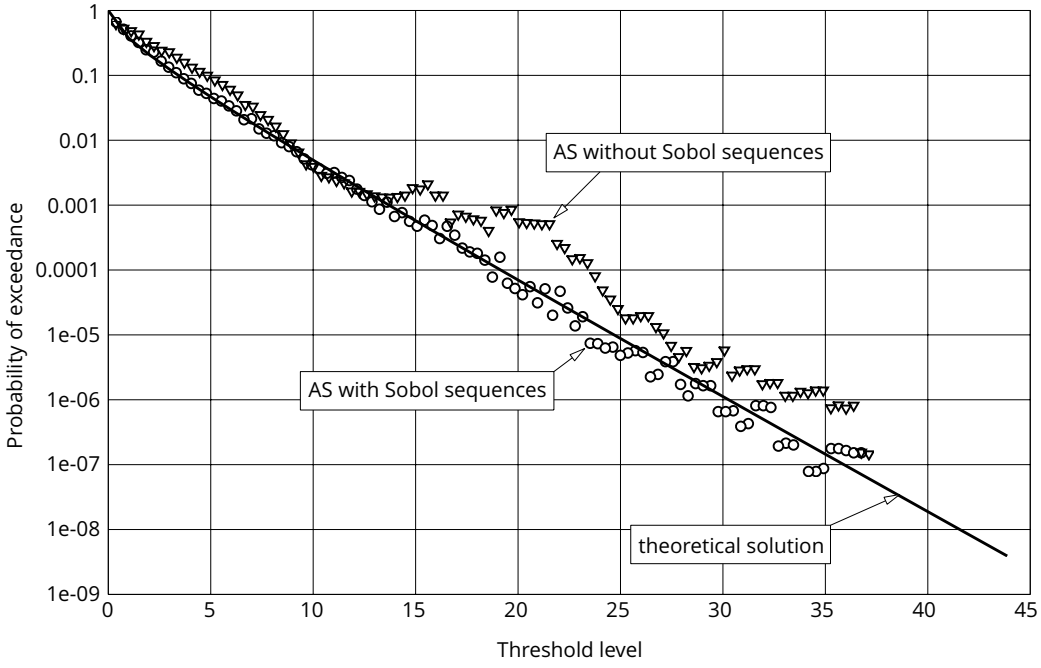

Fig. 3.8: Threshold exceedance probability for function of one variable

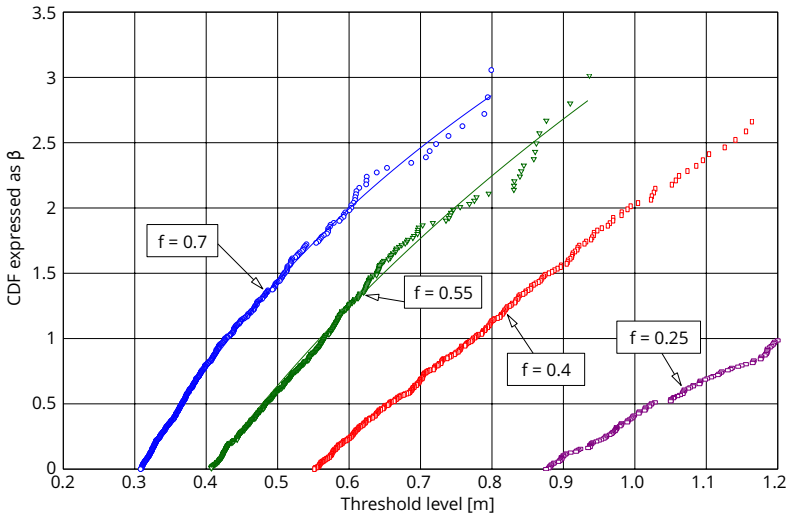

Fig. 3.9: Linear SDOF: stabilized CDFs

3.4 Further numerical examples

3.4.1 Linear SDOF oscillator

Consider a linear SDOF oscillator (see e.g. [Ziegler, 1998]) with mass $m = 2$ kg, stiffness $k = 7$ N/m and damping ratio $\zeta = 0.02$. The excitation is given by a random force with normal distribution with zero mean and standard deviation $\sigma = 1$. This means that the excitation is constituted by a sequence of independent and identically distributed (i.i.d.) random variables. These are assumed to be constant values spaced at the time interval $\Delta t = 0.05$ s. In total a period of 20 seconds is considered. Hence, the total number of steps (as well as the number of dimensions of the system n) is equal to 401.

For this calculations, four support points (scale factors f: 0.7, 0.55, 0.4 and 0.25) are used. The number of evaluations is 1050, 825, 600 and 375, respectively, giving a total of 2850 evaluations.

Figure 3.9 shows the upper part of the CDFs with logarithmic stabilizing curves. As explained in section 3.3.2, the stabilizing approach is particularly useful for the higher scale factors f, as they yield fewer failures for the higher threshold levels. Naturally, for lower threshold levels they yield more failures and, hence, the respective CDFs have there a smoother shape anyway. Therefore, the regression has only be adopted for half of the evaluations, namely for the ones which have resulted in the highest displacements (which corresponds to the part of the CDF with positive values of β). Furthermore, the stabilizing curves were only applied to the CDFs of the two higher scale factor f, as the other ones offer representative numbers of failures in the threshold range of interest anyway.

Figure 3.10 shows the threshold crossing probabilities. As reference, the results of a crude MCS based on 10^5 evaluations are shown. Evidently, AS allows for estimates even at lower probability levels with a significantly reduced number of evaluations. Furthermore, it can clearly be seen that the results based on stabilized CDFs are more accurate. Obviously, results can just be gained for that threshold range that is covered by all CDFs. To obtain exceedance probability estimates for higher threshold levels, the support point belonging to the highest scale factor f could be replaced by an additional one for a lower scale factor f.

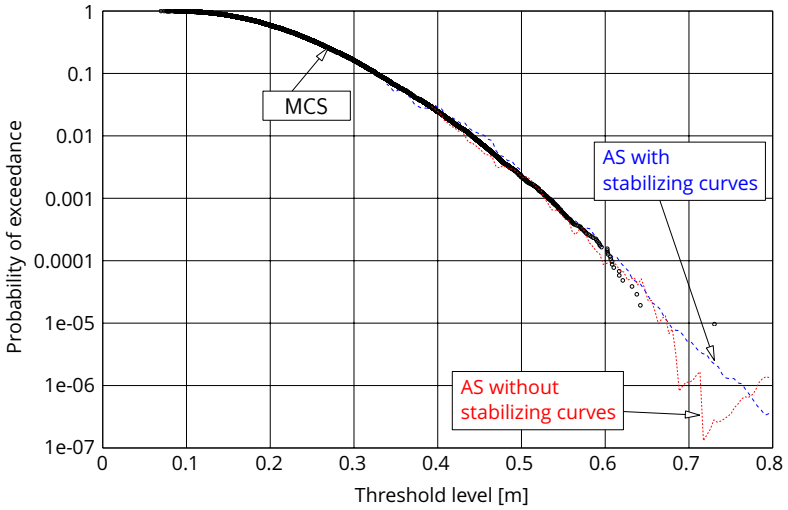

Fig. 3.10: Threshold exceedance probability for linear SDOF oscillator

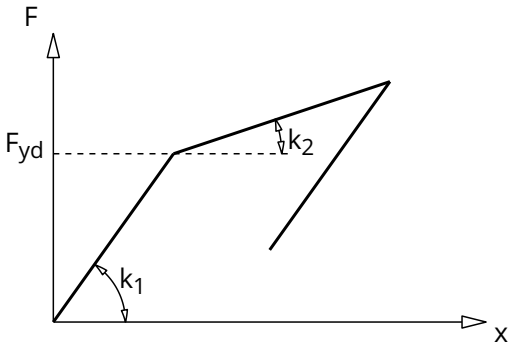

Fig. 3.11: Stress strain behaviour of nonlinear SDOF oscillator

3.4.2 Nonlinear SDOF oscillator

This example is a nonlinear SDOF oscillator. It is taken from [Bamer, 2014]. The nonlinearity is given by an elastoplastic material behaviour, which is shown in fig. 3.11. The parameters are chosen as mass $m = 4$ kg, pre-yield elastic stiffness $k_1 = 80$ N/m, post-yield plastic stiffness $k_2 = 40$ N/m, yield force $F_{yd} = 1$ N and damping ratio $\zeta = 0.05$. The excitation is the same as in the previous example.

Three support points are used (scale factors f: 0.75, 0.6 and 0.45). The number of evaluations is 900, 720 and 540, respectively, giving a total of 2160 evaluations. The CDFs obtained for these scaling levels are shown in fig. 3.12. They are all stabilized by regression curves based on 50% of the CDF points, just as in the previous example.

The results are represented in fig. 3.13 as probability of exceedance over the threshold level. As reference, the results of a crude MCS based on 10^5 evaluations are shown. It is demonstrated that failure probabilities up to approximately 10^{-7} can be estimated by a moderate number of evaluations. The stabilizing technique provides a remarkable increase in accuracy, especially for higher threshold levels.

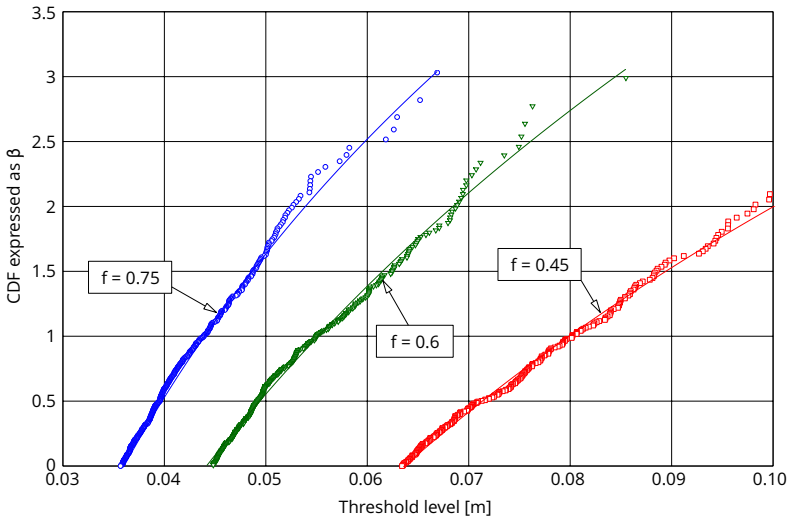

Fig. 3.12: Nonlinear SDOF oscillator: stabilized CDFs

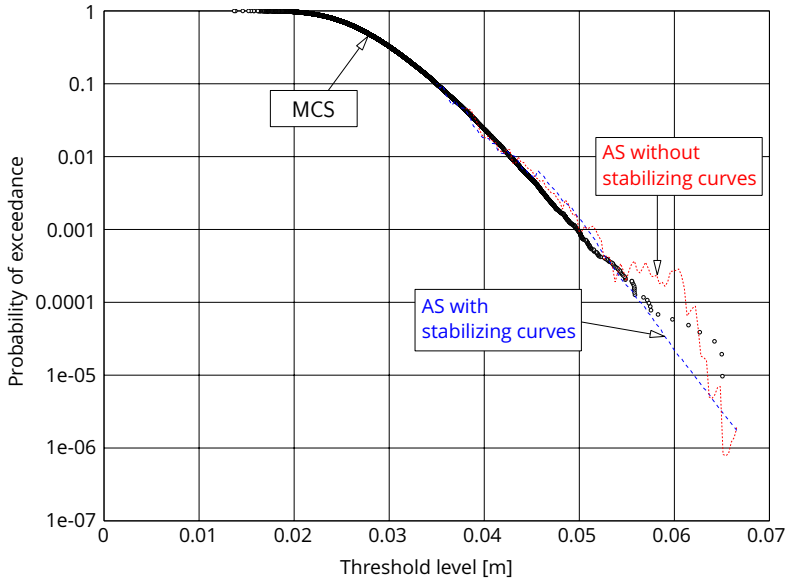

Fig. 3.13: Threshold exceedance probability for nonlinear SDOF oscillator

3.5 Asymptotic sampling using regression surface [2]

In this section, asymptotic sampling (AS) is combined with an alternative approach to estimate small (failure) probabilities: extrapolation of the CDF. First, the two approaches are shortly explained. Subsequently they are combined to a joint regression function. Since the quantity of interest is then a function of two variables (threshold level and scale factor), this regression function is a surface.

3.5.1 Asymptotic sampling

Due to a result by Breitung [Breitung, 1984] it is known that for an arbitrary reliability problem the reliability index β as computed from the First-Order Reliability Method (FORM) is asymptotically exact as the reliability tends to infinity, or alternatively, as the standard deviation of the basic variables in normal space tends to zero. Introducing the scale factor f, which is simply the inverse of the standard deviation, $f = 1/\sigma$, it can thus be stated that the reliability index asymptotically depends linearly on f, or, in scaled notation [Breitung, 1984, Gollwitzer and Rackwitz, 1988]

$$\lim_{f\to\infty} \frac{\beta(f)}{f} = \text{const.} \tag{3.18}$$

This asymptotic property can be exploited when extremely small failure probabilities are to be estimated. In that case, a conventional MCS would be unaffordable, since too many single simulation runs would be necessary in order to obtain a representative number of failure events. However, if the standard deviation of the basic variables is increased, a representative number of failure events can be obtained out of a moderate number of simulation runs. The scaled reliability indices obtained in that way are then used as support points for a regression as shown in fig. 3.1. The reliability index of the original system, i.e. $\beta(f = 1)$, is then obtained by extrapolation.

In order to exploit this asymptotic relation, [Bucher, 2009a] suggested to utilize the formulation

$$\frac{\hat{\beta}(f)}{f} = A + \frac{B}{f^2} \tag{3.19}$$

This choice is motivated in order to satisfy the asymptotic property in equation (3.18), according to which the second term in equation (3.19) has to vanish for $f \to \infty$. However, it was observed that the regression approach should be made more flexible to make it suitable for a broad range of applications. Hence, a third parameter is introduced, which constitutes the exponent of the denominator:

$$\frac{\hat{\beta}(f)}{f} = A + \frac{B}{f^C} \tag{3.20}$$

Assuming C to be positive, also this approach ensures asymptotic convergence to a constant value (here to A) as $f \to \infty$ (which is equivalent to $\sigma \to 0$). The coefficients A, B and C can be determined from a optimization algorithm.

It is pointed out that the asymptotic properties, on which the approach relies, are only valid if the random variables are independent and identically distributed (i.i.d.) with zero mean and standard deviation $\sigma = 1$. Not normally distributed variables and possible correlations among them can easily be introduced using marginal transformations and joint probability density function models such as the widely used Nataf-model [Nataf, 1962, Liu and Der Kiureghian, 1986].

[2] This sections has been published as [Gasser and Bucher, 2017a]. The text here contains some modifications.

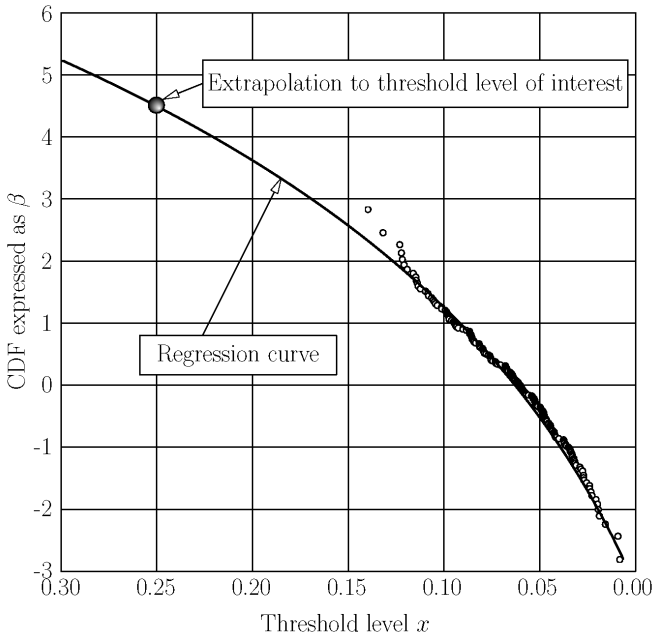

Fig. 3.14: Estimation of small failure probabilities by extrapolation of the CDF

3.5.2 Extrapolation of the cumulative distribution function

A different, but in principle very simple method is presented in this subsection. The basic concept is shown in fig. 3.14. The outcomes of a MCS are represented as cumulative distribution function (CDF) $F_X(x)$ expressed as the reliability index, $\beta = \Phi^{-1}(F_X(x))$. These outcomes could be, e.g., the maximum displacements of a dynamical system excited by a random force. A MCS result representation as in fig. 3.14 is very useful as it indicates the exceedance probabilities for a whole range of threshold levels. For instance, the reliability index for not exceeding the threshold level $x = 0.10$ apparently is approximately $\beta = 1.2$. By using equation (2.26), the probability of exceedance follows therefore as $P_F = 0.115$.

However, it is evident that this representation is not suitable for the estimation of very small exceedance probabilities, since for a limited number of simulation runs, higher threshold levels are rarely or never reached. To overcome this limitation it is proposed to approximate the CDF with a regression function, which is then extrapolated to the threshold level of interest. In fig. 3.14 this approach yields reliability index $\beta \approx 4.5$ for threshold level $x = 0.25$. For the approximation shown in fig. 3.14 the following function was used:

$$\hat{\beta} = A \ln(Bx + C) + D \tag{3.21}$$

The logarithmic approach guarantees monotonicity. The four coefficients A, B, C and D are obtained by an optimization algorithm. It is evident that the regression curve retraces the MCS results very well. It can be assumed that the failure probabilities can be estimated quite accurately with this simple technique, especially for threshold levels not too far away from the range covered by MCS results. This approach was applied to estimate small failure probabilities resulting from earthquakes of moderate intensity in [Gasser and Bucher, 2017b].

However, this technique is not able to really predict the actual behaviour of the system in the probability tails. For instance, referring to fig. 3.14, a sudden change of boundary conditions

occurring at displacement level $x = 0.15$ remains entirely undiscovered because no simulation run yielded such a large displacement.

3.5.3 Probability estimation by regression surface

On the other hand, the AS technique is in principle suitable to explore the system's behaviour in the probability tails, as it is based on a scaling of the standard deviations of uncorrelated normally distributed variables. Hence, it is proposed to combine both approaches described in subsections 3.5.1 and 3.5.2.

For that purpose, for the reliability index β, a regression function is proposed that depends on both variables, the threshold level x und the scale factor f:

$$\frac{\hat{\beta}(x,f)}{f} = a_0 + a_1 x + a_2 \ln x + \frac{a_3}{f^C} + \frac{a_4 x}{f^C} + \frac{a_5 \ln x}{f^C} \tag{3.22}$$

A similar approach has successfully been applied in [Bucher, 2015]. The approach is chosen such that the six parameters a_0 ... a_5 can be obtained by linear regression. The optimal exponent C is found by executing the linear regression with a series of exponents and selecting then the exponent for which the approximation was best in terms of least squares.

In this way, a regression surface is constructed. The exceedance estimates are obtained as a function of the threshold level x when the scale factor is fixed to $f = 1$.

3.5.4 Numerical example

The presented approach is tested on a well-known benchmark example [Schuëller and Pradlwarter, 2007], which is described in the following. It is a MDOF system with Duffing type nonlinearity. This system is driven by an earthquake excitation $a(t)$ which is defined as the output of a 4^{th} order linear filter driven by non-stationary white noise $w(t)$. The noise is defined by its covariance function

$$E[w(t)w(t+\tau)] = I\delta(\tau) \cdot h(t);\ h(t) = \begin{cases} \frac{t}{2} & , \quad 0s \le t \le 2s \\ 1 & , \quad 2s \le t \le 10s \\ \exp\big(-0.1(t-10)\big) & , \quad t \ge 10s \end{cases} \tag{3.23}$$

with $I = 0.08\ \mathrm{m}^2/\mathrm{s}^3$. The linear filter is given by the equations

$$\dot{\mathbf{X}}(t) = \mathbf{A}_{EQ}\mathbf{X}(t) + \mathbf{B}_{EQ}w(t); \qquad a(t) = \mathbf{C}_{EQ}\mathbf{X}(t) \tag{3.24}$$

$$\mathbf{A}_{EQ} = \begin{bmatrix} 0 & 1 & 0 & 0 \\ -\Omega_{1g}^2 & -2\zeta_{1g}\Omega_{1g} & 0 & 0 \\ 0 & 0 & 0 & 1 \\ \Omega_{1g}^2 & 2\zeta_{1g}\Omega_{1g} & -\Omega_{2g}^2 & -2\zeta_{2g}\Omega_{2g} \end{bmatrix} \quad \mathbf{B}_{EQ} = \begin{bmatrix} 0 \\ 1 \\ 0 \\ 0 \end{bmatrix} \tag{3.25}$$

$$\mathbf{C}_{EQ} = \begin{bmatrix} \Omega_{1g}^2 & 2\zeta_{1g}\Omega_{1g} & -\Omega_{2g}^2 & -2\zeta_{2g}\Omega_{2g} \end{bmatrix} \tag{3.26}$$

The numerical values chosen are Ω_{1g} =15 rad/s, $\omega_{2g} = 0.3$ rad/s, $\zeta_{1g} = 0.8$ and $\zeta_{2g} = 0.995$. The MDOF system is governed by the equations

$$\mathbf{M}\ddot{\mathbf{u}}(t) + \mathbf{C}\dot{\mathbf{u}}(t) + \mathbf{K}(\mathbf{u}(t))\mathbf{u}(t) = \mathbf{m}a(t) \tag{3.27}$$

in which the matrices are given as

$$\mathbf{M} = \begin{bmatrix} m_1 & 0 & \dots & 0 \\ 0 & m_2 & \dots & 0 \\ \vdots & \vdots & \ddots & \vdots \\ 0 & 0 & 0 & m_{10} \end{bmatrix}; \quad \mathbf{m} = \begin{bmatrix} m_1 \\ m_2 \\ \vdots \\ m_{10} \end{bmatrix} \tag{3.28}$$

$$\mathbf{C} = \begin{bmatrix} c_1 + c_2 & -c_2 & \dots & 0 \\ -c_2 & c_2 + c_3 & \dots & 0 \\ \vdots & \vdots & \ddots & \vdots \\ 0 & 0 & \dots & c_{10} \end{bmatrix} \quad \mathbf{K} = \begin{bmatrix} \bar{k}_1 + \bar{k}_2 & -\bar{k}_2 & \dots & 0 \\ -\bar{k}_2 & \bar{k}_2 + \bar{k}_3 & \dots & 0 \\ \vdots & \vdots & \ddots & \vdots \\ 0 & 0 & \dots & \bar{k}_{10} \end{bmatrix} \tag{3.29}$$

$$\bar{k}_i = k_i \left(1 + \epsilon \left(\frac{u_i(t) - u_{i-1}(t)}{\delta u_{ref}} \right)^2 \right); \qquad i = 1, \cdots, 10 \tag{3.30}$$

The system parameters are chosen as $\delta u_{ref} = 0.02$ m, $\epsilon = 0.1$, $m_1 = \cdots = m_{10} = 10{,}000$ kg, $k_1 = k_2 = k_3 = 40$ MN/m, $k_4 = k_5 = k_6 = 36$ MN/m, $k_7 = k_8 = k_9 = k_{10} = 32$ MN/m, $c_i = 2\zeta_i \sqrt{m_i k_i}$ and $\zeta_i = 0.04$ for $i = 1, \cdots, 10$. The time duration is $T = 20$ s and the time step is chosen as $\Delta t = 0.005$ s [3]. Therefore the load discretization requires 4000 random variables. The failure criterion is the relative displacement between stories 9 and 10 exceeding a threshold level x.

The AS procedure is carried out for five different scale factors f equally spaced between 0.4 and 1. It has been observed that, in order to save computation time, the number of simulation runs may be reduced as the scale factor is reduced, cf. subsection 3.3.3. The reason is that for smaller scale factors, high threshold levels are covered well anyway, even at a significantly reduced number of runs. Hence, the number of simulation runs per scale factor level was chosen as $n_{runs}(f) = n_{init} f$. The initial number of runs was chosen as $n_{init} = 800$, thus in total 2800 runs are performed. For the construction of the regression surface according to equation (3.22), only support points with a positive reliability index β are used, see fig. 3.15. Furthermore, samples above threshold level $x = 0.05$ m are truncated.

Eventually, the estimation of exceedance probability as function of the threshold level is obtained by fixing the scale factor to $f = 1$ (which corresponds to the original system), see fig. 3.16. In this graph, also the reference results from the benchmark study are indicated. These were obtained by conventional MCS with 74,700,000 runs, evaluating the exceedance probabilities for the threshold levels $x = 0.024$ and $x = 0.028$. It is evident that the agreement with the proposed approach, which is based on 2.800 runs, is very good.

3.6 Summary and conclusions

Asymptotic sampling is a novel Monte Carlo based simulation technique for calculating small failure probabilities. It has been shown that very small probabilities can be estimated with sample sizes between 1000 and 3000. The method is suitable for a wide range of applications, including highly nonlinear problems.

The results have been represented as threshold exceeding probabilities, providing the analyst comprehensive information about the systems expected behaviour. It has been explained how these additional informations can be easily educed from the CDFs resulting from the simulations.

[3] The smallest natural period of the system equals 0.0532 s.

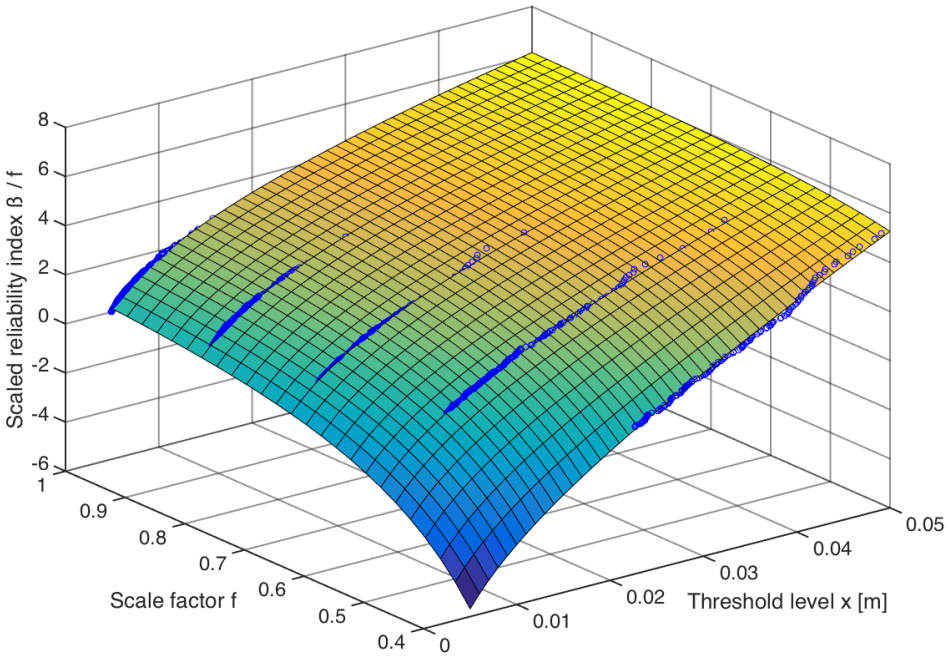

Fig. 3.15: Support points with regression surface

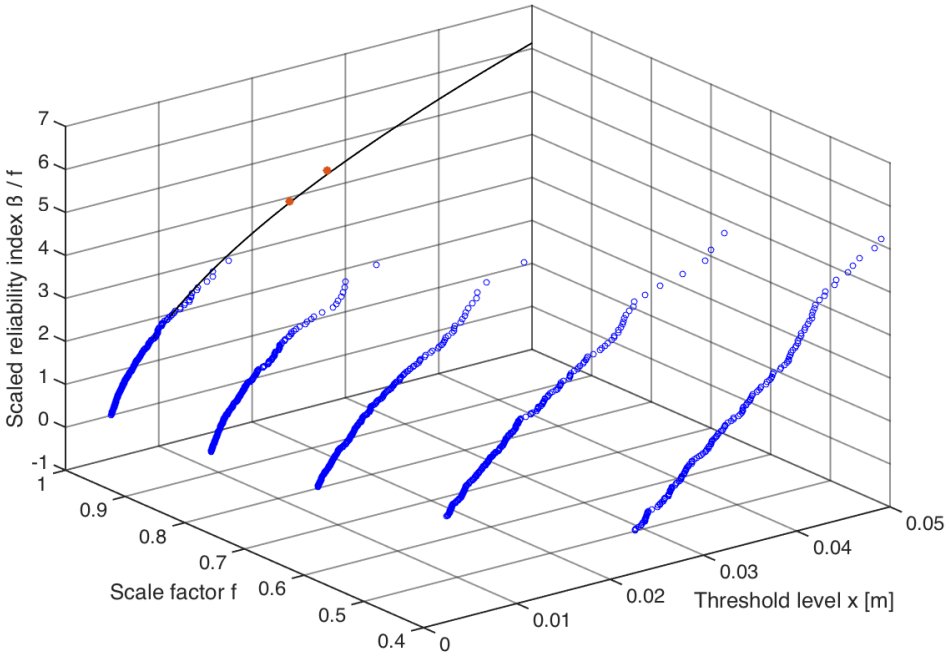

Fig. 3.16: Support points with resulting threshold exceedance probability curve, as well as reference results (red dots) taken from [Schuëller and Pradlwarter, 2007]

It has been shown that for low-dimensional problems, well known low-discrepancy sampling methods can be applied effectually. For problems involving many variables, a new technique was presented, which is able to increase the accuracy of the results by stabilizing the support points for the regression.

The chosen regression function with three parameters has proven to be suitable for fitting the support points and yielding the reliability index by extrapolation. Future research could focus on how to determine the optimal exponent in this regression function.

In a second approach, a regression *surface* was constructed based in the generated samples, and an extrapolation in two directions was performed. The approach was tested on a benchmark example of a MDOF oscillator with Duffing-type nonlinearity. The results are in good agreement with the reference results. However, the number of simulation runs necessary is smaller by several orders and threshold range for which exceedance probabilities can be estimated is very wide. Further research might focus on the approach used for the regression surface.

Chapter 4

Seismic safety analysis of an arch dam

4.1 Probabilistic seismic analysis

In seismic engineering practice, structures are usually designed to withstand earthquakes with a certain intensity. For a given location, any intensity level may be associated with a certain return period by means of seismological investigations. Additionally to the location of the structure, the choice of the design intensity level depends obviously on its importance. The aim is to prevent damages, respectively failure, whereby one seeks to stay always on the safe side by applying safety factors. This is necessary because of the lack of exact knowledge about the resistances and loadings and because of their inherent randomness in general. Furthermore, it is impossible to represent a real structure by a model exactly. However, apart from certain analytical cases, any safety factor concept is eventually inappropriate to design a structure such that damage/failure will not occur during the lifetime with a *given* probability, cf. chapter 2.

Two methods for earthquake analysis used in practice are the response spectrum method and the time history analysis. An advantage of the response spectrum method is that dynamic analyses are avoided, hence making it practicable for most engineering companies. Furthermore, response spectra for design purposes are available for wide areas of the world. The stochasticity of ground accelerations is considered by these design spectra in the way that they are smoothened median values (or other percentiles) of the spectral responses to a set of ground accelerations which are to be expected in that location with a given return period. The major disadvantage of this method is its incapacity of representing the real behaviour of the structure since it relies on some superposition of responses of linear SDOF oscillators. In particular, this concerns the material behaviour beyond linear elasticity, including the dissipative effects of ductile components, which are of high relevance in earthquake engineering [Adam and Jäger, 2012]. Instead, these effects may only be included in the dimensioning by some generic factors [Chopra, 2012a].

This shortcoming motivates to perform a time history analysis. The real performance of the structure is studied by implementing inelasticities and nonlinear behaviour in general [Adam, 2001]. This approach constitutes the first step of the concept called performance-based earthquake engineering (PBEE) [Deierlein et al., 2003]. Instead of using a design spectrum, one needs to apply a ground motion time history pertinent to the location and the desired return period. Although characteristics of the time history, such as intensity and frequency content, may be chosen skilfully by considering the geophysics of the site, one has to keep in mind that it is an inherently random signal. This kind of uncertainty is also referred to as aleatoric uncertainty, which means not reducible by more elaborate investigation. Of course, this high degree of randomness is then reflected in the response of the structure. On the other hand, uncertainties of other model parameters, such as concrete strength parameters, are comparatively small and, in principle, may be further reduced by more elaborate testing as well as by more exact production processes (epistemic uncertainties).

In fact, consideration of both the real (nonlinear) behaviour and the stochasticity of ground motions and other parameters call for an analysis framework that results in a probabilistic

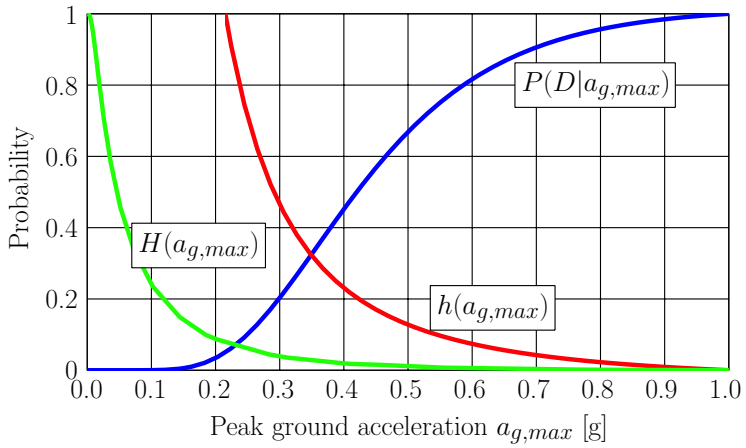

Fig. 4.1: Seismic hazard curve $H(a_{g,max})$, probability density function of PGA, $h(a_{g,max})$, and fragility curve $P(D|a_{g,max})$, conceptually

representation of a structure's response given its seismic environment. Such an analysis framework is called probabilistic seismic demand analysis (PSDA). In PSDA, certain quantities, so called engineering demand parameters (EDPs), are selected which are representative for the structural performance. These EDPs may be stresses, displacements, damage indices, energies or other quantities which may be associated with defined limit states. PSDA has primarily been established in the context of buildings, see e.g. [Carballo and Cornell, 2000, Shome, 1999].

The randomness of the ground motions, as well as of all other model parameters, may be accounted for by means of Monte Carlo simulation (MCS). In the context of earthquake engineering, one has to consider that it is not sufficient to calculate the probability of damage just for a predefined intensity level (maybe the one with return period equal to expected life time) since there is also some (lower) damage probability for lower intensity levels and some (higher) damage probability for higher intensity levels.

Eventually, these reflections lead to the following equation for the calculation of the damage probability (cf. [Cornell and Krawinkler, 2000])

$$P_D = \int_0^\infty h(a_{g,max}) P(D|a_{g,max}) da_{g,max} \tag{4.1}$$

where the peak ground acceleration (PGA) level $a_{g,max}$ serves as intensity measure (IM).

Conceptually, the two terms of the integrand are shown in fig. 4.1.
The red curve shows $h(a_{g,max})$, the probability density function of PGA, which is the negative derivative of the seismic hazard curve $H(a_{g,max})$:

$$h(a_{g,max}) = -\frac{dH(a_{g,max})}{d(a_{g,max})} \tag{4.2}$$

$H(a_{g,max})$ gives the probability that the PGA at a site will equal or exceed level $a_{g,max}$ in a given period of time. It is provided by seismological services. Consequently, P_D then refers to the same period of time, which is typically 50 years. The other term in equation (4.1), $P(D|a_{g,max})$, is a damage probability of the structure subjected to an earthquake with PGA equal to $a_{g,max}$, and it is called fragility curve. While the term $h(a_{g,max})$ is merely location-referred, the fragility

curves $P(D|a_{g,max})$ refer to the structure itself. So, the two terms can conveniently be treated separately. [1]

In the following, focus will be on the efficient construction of the fragility curves. Indeed, there is a single fragility curve for each limit state of a structure, especially for any damage or failure mechanism which can be identified and defined by professional judgement. Naturally, in the MCS, the simulation runs do not have to be performed separately for different limit states, in general. However, as a fragility curve $P(D|a_{g,max})$ for a damage - respectively $P(F|a_{g,max})$ for failure - represents a probability conditional on the PGA level, several MCS estimates (for different PGA levels) are needed. Hence, the computational cost of a complete seismic safety analysis resulting in damage probabilities P_D - respectively in failure probability P_F - may be excessively high. Therefore, possibilities will be tested to reduce the number of simulation runs.

4.2 Seismic analysis of dams

In the past decades, special attention has been given to the evaluation of earthquake safety of dams since failure would have catastrophic consequences. The challenges, which were faced in modelling this kind of structures, regarded dam-reservoir interaction, proper modelling of earthquake input [Hall, 1998], and consideration of the effects of radiation damping [Chopra, 2012b]. In the case of arch dams, a realistic modelling allows for opening of the contraction joints [Hall, 1998] and, at best, includes a damage model for the concrete. Extensive research about all of the mentioned topics has been done by Zhang and his research team at Tsinghua University. A collection of their papers has been published in [Zhang et al., 2013].

Herein, a probabilistic approach is used for the seismic safety analysis of an arch dam. So far, similar research work focused primarily on gravity dams [Kisliakov, 1997, de Araújo and Awruch, 1998, Tekie and Ellingwood, 2003, Ghanaat et al., 2012, Ju et al., 2015, Bernier et al., 2016], where especially the sliding safety was investigated. Moreover, a number of recent publications by Hariri-Ardebili and Saouma (and co-authors), see e.g. [Hariri-Ardebili and Kianoush, 2014, Hariri-Ardebili et al., 2016, Hariri-Ardebili and Saouma, 2016a, Hariri-Ardebili and Saouma, 2016b], is concerned with (nonlinear) dam behaviour and possible failure mechanisms. Mostly, probabilisitic methods are involved and results are presented as fragility curves or surfaces. A review of these and other relevant papers can be found in [Hariri-Ardebili and Saouma, 2016c]. Yet, analogous research on arch dams has rarely been done [Varbanov et al., 2012, Hariri-Ardebili et al., 2016, Wang et al., 2018]. This is maybe also because of the high effort of implementation and computation since analysis of arch dams necessarily involves a three-dimensional model.

However, as earthquakes are highly stochastic processes, they are the main source of uncertainty in the response of a structure (in an earthquake-prone region), cf. [Tekie and Ellingwood, 2003, Gasser and Bucher, 2017b]. Hence, it seems natural to investigate the response by probabilistic means. Additionally to seismic excitation, the damping of a structure is a highly uncertain mechanism. Moreover, in the case of a dam, the water level of the reservoir is subjected to high variation. Besides, in principle, also all other loads and resistances constitute random

[1] In modern PBEE - more specifically, within the framework of the *PEER PBEE methodology*, developed by the Pacific Earthquake Engineering Research Center (PEER), - an extended integral is proposed, instead of the one in equation (4.1), see e.g. [Deierlein et al., 2003], [Porter, 2003] (for summary), or [Krawinkler, 2005] (for benchmark study). It involves in particular *decision variables*, "which translate damage measures into quantities that relate to risk management decisions concerning economic loss and life safety" [Deierlein et al., 2003]. This approach is not treated in this thesis. It would be beyond the scope: One only needs the think about the fact that a (quantitative) assessment of life safety would require an estimation of the inundated area if the dam fails.

variables, which influence the safety of a structure to a greater or lesser extent. [2] The complete list of parameters that are considered in a stochastic way in this study is presented in section 4.5.

To assess the safety of a structure, it is necessary to identify possible damage and failure mechanisms. The damage mechanisms investigated in this work are concrete cracking, opening of a block joint (exceeding a defined limit), cracking of the grout curtain, and sliding safety. These mechanisms are described in detail in section 4.6. For each of them, a fragility curve will be derived.

The most realistic scenario of a complete failure of an arch dam under earthquake excitation is excessive tensile cracking of the concrete [Zhang et al., 2013, Chopra, 1992]. However, a localized and temporary exceedance of the tensile strength will lead to a small crack but not to failure of the dam. Hence, exceedance of a (strength) parameter cannot simply be used as an indicator for total failure. This fact represents a challenge to the framework of probabilistic safety assessment since it usually associates failure with a certain scalar limit state. Instead, the present work aims to clarify if abortion of the numeric calculation can be used as an indicator for loss of equilibrium and hence for failure. For that purpose, damage and stiffness degradation under cyclic loading is modelled by implementing the plastic-damage model developed by Lubliner et al. [Lubliner et al., 1989] and Lee and Fenves [Lee and Fenves, 1998b].

4.3 The arch dam model

The application object is an arch dam whose seismic behaviour was studied in the dissertation of Goldgruber [Goldgruber, 2015]. The structure is fictitious, however its shape and properties are typical for a real dam in a region with moderate seismicity, like the Alps. The finite element model is shown in figs. 4.2 and 4.3.

The dam is 220 m high. The width of the valley is approximately 80 m at the bottom and 430 m at the crest. The total model, which includes also part of the reservoir and of the foundation, has a quadratic ground plan of 1000 m length and a height of 500 m.

Simulations are performed in Abaqus. The number of finite elements is approximately 20,000 (depending on the reservoir level). For the solids, linear brick elements with reduced integration are used. They have eight nodes and one integration point, and are labelled C3D8R. The water is modelled by eight-node acoustic linear elements labelled AC3D8. Consequently, the acoustic wave equation has only one degree of freedom - which is pressure. Compressibility is expressed by the bulk modulus, $K_w = 2200$ MPa.

As for the sequence of the simulation steps, in the first second, the self weight of the dam is applied gradually, followed by the hydrostatic load in the next second. During these two steps, fixed boundary conditions are adopted at the outer boundaries of the foundation. Subsequently, earthquake excitation is applied additionally for 10 seconds. For this, the fixed boundaries are

[2] At this point, the author would like to emphasize once again the difference between aleatoric and epistemic uncertainties. The relevance of the response uncertainty attributable to the earthquake excitation (record-to-record variability) arises primarily by the fact that this is about an aleatoric uncertainty. As for the other parameters' uncertainties, they can be (quite clearly) classified as epistemic. This means that they are in principle reducible. And, in fact, it should be the primary aim of the engineer to reduce the uncertainties of the relevant parameters and to understand the essential mechanisms as best as possible, cf. the problem of seismic input modelling described in subsection 4.3.3. The specification of a parameter as a random variable (especially the specification of the dispersion) leads to the conceptional contradiction described in footnote 10 of chapter 2. This contradiction applies especially for cases where the dispersions of quantities can hardly be estimated statistically - a statistical estimate would be possible, e.g., for strength parameters of a component of a certain material produced in a certain factory -, but on expert opinions, experience and (unsystematic) measurements. This is rather the case here, where a prototype (the arch dam) is built in a given and unique environment (the river valley).

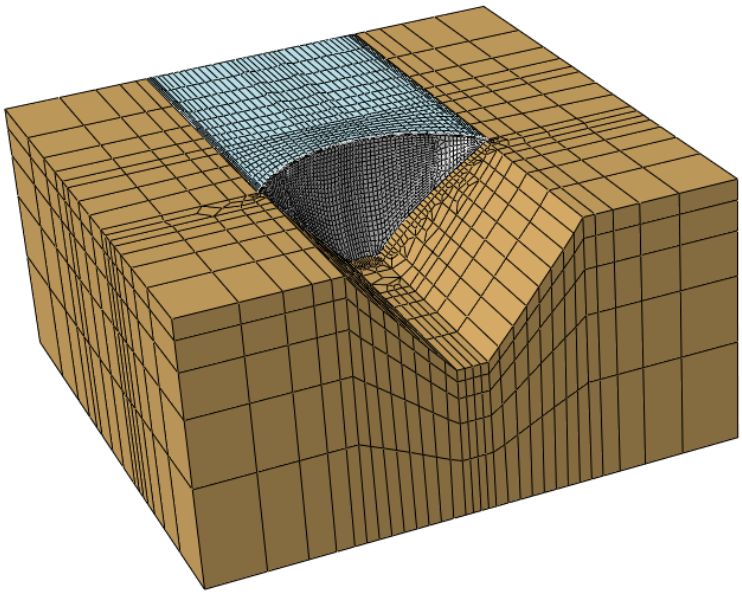

Fig. 4.2: Finite element model of dam, reservoir and foundation [Goldgruber, 2015]

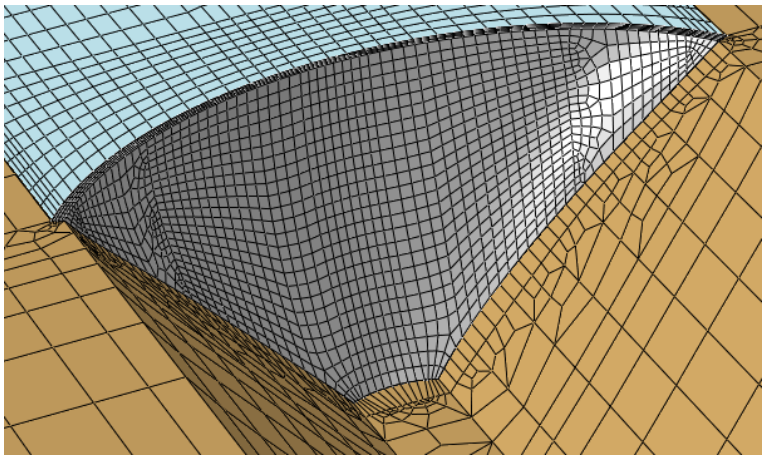

Fig. 4.3: Finite element model: detail [Goldgruber, 2015]

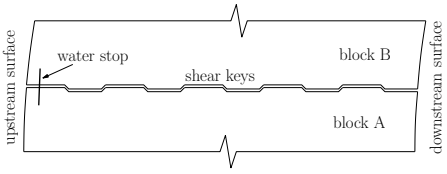

Fig. 4.4: Shear keys and water stop between two blocks of an arch dam

replaced by acceleration time histories, which act in all three directions. A detailed description of the seismic excitation is given in section 4.4.

4.3.1 Contact modelling

The acoustic fluid continuum approach enables for realistic fluid-structure interaction. For the contact between the dam and the reservoir, a tie constraint is defined. This type of constraint allows neither separation nor relative slip, which also applies to the acoustic fluid elements among themselves. At the back-end boundary of the reservoir, a non-reflecting (viscous) boundary condition is adopted, hence waves are absorbed. No boundary conditions are specified on the valley sides, which results in total reflection [Goldgruber, 2015].

Arch dams are subdivided in vertical blocks in order to limit thermal stresses during hydration. The blocks have shear keys on their edges which allow relative displacement in vertical direction but not in radial direction, see fig. 4.4. In the finished state, the joints between the blocks are grouted so that the dam behaves like a monolithic structure. However, during a strong earthquake the grouting may break up, leading to a separation of the blocks and to some displacement between them.

In the model, the dam is separated into 18 vertical blocks. Stresses may be transmitted between the blocks. However, separation is allowed as well as relative displacement between the blocks. To take account of the shear keys, an anisotropic contact formulation is chosen: In radial direction, a very high friction coefficient ($\mu = 5$) basically inhibits relative displacement, as long as the joints are under pressure. An essentially smaller friction coefficient for the second surface direction allows differential sliding of the blocks vertically. Because of the high uncertainty of this contact behaviour it is implemented as a random variable, see table 4.1.

Similarly, also for the interface between dam and foundation, a modelling was chosen that allows for separation as well as relative displacement. Here, the (isotropic) friction coefficient is $\mu = 1$.

4.3.2 Concrete modelling

The strength class of the concrete is C20/25 [EN1992, 2015] with mean compressive strength $f_{cm} = 28$ MPa and density $\rho = 2400$ kg/m^3. The uniaxial compressive stress-strain behaviour is modelled by three segments, see fig. 4.5. The initial linear branch ends at $0.4 f_{cm}$. The second ascending segment [fib, 2012] is quadratic and reaches f_{cm}. The third (descending) segment describes softening [Krätzig and Pölling, 2004]. It depends on the fracture energy and on the characteristic length l_{eq} [Bažant and Oh, 1983]. The use of the fracture energy, a material parameter, was originally derived for *tension* softening in the smeared crack idealization [Krätzig and Pölling, 2004]. The fracture energy concept was transferred to softening under compression by Feenstra [Feenstra, 1993]. The characteristic length l_{eq}, which originally refers to the dependency on sample size observed in experiments, here depends on the finite elements, basically on their

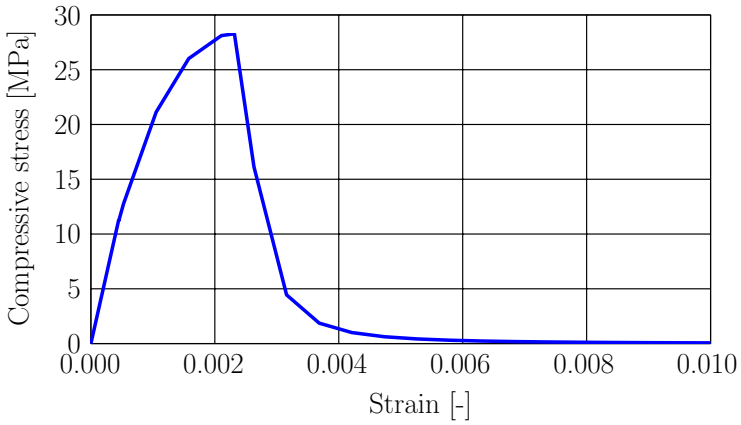

Fig. 4.5: Uniaxial compressive behaviour of concrete

size. The element size of the dam model is in the order of three meters, thus very large. As a consequence, the descent of the third segment in fig. 4.5 is particularly steep. A mathematical description of the three segments can be found in [Alfarah et al., 2017].

For the material damping, the Rayleigh model is used. Thereby, it is assumed that the damping matrix is proportional to the mass and the (initial) stiffness matrix. The proportionality factors are α for the mass and β for the stiffness. The intensity of the damping must be specified by predefining the damping ratio for two (basically arbitrary) frequencies. In practice, the fundamental frequency and the frequency at which the sum of effective modal masses reaches 90% of the total mass are used. For the dam under investigation, these frequencies are 1.54 Hz and 2.29 Hz (fourth natural frequency of the deterministic model) [Goldgruber, 2015]. Since damping mechanisms are inherently highly uncertain, the predefined damping ratios are treated as random variables (see section 4.5).

4.3.2.1 Plastic-damage model

As mentioned earlier, it is of particular interest to study the ultimate capacity of the dam, which will be reached when (cracking) damage of the concrete is so severe and extensive that equilibrium between acting forces and resistances does not subsist anymore. For this purpose, the modelling of the concrete has to be extended such that it can reproduce degradation of stiffness and strength under dynamic loading (see e.g. [Hofstetter and Mang, 1995]).

Such a model has been developed by Lubliner and coauthors [Lubliner et al., 1989] and further developed by Lee and Fenves [Lee and Fenves, 1998b]. In Abaqus it is called *Concrete Damaged Plasticity* [Abaqus, 2014a], see fig. 4.6. It uses the concept of fracture-energy-based damage [Hillerborg et al., 1976] to describe tension cracking and compression crushing. The effect of different damage states on elastic stiffness is controlled by two damage variables, one for tensile damage, d_t, and the other for compressive damage, d_c [Lee and Fenves, 1998b]. The yield function (respectively, failure function, in the strain-softening regime) accounts for different evolution of strength under tension and compression [Abaqus, 2014a]. Recovery of compression stiffness upon crack closure as the load changes from tension to compression can be accounted for (by parameters w_c and w_t) [Abaqus, 2014a].

Lee and Fenves have used their plastic-damage concrete model to study the response of Koyna dam in India in the 1967 Koyna earthquake [Lee and Fenves, 1998a]. This concrete gravity dam sustained several horizontal cracks at the upstream and downstream surfaces [Lee and Fenves,

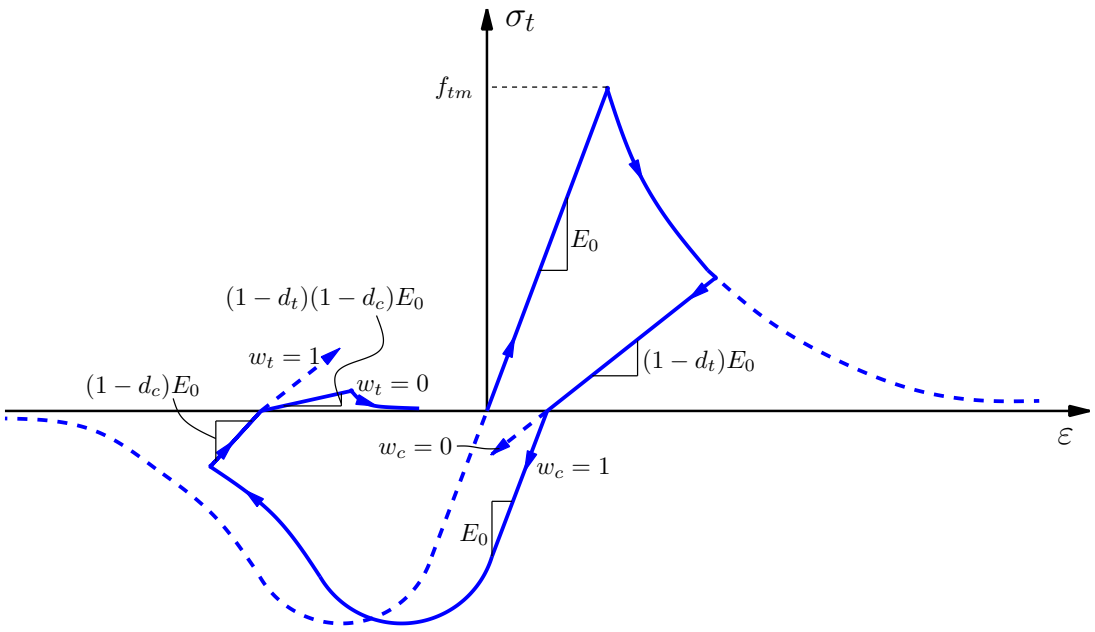

Fig. 4.6: Plastic-damage model: Uniaxial load cycle (tension-compression-tension) assuming stiffness recovery factors $w_t = 0$ and $w_c = 1$, according to [Abaqus, 2014a]

1998a]. To date, it is one of few dams that have been damaged substantially by an earthquake. An accelerograph in the inspection gallery recorded the transverse and vertical accelerations, which, since having been registered in such a massive structure, can be considered representative of the free-field ground motion. Because of these circumstances the crack formation at Koyna dam has been an event that attracted many scientists to perform investigations, both numerically and experimentally [Lee and Fenves, 1998a, Chopra and Chakrabarti, 1972, Chopra and Chakrabarti, 1973, Bhattacharjee and Léger, 1993, Ghrib and Tinawi, 1995, Cervera et al., 1996].

The seismic analysis of Koyna dam by means of the plastic-damage model is given as an example problem in Abaqus Example Problems Guide [Abaqus, 2014b]. There, a two-dimensional model of the gravity dam is excited by the Koyna earthquake and the crack formation is simulated. Because of the similarity in problem type and mesh size, the concrete tensile properties used in that investigation are adopted for the present dam study: Figure 4.7 (a) shows the response of concrete to uniaxial post-failure loading in tension, which is commonly referred to as "tension stiffening"; (b) shows the evolution of the tensile damage variable d_t, which is a non-decreasing variable ranging from 0 (no damage) to 1 (fully cracked). Both quantities are given as functions of cracking displacement rather than strain. This is because in cases with little or no reinforcement, the specification of a post-failure stress-strain relation introduces unreasonable mesh sensitivity in the results. However, it is generally accepted that the fracture energy proposal by Hillerborg [Hillerborg et al., 1976] is adequate to alleviate this handicap for many practical purposes. Hillerborg defines the energy required to open a unit area of crack, G_f, as a material parameter. With this approach, the brittle behaviour of concrete is specified by a stress-displacement response, see [Abaqus, 2014a].

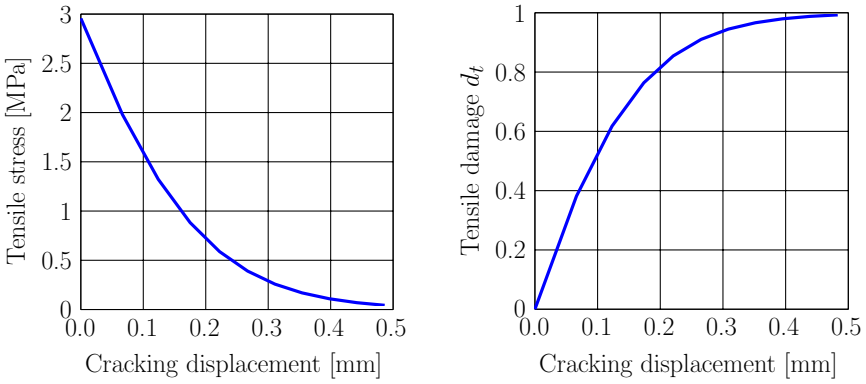

(a) Tension stiffening (b) Tensile damage variable

Fig. 4.7: Concrete post-failure tensile properties; modified from [Abaqus, 2014b]

The mean tensile strength of C20/25 type concrete is 2.2 MPa. Yet, it is well known that this value is higher if the load is applied rapidly. The dependence of strength parameters on the strain rate is controversial. Zhang et al. [Zhang et al., 2013] suggest to increase the tensile strength by 30% in the context of seismic excitation of dams. This value is also accepted in this work, resulting in dynamic tensile strength $f_{tm} = 2.9$ MPa [3].

As unreinforced structures, arch dams are susceptible to failure mechanisms caused by tensile cracking, whereas compressive stresses will hardly exceed the compressive strength. Hence, compressive damage (crushing) is not considered in this model ($d_c = 0$). Full recovery of compression stiffness upon crack closure is assumed ($w_c = 1$), whereas recovery of tension stiffness as the loading changes from compression to tension is neglected ($w_t = 0$). This corresponds to the default settings.

As for the plasticity parameters that are required in the plastic-damage model, the Abaqus default values are chosen likewise, i.e. dilation angle $\psi = 35°$, flow potential eccentricity $\epsilon = 0.1$, ratio of initial equibiaxial compressive yield stress to initial uniaxial compressive yield stress $f_{b0}/f_{c0} = 1.16$, parameter for the deviation of yield surface in a deviatoric plane from circularity $K_c = 2/3$, viscosity parameter $\mu = 0$.

It should be noted here that for the *Concrete Damaged Plasticity* model, Abaqus calculates the stiffness proportional damping stress based on the undamaged elastic stiffness. This may introduce large artificial damping forces on elements undergoing severe damage [Abaqus, 2014a]. On the other hand, in this way, potential negative damping - which would increase the seismic response, but would be physically nonsensical - is avoided.

4.3.3 Foundation modelling

Proper modelling of the foundation and the earthquake input mechanism is a topical research field. The problem is conceptually shown in fig. 4.8. Since dams are relatively stiff structures, their dynamic behaviour is considerably influenced by the surrounding rock foundation, which hence should be included in the finite element model. The seismic excitation is then typically applied as acceleration input at the rock foundation boundaries. As a consequence, however, the signal will be altered in amplitude and frequency content as it travels through the ground. So, as it reaches to the dam-foundation interface it will not correspond anymore to the signal which

[3] Naturally, also resistance parameters could be considered as random variables. Here, however, deterministic values are assumed. This is a requirement for some of the subsequent evaluation techniques.

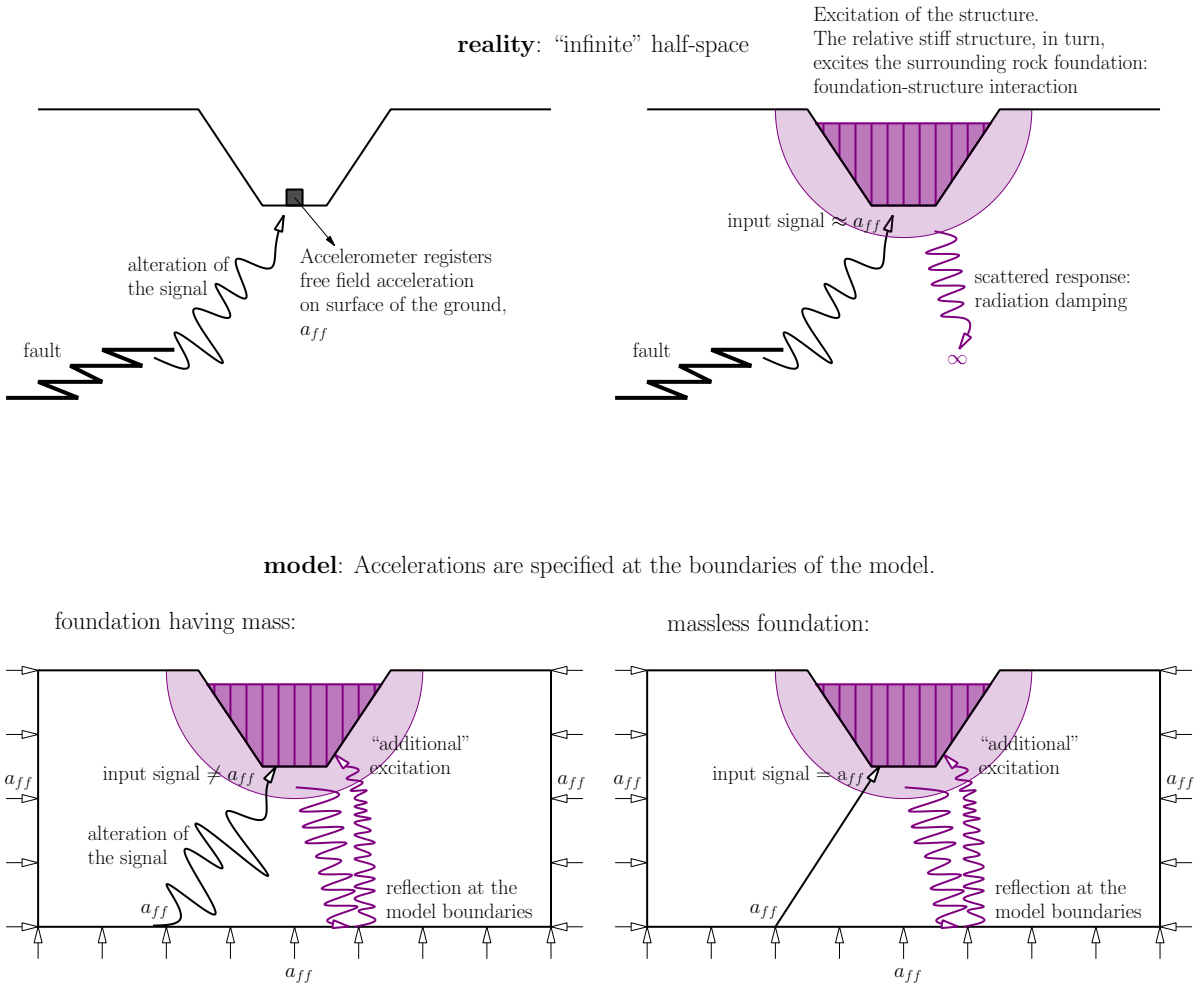

Fig. 4.8: The problem of modelling foundation, boundary conditions and seismic input

an accelerometer has registered on the surface of the ground. In this case, the object of interest, i.e. the dam, would basically be excited arbitrarily.

To circumvent this problem, Clough [Clough, 1980] proposed to implement a massless foundation. That approach, traditionally applied in seismic dam engineering, is also used in this research work. For simplicity, the material damping for the foundation is defined just as for the dam concrete, i.e. by the Rayleigh model, whereby the prescribed damping ratios are 10%. It was observed that different damping ratios do not significantly influence the ground motions that occur at the bottom of the dam (applying massless foundation); for a wide range of damping ratios, they are almost identical to the free-field ground motions applied on the model boundaries in terms of PGA and root-mean-square acceleration.

In recent years, this approach has been criticized, see e.g. [Chopra, 2012b], because of its incapacity of simulating radiation damping. Conceptually, the argument is legitimate. If the excitation is applied as acceleration at the model boundaries, waves are reflected at these artificial boundaries instead of propagating to infinity, as they do in the real half-space. This may lead to an overestimate of the response of the structure.

Several methods have been proposed to simulate radiation damping with finite elements [Lysmer and Kuhlemeyer, 1969, Saouma et al., 2011, Zhang et al., 2009, Wang and Chopra,

2010, Løkke and Chopra, 2018]. The strategy to apply in most commercial finite element codes is to include the mass of the foundation rock and to use viscoelastic boundaries. In order that the waves are absorbed by these boundaries, the seismic excitation has to be applied as forces instead of accelerations. As reported by other authors, in general, the structural response resulting from this method is lower than when using a massless foundation with fixed boundaries. According to [Zhang et al., 2009] the reduction may reach 25-40% in terms of peak tensile stresses and crest displacement. Penner et.al. [Penner et al., 2017] applied a sine-sweep input ground motion and compared the resulting crest displacements. They observed higher responses in the massless foundation model, however just for frequencies higher than 5 Hz. For lower excitation frequencies both approaches yielded almost identical results.

It is important to underline that a seismic analysis employing absorbing boundaries in a 3D model is associated with great difficulties. They primarily stem from the need to apply forces at the model boundaries that lead to accelerations at the dam-foundation interface that are consistent with the target free-field motions. The specification of these forces generally requires a deconvolution procedure run before or in parallel to the actual finite element simulation (eight auxiliary analyses for each of the three components of ground motion, according to [Løkke and Chopra, 2018]). Since the canyon and the dam itself lead to complicated reflexions, in iterative procedure may be necessary to match approximately the target intensity.

For the present study, which involves MCS, such a procedure would be impracticable and it is furthermore beyond the scope. Since the main frequency content of the ground motions as well as all relevant eigenfrequencies of the dam are below 5 Hz, the massless foundation approach is applied.

4.4 Seismic modelling

Frequently, scaled records of real ground motions are used in stochastic seismic analysis, see e.g. [Wang et al., 2018]. In this study, however, artificial ground accelerations serve as excitation for the MCSs. They are applied on the finite element model as boundary conditions in all three directions.

Their frequency content is controlled by a Kanai-Tajimi filter, cf. e.g. [Clough and Penzien, 1993, Bucher, 2009b]. Thereby, first, a raw acceleration $b(t)$ is defined as a linear combination of the displacement and velocity of a system with a SDOF. This SDOF system is characterized by its natural frequency ω_g and the damping ratio ζ_g, whereby these parameters represent some characteristic frequency and damping ratio of the ground, respectively [Clough and Penzien, 1993]. The input $w(t)$ to this filter is white noise with a power spectral density S_0. The equation of motion of this filter is

$$\ddot{z} + 2\zeta_g\omega_g\dot{z} + \omega_g^2 z = w(t) \tag{4.3}$$

The (raw) acceleration $b(t)$ is then defined as

$$b(t) = 2\zeta_g\omega_g\dot{z} + \omega_g^2 z \tag{4.4}$$

A realization for the values $\zeta_g = 0.6$, $\omega_g = 17$ rad/s and $S_0 = 0.0372$ m^2/s is shown in fig. 4.9 (a). The time interval considered is 10 s, the time step $dt = 0.01$ s, giving a total of 1000 time steps. The power spectral density for the random process defined by equation (4.4),

$$S_{bb}(\omega) = S_0 \frac{4\zeta_g^2\omega_g^2\omega^2 + \omega_g^4}{(\omega_g^2 - \omega^2)^2 + 4\zeta_g^2\omega_g^2\omega^2} \tag{4.5}$$

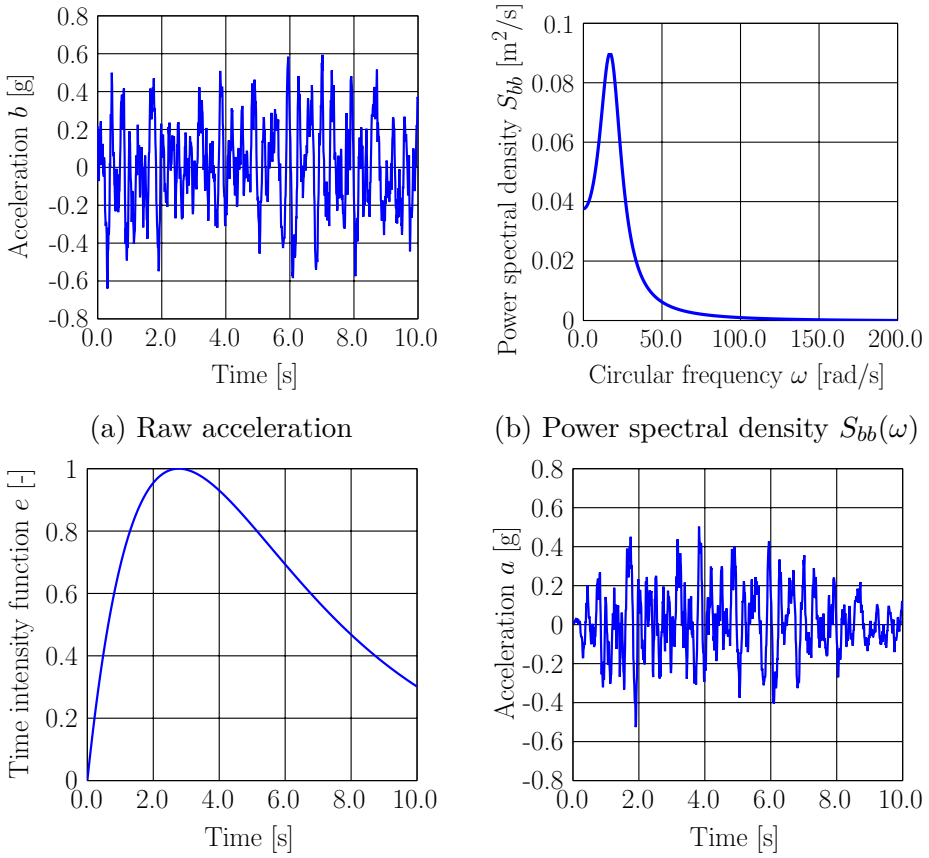

(a) Raw acceleration

(b) Power spectral density $S_{bb}(\omega)$

(c) Time intensity function

(d) Ground acceleration

Fig. 4.9: Generation of ground accelerations

is shown in fig. 4.9 (b). Afterwards, the random process is superposed by a deterministic time intensity function

$$e(t) = 4[exp(-0.25t) - exp(-0.5t)] \tag{4.6}$$

(see fig. 4.9 (c)) to take account of the non-stationary history of real earthquakes:

$$a(t) = e(t)b(t) \tag{4.7}$$

Moreover, a baseline correction is applied in order to avoid permanent drift in displacement or velocity. A sample realization of such a ground acceleration $a(t)$ is shown in fig. 4.9 (d). The excitation in vertical direction was reduced by factor 0.67 in time domain, cf. [EN1998, 2017].

For the construction of the fragility curves, MCSs have to be performed for different intensity levels. However, in the present work, the ground motion intensity is not specified by the PGA (directly). Instead, the input quantity is power spectral density S_0, see equation (4.5). More specifically, for each simulation run just the one power spectral density is chosen that yields the desired PGA *in the mean*. The relationship between the two intensity quantities is $a_{g,max} = const\sqrt{S_0}$. The specific value *const* (which applies to the seismic model specified here) has been determined beforehand by simulating a large number of ground motions: $const \approx 28.28$.

As for the selection of the intensity measure (IM), there seems to be some consensus among authors that PGA might be not the best choice, see e.g. [Deierlein et al., 2003, Hariri-Ardebili and Saouma, 2016b] [4]. Major concerns about representativity of PGA for the earthquake intensity stem from the fact that a single very high peak in the acceleration time history might have relatively little effect on the structural response. In this regard, a spectral IM (which may refer to e.g. the structure's fundamental period) would seem more appropriate, see. e.g. [Baker and Cornell, 2005, Adam et al., 2017]. In general, researchers tend to assess the appropriateness of an IM essentially based on its *efficiency*, where they call an IM parameter efficient if it will reduce the EDP variability for a given IM value. However, the author has some doubts about the consistency of that assessment criterion because, as a matter of fact, the probability of exceeding a limit state depends on the variance of the respective sample results. Specifically for PSDA, it is important to note that a high variability of EDP responses implies a higher probability of exceeding a limit state, as long as the mean response is lower than that limit state.

Anyway, the author believes that specifying the earthquake intensity by means of power spectral density seems appropriate, especially because it avoids the classification of a ground motion merely based on a single peak value. As ("illustrating") abscissa quantity in subsequent diagrams, however, PGA is used since it is an intuitively more accessible IM than a power spectral density measure. As outlined above, these PGA values are just expected values - the real PGA of a simulation run can (and will) actually be different.

4.5 Uncertain Parameters

Apart from the stochastic ground motions, the probabilistic nature of the present research arises due to the fact that a number of selected parameters are considered as random variables. Their distributions are listed in table 4.1. The selection is motivated by the fact that some parameters of the model are associated with high inherent uncertainty or with some variability that may affect the response of the system considerably. For other parameters this is not the case (e.g. density of the concrete), hence they are defined deterministically, for simplicity. The actual values of the distributions here are chosen freely and constitute typical values of the respective quantities.

Tab. 4.1: Parameters of the model which are considered as random variables

Parameter	unit	Type of PDF	Mean value	C.o.V.
Elasticity modulus concrete E_c	MPa	Normal	27000	2000
Poisson's ratio concrete ν_c	-	Normal	0.167	0.02
Elasticity modulus rock E_r	MPa	Normal	45000	5000
Poisson's ratio rock ν_r	-	Normal	0.25	0.02
Mass prop. damping factor α	-	Uniform	0.347 - 1.157	-
Stiffness prop. damping factor β	-	Uniform	0.0025 - 0.0083	-
Block friction coeff. (vertical) μ	-	Uniform	0.5 - 1	-
Natural frequency rock ω_g	rad/s	Normal	17	2
Damping ratio rock ζ_g	-	Normal	0.6	0.1
Water level	m	Uniform	110 - 220	-

Following the recommendation of the International Commission on Large Dams [ICOLD, 2010], a uniform distribution between 3 and 10% is assumed for the material damping of the concrete. These damping ratios were converted to the factors α and β required for the Rayleigh model.

[4] However, others have found that PGA is most suitable for many applications [Padgett et al., 2008].

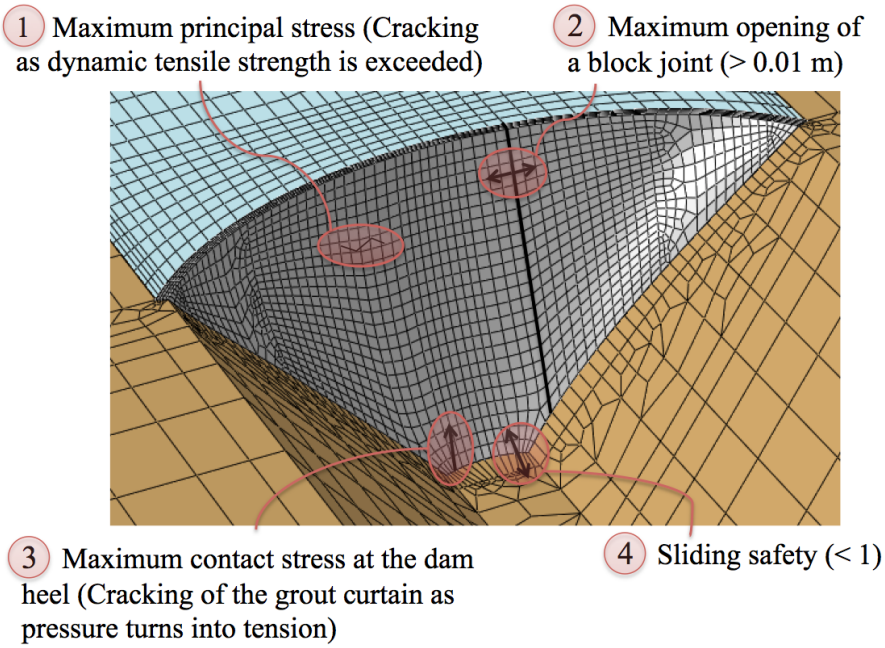

Fig. 4.10: Selected EDPs and associated damage mechanisms

Regarding computational implementation, the procedure is as follows: Each input file for the finite element simulations is a text file which contains: (1) general informations about the model which are equal in each text file, including the deterministic parameters; (2) an individually generated ground acceleration time history according to the target PGA, which acts in all three directions (values are reduced by 2/3 in vertical direction), and a sample of the ten variable parameters listed in table 4.1. No correlation is assumed between the parameter values. The input files are then sent to the solver (CAE Cluster of TU Wien). The results are saved in odb output files. The informations of interest (e.g. maximum stresses) are extracted from these files using purpose-built Python scripts.

4.6 Damage and failure mechanisms

Four damage mechanisms are investigated. They are described in the following subsections. Usually, a damage mechanism can be characterized by the fact that a certain engineering demand parameter (EDP), e.g. a stress or displacement value, exceeds a defined limit. The four EDPs and the associated damage mechanisms are represented in fig. 4.10. By way of illustration, for each damage mechanism, a time history of the corresponding EDP is presented in the following. Hereby, the PGA of the earthquake excitation is equal to 0.556 g. Finally, the ultimate limit state of the dam is explained.

4.6.1 Concrete cracking

As arch dams are in general unreinforced, they are designed such that all parts are under pressure in normal conditions. However, strong ground motions may cause the concrete to be exposed to tension. If the stresses exceed the tensile strength in some part, a crack will form. This damage mechanism is defined as the maximum principal stress exceeding the dynamic tensile

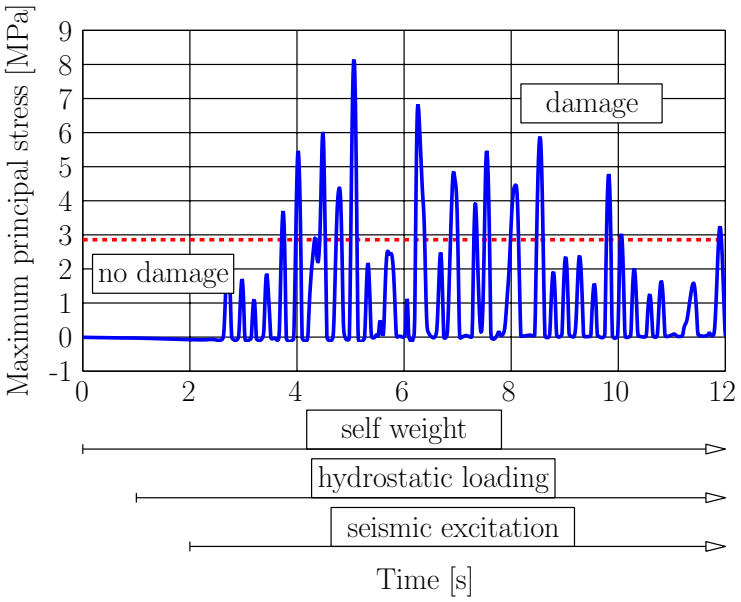

Fig. 4.11: Maximum principal stress in an element of the downstream surface; PGA = 0.556 g

strength, f_{tm} = 2.9 MPa, in *any* element of the dam surface *anytime* during the earthquake. This means that the maximum value is determined by a double loop over all time steps and all surface elements.

However, as long as such loadings are localized and of very short duration, forces will be transferred to alternative load bearing paths, and cracks will remain superficial. Hence, a (single) exceedance of the dynamic tensile strength can be defined as a damage mechanism that is clearly tolerable for maximum credible earthquake.

As an illustrative example, fig. 4.11 shows the maximum principal stress in an element of the downstream surface, situated at approximately 2/3 of the total height. The diagram shows that there are no positive principal stresses in the first two seconds, which is to say that there are no tensile stresses under normal loading conditions. However, during excitation, the dynamic tensile strength is clearly exceeded many times.

4.6.2 Opening of a block joint

Arch dams are built in vertical blocks. The joints between them are sealed with elastic water stops. It is known that strong motions may cause a separation of the blocks. As long as the gap is not too wide, the water stops will prevent that water from the reservoir gets into the joints. Such a penetration of water would cause also the inner faces of the blocks to be subjected to hydrostatic pressure. Furthermore, if the opening is so wide to exceed the thickness of the shear keys, the stability of the dam would be endangered. Hence, it is of interest to study whether a separation of the blocks takes place during the ground excitation. Specifically, the limit state is defined as an opening of 10 mm of any of the block joints. However, a block opening of that magnitude should be classified as tolerable in a strong earthquake.

The opening at the top node of the central block joint is illustrated in fig. 4.12. The limit of 10 mm is exceeded once during the earthquake.

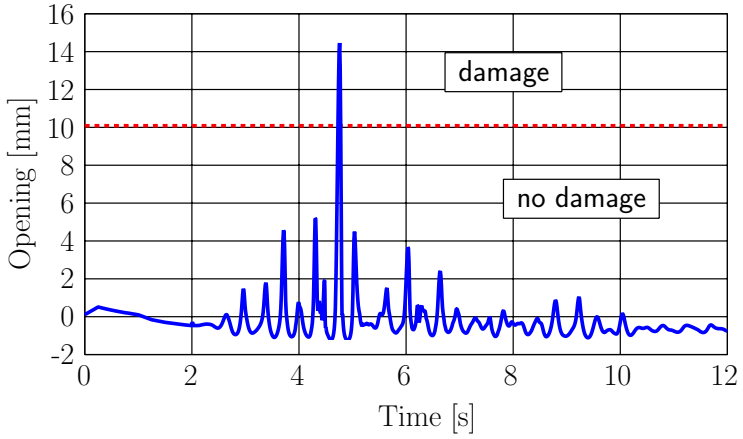

Fig. 4.12: Opening of a block joint; PGA = 0.556 g

4.6.3 Cracking of the grout curtain

Mostly, underneath a dam, a grout curtain is installed, which inhibits undermining due to constant water flow and reduces the uplift water pressure at the bottom of the dam. Usually, it reaches some dozens of meters into the ground and is located some meters behind (i.e. in the downstream direction) the (upstream) heel of the dam. Naturally, it is important that the grout curtain stays permanently connected to the dam itself. This connection may crack open already at the first impounding of the reservoir if the hydrostatic load is strong enough to cause a lift-off of the heel. Then a re-grouting will be necessary. The same might occur during an earthquake. Hence, here, this damage mechanism is defined as the occurrence of any loss of contact pressure in the second finite element row (of four) at the dam-foundation interface behind the dam heel during the ground motions.

The vertical normal stress (contact stress) in such an element is shown in fig. 4.13. It is evident that the self weight of the dam causes contact pressure of approximately 3 MPa at the interface. On the other hand, the impounding of the reservoir leads to reduction of the pressure, though not to lift-off of the dam heel. However, during the ground motions, the normal stresses change from pressure to tension temporarily, implying that cracks could form in the grout curtain.

4.6.4 Sliding safety

Additionally to hydrostatic pressure from the reservoir, ground accelerations exert horizontal forces, which potentially endanger the sliding safety of the dam. The resistance against sliding arises from the shear strength, which, according to the Mohr-Coulomb model,

$$\tau_f = c + \sigma \tan \phi \tag{4.8}$$

depends on normal stress σ, friction angle ϕ and cohesion c. In practice, the sliding safety of an arch dam depends considerably on its morphological anchorage in the valley rock and on the schistosity of the rock, see, e.g., [Wittke, 2014, Kolymbas, 2011]). However, here a simplified criterion is applied that assumes loss of sliding safety if the horizontal loads exceed the vertical loads. This corresponds to the case where $\phi = 45°$ and $c = 0$.

The ratio of all vertical forces to all shear forces in valley direction at the dam-foundation interface is shown in fig. 4.14. Since the self-weight acts vertically, the sliding safety increases

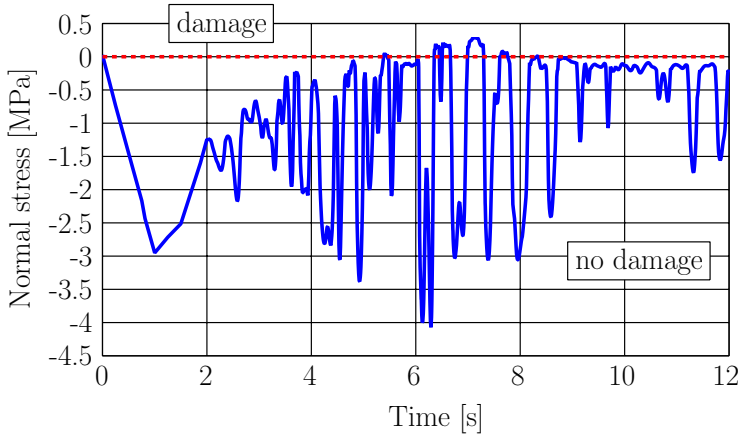

Fig. 4.13: Contact stress at the interface between dam and grout curtain; PGA = 0.556 g

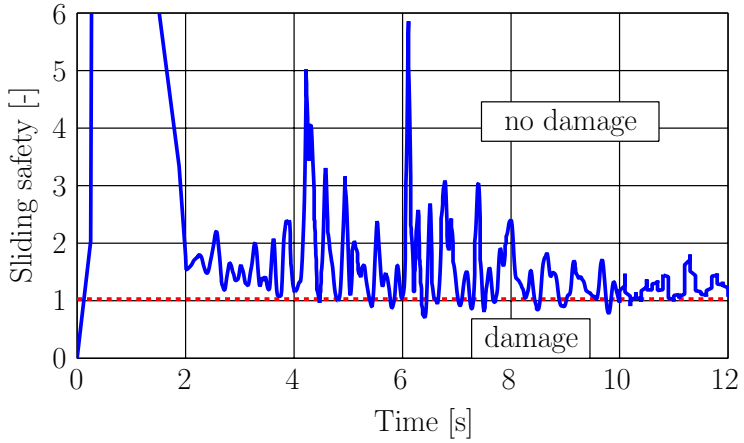

Fig. 4.14: Sliding safety; PGA = 0.556 g

abruptly at the beginning of the simulation, whereas the ratio settles down to approximately 1.5 after application of the primarily horizontally acting water pressure. The ground motions - which not only accelerate the dam vertically and horizontally, but also cause hydrodynamic pressure - lead to strong oscillations of the sliding safety. The sliding safety criterion is violated several times, leading to some horizontal displacement of the dam in the model.

4.6.5 Failure due to exceedance of material strength

As already explained, a single exceedance of material strength leads to a crack but not immediately to failure. However, when a once damaged part is reloaded during the earthquake, the cracks extend and gradually seize more and more parts of the dam. Eventually, the remaining strength does not suffice to transfer the loads to the ground - equilibrium does not subsist anymore.

In this case a finite element simulation is aborted. This fact may potentially be utilized in the MCSs as an indicator for failure. Hence, for this failure criterion, the plastic-damage model is implemented, which is able the represent the progressive deterioration of the concrete. Admittedly, it should be noted that non-convergence of a finite element simulation can also be

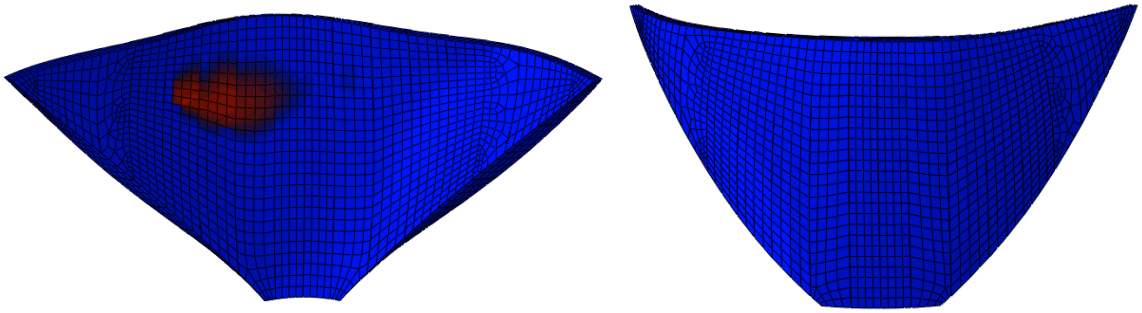

(a) time = 2.12 s (beginning of cracking)

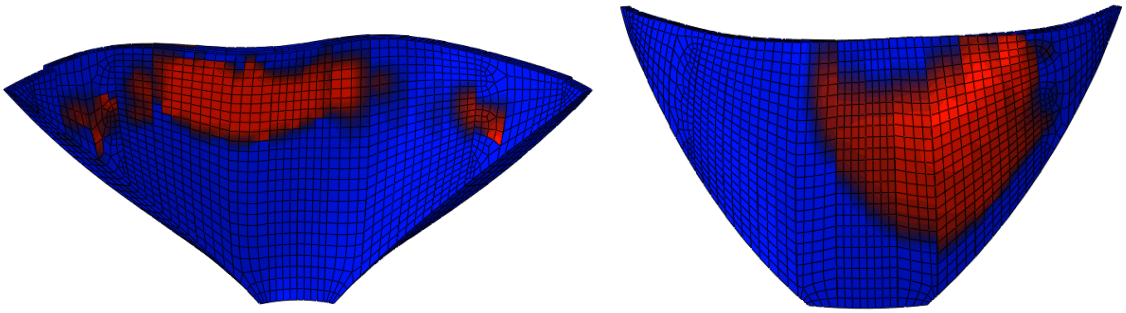

(b) time = 3.00 s

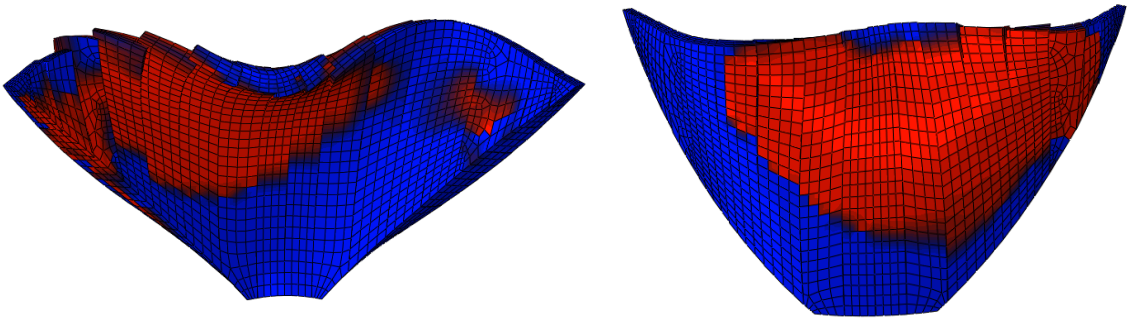

(c) time = 3.96 s (abortion of simulation)

Fig. 4.15: Evolution of tensile damage at downstream and upstream face; PGA = 0.556 g

due to other reasons, especially numerical problems. However, since in the earlier simulations without the plastic-damage model (for the damage mechanisms described above) not a single abortion was observed, there is considerable evidence that abortion is caused by material failure. Further evidence is given by plausibility of subsequent results (fig. 4.15 and fig. 4.20).

The propagation of damaged areas can be observed in fig. 4.15. The pictures on the left side show the downstream surface, the ones on the right side show the upstream surface. The deformations are scaled 200 times. The red colour indicates fully cracked areas (tensile damage variable $d_t \approx 1$). It can be seen that cracking starts in the upper part of the downstream surface at about 2.12 seconds after beginning of the earthquake, while the upstream side is still intact at this stage. After three seconds, damaged areas cover considerable parts of the downstream and upstream surfaces. Finally, the simulation is aborted after 3.96 seconds, as the tensile strength of concrete is exhausted in nearly the whole upper part of the dam.

4.7 Sampling methods

Seismic fragility curves show probabilities of occurrence as functions of the ground motion intensity, here represented by the PGA. In general, it is necessary to calculate these probabilities for several different intensity levels so that a sufficient number of support points is available to construct a fragility curve by regression. The single support points are conveniently obtained by MCS: The number of simulation runs that result in damage (resp. failure) indicates the damage (resp. failure) probability for the respective intensity level.

In terms of design of the experiment, the MCS should be adjusted to the particular problem. Indeed, the fact that the fragility curves, and hence also the overall damage (resp. failure) probabilities according to equation (4.1), depend on multiple single probability estimates, increases the computation effort. On the other hand, the accuracy of a single MCS estimate becomes less important, since it constitutes only one of several support points on which the fragility curve (and hence the overall probability) is based. As a consequence, the number of runs of a single MCS estimate may be kept rather small, here 100 was chosen.

Certainly, this arises the question if *small* occurrence probabilities can be estimated at all. In the present case, this concerns the moderate ground motion intensity levels that rarely cause damage or even failure. However they occur more frequently and, hence, might contribute nevertheless considerably to the integral in equation (4.1). This question will be studied in section 4.9.

In general, the accuracy of a MCS estimate can be increased by applying a low-discrepancy sampling method like Latin Hypercube sampling [Olsson et al., 2003] or Sobol sequences [Hong and Hickernell, 2003]. Though, for the present application any such method can hardly be applied to advantage. The reason is called *curse of dimensionality* and lies in the number of random variables. As in the generated ground accelerations, the value for each of the 1000 time steps constitutes a random variable, the dimensionality of the present problem amounts to 1000 due to the earthquake excitation alone (and is slightly further increased by the random variables listed in table 4.1). In fact, there are certain problems with high (nominal) dimensionality that can be treated much more efficiently by applying low-discrepancy sampling [Caflisch et al., 1997, Kucherenko et al., 2011], however this is not this case here. Specifically, the *curse of dimensionality* cannot be allayed in case that the quantity of interest depends on a random processes composed of nearly equally important and interacting input variables [Gasser and Bucher, 2018, Sobol and Asotsky, 2003, Kucherenko et al., 2011], cf. subsection 3.3.1.

While conventional methods to reduce the cost of MCS estimates fail in case of random time histories, some simulation cost reduction may be gained by addressing the fragility curve construction directly. In the following, two methods will be tested in this regard.

Common to both methods is the assumption that the fragility curves are lognormally distributed (cf. [Shome, 1999]). In fact, two-parameter lognormal distribution functions are traditionally used for the construction of fragility curves [Shinozuka et al., 2000]. This can be justified as reasonable because they can adequately represent the statistical variation of many material properties and seismic response variables, provided one is not primarily interested in the tails of the distribution [Office of Nuclear Regulatory Research, 1983]. [5] Moreover, it is well known that the product of many positive, but apart from that arbitrary, random variables tends to be lognormally distributed, cf. subsection 2.1.2.

For the purpose of higher representativeness, the two methods are described in detail in the next section where also the respective results are presented.

[5] As stated above, the impact of the *tails* of the distribution - which here means the very small damage/failure probabilities in case of moderate earthquakes - will be studied in section 4.9.

4.8 Results and discussion

4.8.1 Binary outcome regression

Here, MCS is modified such that the ground motion intensity is increased in each run, so to cover the whole range of conceivable PGAs uniformly. The results of the single runs are either 0 (no damage/failure) or 1 (damage/failure). For that reason, this approach is here referred to as *binary (outcome regression)* approach. The fragility curves are then fitted to these outcomes by means of the maximum likelihood method. Shinozuka et al. [Shinozuka et al., 2000], who proposed this approach, used it to derive empirical and analytical fragility curves for bridges.

In the present case, the lognormal distribution function has the form [Shinozuka et al., 2000]

$$F(a_{g,max}) = \Phi\left[\frac{\ln(\frac{a_{g,max}}{c})}{\zeta}\right] \tag{4.9}$$

in which c and ζ are parameters that are chosen such as to maximize the likelihood function [Shinozuka et al., 2000]

$$L = \prod_{i=1}^{N} [F(a_{g,max,i})]^{x_i}[1 - F(a_{g,max,i})]^{1-x_i} \tag{4.10}$$

in which N is the number of simulation runs and $x_i = 1$ or 0 depending on whether or not the EDP exceeds the limit value, i.e. damage occurs, under PGA $= a_{g,max}$.

Computationally it is more convenient to maximize the natural logarithm of L, so that the condition for determining c and ζ becomes

$$\frac{d\ln L}{dc} = \frac{d\ln L}{d\zeta} = 0 \tag{4.11}$$

This calculation is solved by implementing a straightforward optimization algorithm.

Figures 4.16 to 4.20 show the fragility curves for the limit states defined in section 4.6. The small (blue) dots represent the binary outcomes (limit state exceeded or not) of the simulations with steadily increasing ground motion intensity. In total, 100 simulations runs are performed which equally cover the intensities between 0.01 and 1 g, expressed in terms of PGA. The fragility curves are then built by fitting lognormal distribution functions (blue lines) to these data points. The (brown) circles show the occurrence probabilities, calculated by conventional MCS, for some selected intensity levels. Each of these points - also they could be used as support points for regression of fragility curves - is based on 100 simulation runs.

Figure 4.16 represents the probabilities that a crack forms, i.e. that the maximum principal stresses exceed the dynamic tensile strength somewhere on the dam surface. This limit state is reached at relatively moderate ground motion intensities; in the conventional approach, even the MCS for PGA = 0.145 g indicates some small occurrence probability, while in the binary approach, exceedance of this limit state is first encountered at PGA = 0.17 g. Eventually, an earthquake with PGA = 0.4 g will lead to cracking almost certainly, according to what is predicted by both approaches. By comparing the lognormal fragility curve fitted to the binary results with the occurrence probabilities calculated by the conventional approach, a very satisfying accordance is observable.

Figure 4.17 shows the probabilities that the opening of any block joint exceeds 10 mm. The fragility curve is more stretched since there is no clear shift from *no damage* to *damage*. The binary approach yields almost identical results as the conventional approach.

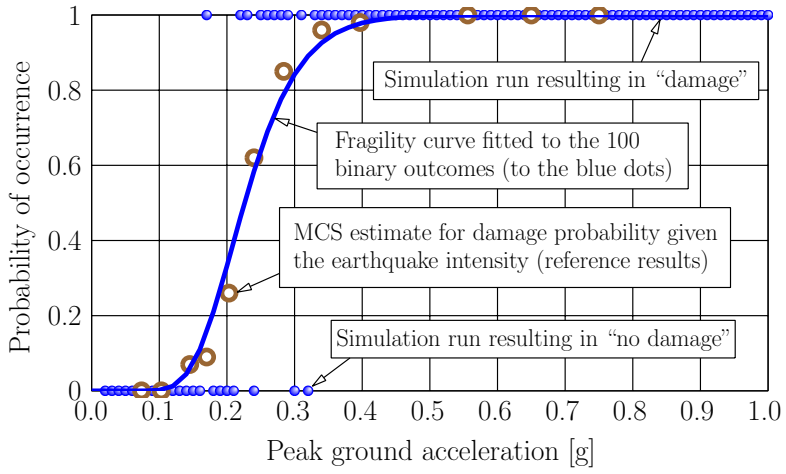

Fig. 4.16: Fragility curve for exceedance of dynamic tensile strength (formation of a crack on the surface of the dam)

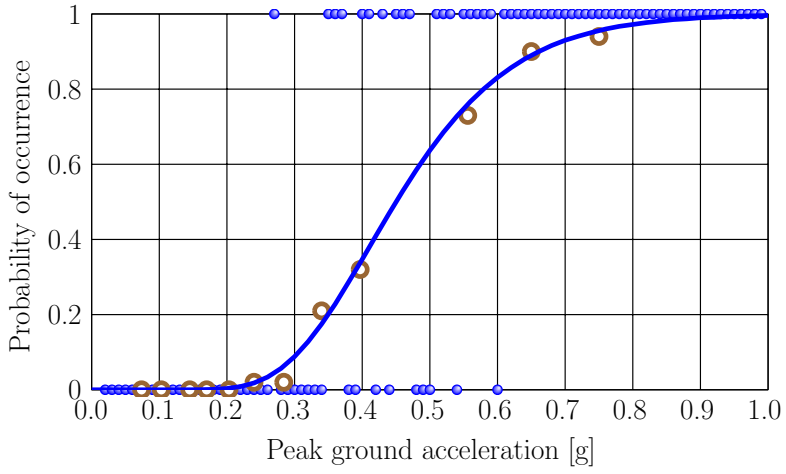

Fig. 4.17: Fragility curve for the opening of a block joint to exceed 10 mm

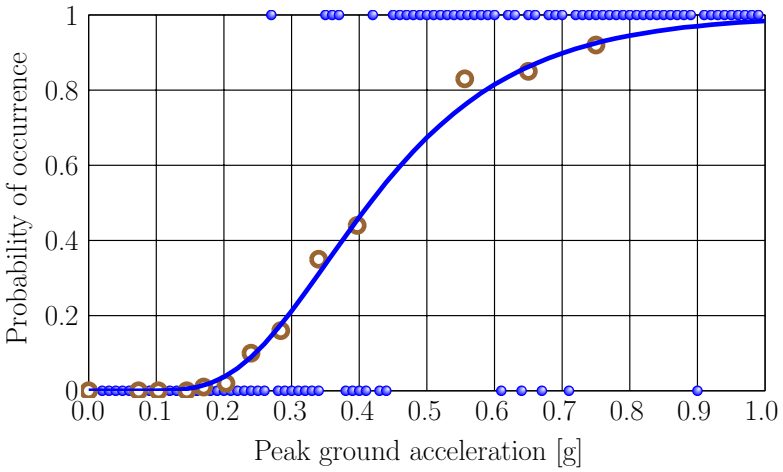

Fig. 4.18: Fragility curve for cracking of the grout curtain

The probabilities that a crack forms at the interface of dam and grout curtain are shown in fig. 4.18. As opposed to damage mechanism 1) (fig. 4.16), it is apparent that there are also some extremely strong motion events that do not lead to exceedance of the limit state. Hence, the fragility curve increases more slowly, similarly to the fragility curve in fig. 4.17. The physical reason might be that the interface of dam and grout curtain is a small area (one element row). Hence, there is some chance for it to escape tensions also during extreme ground motion. On the other hand, the surface of the dam is a big area represented by some hundreds of elements which is subjected to very inhomogeneous stress states even at one point of time. So, the chances are low that each element stays below the tensile strength during the whole earthquake excitation.

Figure 4.19 shows the sliding probabilities. Especially for the binary approach, a quite sudden jump is observable around PGA = 0.4 g. While the onset of occurrence probability is similar for both approaches, apparently there is a divergence in the higher probability levels. For the binary approach, a posterior increase of the sampling density in locations where a sudden shift occurs might be advisable. This is done in the range between 0.3 and 0.6 g, see pink dots. The dashed purple line shows the updated fragility curve, which apparently matches the reference data points better.

Figure 4.20 shows the occurrence probability of failure due to exceedance of material strength, which is defined by abortion of the simulation. According to the results, the failure probability is nearly zero up to a PGA of almost 0.3 g. Then, it rises quite sharply. However, also for very strong earthquakes, some probability of survival can be observed. Failure, evaluated by means of the plastic-damage model for concrete, is a complex mechanism which occurs after ever-increasing damage in vast parts of the dam. Hence, this mechanism does not depend merely on the intensity of the ground motion, but also substantially on chance, or more technically speaking, on the specific acceleration time history as well as on the other random parameters (table 4.1).

4.8.2 Cloud analysis

Although the binary outcome regression approach presented before yields satisfactory results, it is clear that it ignores a lot of information actually contained in the results of the single simulation runs. That is to say, by fitting a fragility curve to data points having value one or zero, the actual value of the respective EDP is not considered.

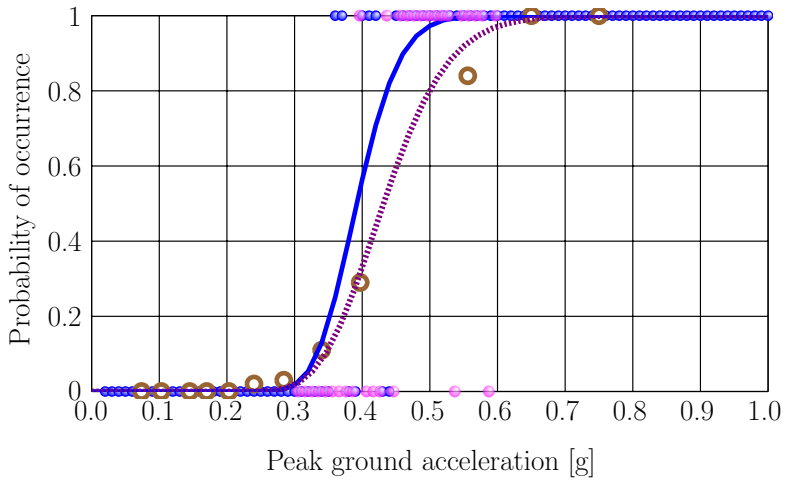

Fig. 4.19: Fragility curve for sliding safety < 1

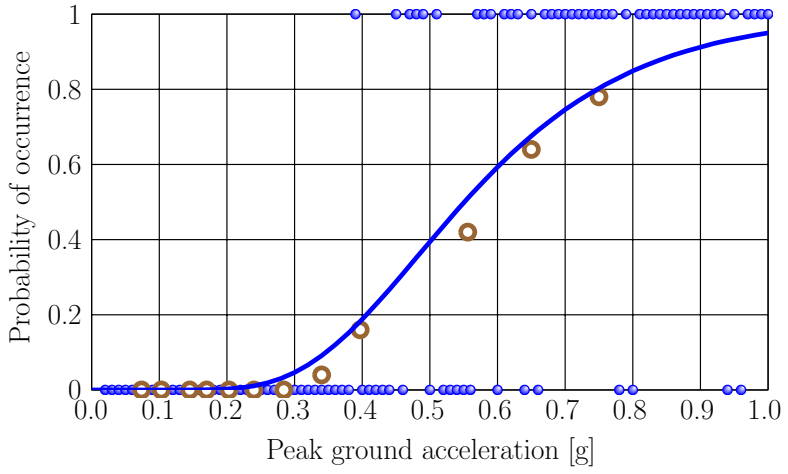

Fig. 4.20: Fragility curve for failure due to exceedance of material strength (abortion of simulation)

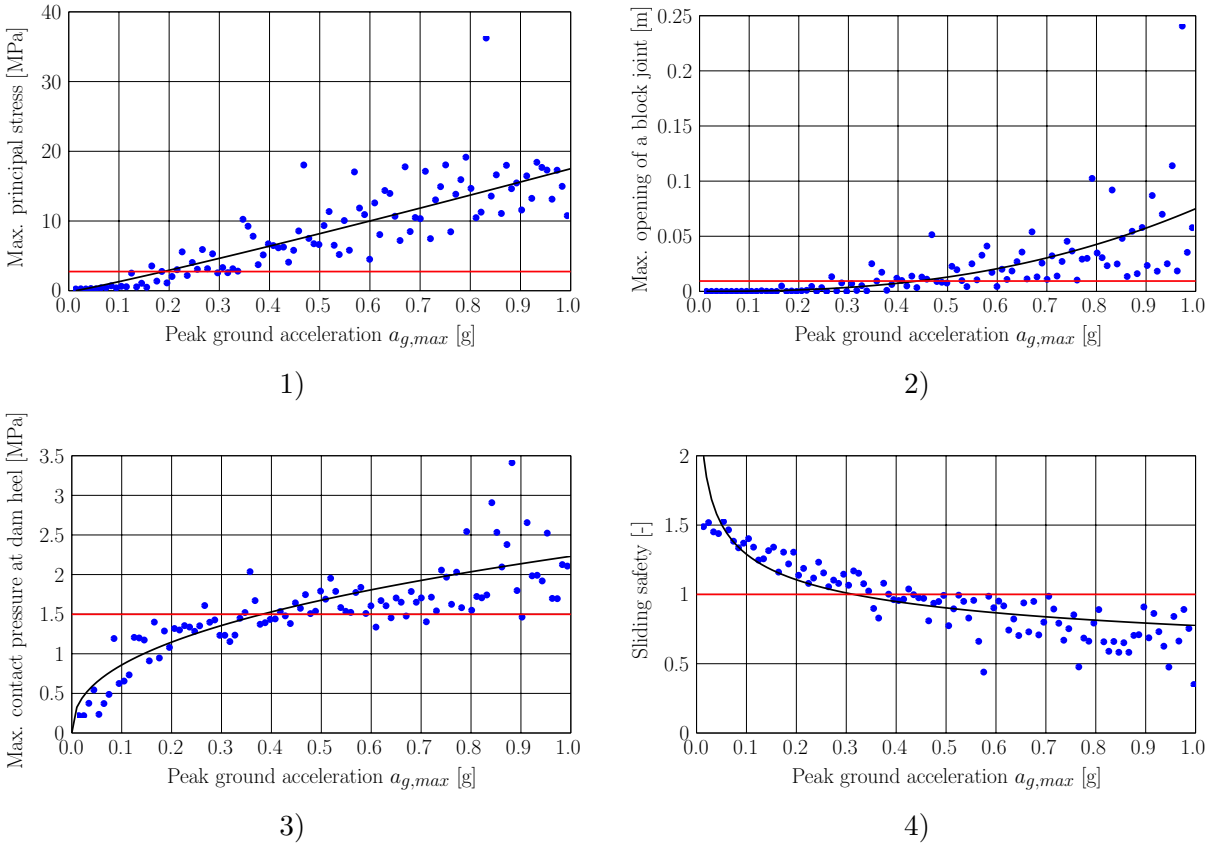

Fig. 4.21: EDP values versus PGA corresponding to damage mechanisms: 1) Cracking as dynamic tensile strength is exceeded; 2) Maximum opening of a block joint > 0.01 m; 3) Cracking of the grout curtain; 4) Sliding safety < 1

Hence, a kind of corresponding cloud analysis, which here means an analysis involving all available result data, is performed to compute the fragility curves. For that purpose, the values of the four selected EDPs [6] are represented versus PGA, as scatter plots or "clouds" of result data, see fig. 4.21. As for diagram 3), which shows the maximum stress at the dam heel, the values have all been shifted to the positive range by adding a value of 1.5 MPa to each of them. This was necessary since the MCS yielded a number of negative stress values (when the dam heel is - so as it should be - under pressure throughout the ground motions), however, for the subsequent approach just positive values are admissible. The corresponding damage criterion, namely the occurrence of any tensile stress (i.e. any positive stress value), was therefore simply changed to any value above 1.5 MPa.

The data points are then fitted by a power function [Hariri-Ardebili and Saouma, 2016b]:

$$\eta_{EDP|a_{g,max}}(a_{g,max}) = u(a_{g,max})^v \tag{4.12}$$

where u and v are regression constants and $\eta_{EDP|a_{g,max}}$ is the median value of EDP given $a_{g,max}$.

[6] This approach is applied to the four damage mechanisms only. Since "failure due to exceedance of material strength" is characterized by binary outcomes, it is not amenable to cloud analysis.

The lognormal fragility curve is then constructed by [Cornell et al., 2002]

$$P[EDP \geq edp|a_{g,max}] = 1 - \Phi\left[\frac{\ln(edp) - \ln(u(a_{g,max})^v)}{\beta_{EDP|a_{g,max}}}\right] \tag{4.13}$$

where $\Phi(.)$ is the standard normal cumulative distribution function and $\beta_{EDP|a_{g,max}}$ the logarithmic standard deviation (also called dispersion) of the EDP conditioned on the $a_{g,max}$. It is given by [Jalayer, 2003]

$$\beta_{EDP|a_{g,max}} \cong \sqrt{\frac{\sum \left(\ln(edp_i) - \ln(u(a_{g,max})^v)\right)^2}{N-2}} \tag{4.14}$$

This approach has been used also by [Hariri-Ardebili and Saouma, 2016b] for the generation of fragility curves for a gravity dam.

The resulting fragility curves are shown in fig. 4.22 (in green). For comparison purposes, the diagrams contain also the previously calculated probabilities. Evidently, the quality of the single results is varying for different damage mechanisms. As for damage mechanism 3), the cloud analysis yields quite satisfactory results. Also the fragility curves for damage mechanisms 1) and 2) seem acceptable, although the consistently higher occurrence probabilities predicted for damage mechanism 1) by the cloud analysis stand out. However, the results for damage mechanism 4) must be considered as unacceptable.

In the following, it is attempted to find the reasons for the mismatches and solution strategies. In the case of damage mechanisms 1) and 4), the transition from *no damage* to *damage* takes place within a relatively narrow intensity range (according to the reference results). Similarly as for the binary outcome regression, also for the cloud analysis this means that the two regression parameters are substantially determined by EDP values for intensity levels outside the "crucial" range.

Hence, the regression according to equation (4.12) is subsequently limited to the values within the "crucial" range, i.e. the range where the transition occurs. Figure 4.23 shows the corresponding regression curves, in fig. 4.24 the resulting fragility curves are shown as dashed green curves. In the case of damage mechanism 1), the matching between cloud analysis and reference results is now nearly perfect. For damage mechanism 4), the fragility curve has now a similar shape as the one obtained by binary outcome regression. However, it indicates more conservatives results.

As for damage mechanism 2), the respective diagram in fig. 4.21 shows that the regression curve evidently approximates the data points very well. However it stands out that the scatter of results increases strongly as the PGA increases. The physical explanation for this result pattern is that during weak ground motions, the blocks of the dam do not separate at all (so, the maximum opening of the joints is equal to zero), while, for strong motions, there is a strong dependence of this EDP on the specific ground motion time history. In contrast to that, a constant logarithmic standard deviation is implied by equation (4.14).

Hence, the fragility curve is developed again by adopting a moving standard deviation. Instead of calculating the standard deviation of all data points, it is now computed for each data point separately based on ten neighbouring values. In fig. 4.25 the dashed green curve represents the resulting fragility curve. It matches the reference results well.

Comprehensively, it can be concluded that cloud analysis may be used for constructing fragility curves. However, the regression of the data points has to be carried out with care. Especially, it should be made sure that the data points are fitted well near the limit value that indicates damage. If the variance of results strongly depends on the intensity level, a moving standard deviation should be adopted.

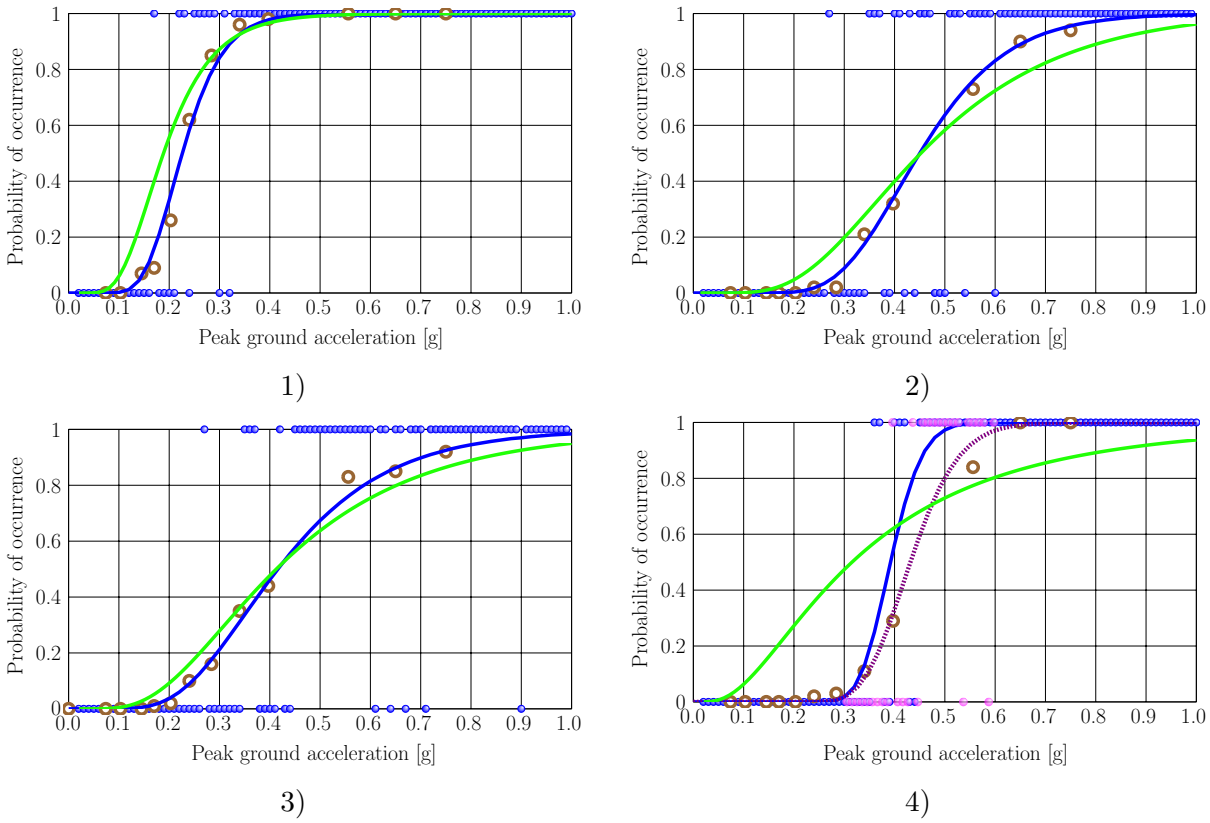

Fig. 4.22: Fragility curves for the damage mechanisms: 1) Cracking as dynamic tensile strength is exceeded; 2) Maximum opening of a block joint > 0.01 m; 3) Cracking of the grout curtain; 4) Sliding safety < 1

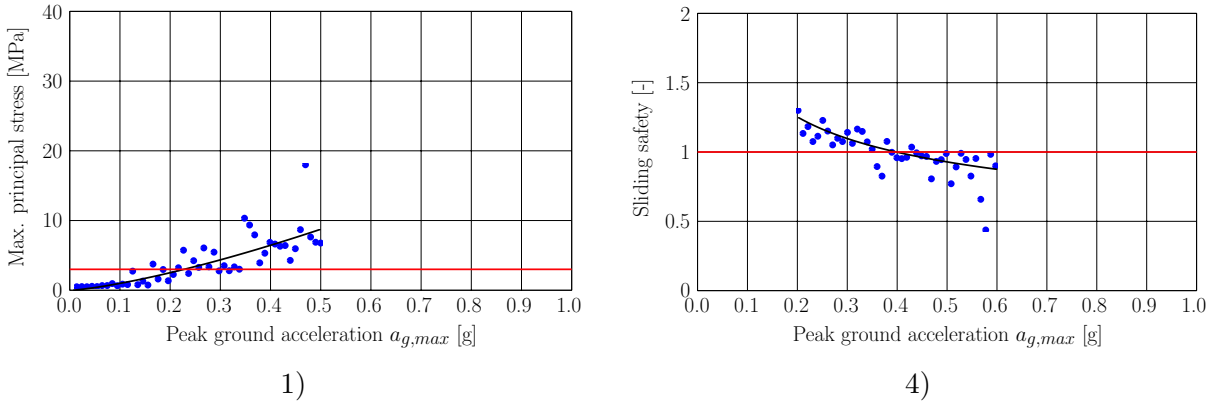

Fig. 4.23: "Crucial" EDP values versus PGA corresponding to damage mechanisms: 1) Cracking as dynamic tensile strength is exceeded; 4) Sliding safety < 1

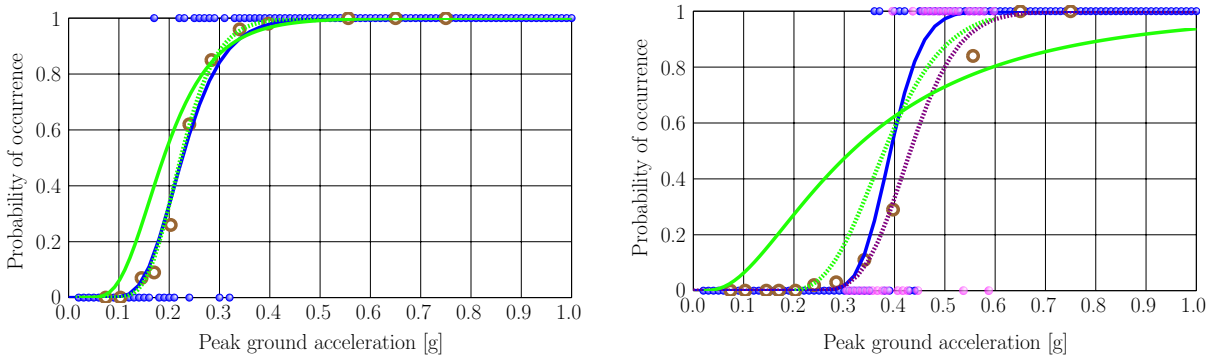

1) 4)

Fig. 4.24: Updated fragility curves for damage mechanisms: 1) Cracking as dynamic tensile strength is exceeded; 4) Sliding safety < 1

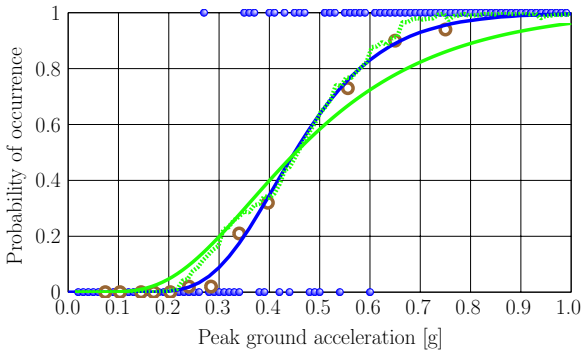

Fig. 4.25: Updated fragility curves for damage mechanisms 2) Maximum opening of a block joint > 0.01 m

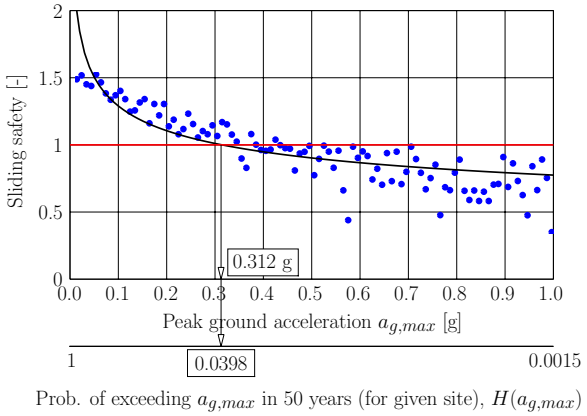

Fig. 4.26: Concept of limit exceedance estimation by means of EDP scatter plots "directly" using the example of damage mechanism 4) Sliding safety < 1

Additionally, from a practical point of view, it is emphasized that the EDP versus intensity plots in fig. 4.21 by themselves constitute a useful and expressive source of information about the performance of a structure. Actually, it is difficult to associate a damage mechanism with a certain metric, say an EDP exceeding a deterministic limit value. This is even more the case for total failure of the structure [Gasser et al., 2019b] - though also for dams different damage and failure indices have been proposed [Hariri-Ardebili and Saouma, 2014, Hariri-Ardebili and Saouma, 2016a, Wang et al., 2018]. However, the assessment of the safety of a projected or existing structure should be based on a comprehensive evaluation of its individual behaviour under the given exposures, taking into account all conceivable risks and the uncertainties of the models used. The author believes that this is especially true for dams and other infrastructures whose structural properties can hardly be standardized, unlike for frame structures and buildings in general, for which a wide PSDA toolset has been published in the last twenty years [Cornell et al., 2002, Barroso and Winterstein, 2002, Ramamoorthy et al., 2006, Jalayer et al., 2007, Padgett et al., 2008, Adam et al., 2017]. In that sense, it is believed that scatter plots, as in fig. 4.21, showing the outcomes of different simulation runs including their variations can serve as useful decision basis for dam experts.

Basically, it would even be possible to read off approximate damage probabilities from the scatter plots directly. The concept is shown in fig. 4.26: One would only have to find the intersection between the regression curve and the limit value for the respective damage mechanism. The respective PGA value would then provide a direct estimate for the limit exceedance probability, as, for a given site, each PGA level in turn may be associated with an exceedance probability in terms of the seismic hazard curve $H(a_{g,max})$.

For that purpose, naturally, any other suitable regression function could be used for fitting the results - instead of equation (4.12) -, especially a three parameter power function,

$$\eta_{EDP|a_{g,max}}(a_{g,max}) = u(a_{g,max})^v + w \tag{4.15}$$

In principle, it might also be used for the cloud analysis as presented before. However, this function easily attains negative values when used for fitting data points near zero. Hence, it could not be inserted directly in equations (4.13) and (4.14) - since the logarithm is not defined for negative values. Instead, some artificial shift to the positive range would be necessary.

Turning to fig. 4.26, the approach seems very appealing for its easiness. However, it totally ignores the dispersion of results, which naturally influences the exceedance probabilities of interest. Hence, this approach lacks consistency. Nevertheless, a numerical comparison of results is presented in the next section.

4.9 Integration with local seismicity

In this section, the fragility curves will be combined with the site-referred seismic hazard, as required to calculate damage occurrence probabilities in a given period of time, according to equation (4.1), see also [Gasser et al., 2019a]. The aim is to see how the occurrence probabilities are distributed over the intensity range. Naturally, this will depend on one hand on the structure and on the damage mechanism of interest, and on the other hand on the local seismic hazard.

Hence, three locations in the Alps with different seismicity are selected. Their corresponding seismic hazard is paired with the four fragility curves of the damage mechanisms of the arch dam. The twelve resulting combinations are shown in fig. 4.27. The red curves show the probability density functions of PGA, $h(a_{g,max})$, which are the negative derivatives of the corresponding exceedance probabilities $H(a_{g,max})$, which refer to a period of 50 years and to rock foundation. They are taken from [EFEHR, 2017]. The geographical coordinates of the three locations are listed in table 4.2.

Tab. 4.2: Selected locations with coordinates

City name	Bozen	Innsbruck	Tolmezzo
Seismic risk	low	moderate	high
Longitude	11.38	11.38	12.98
Latitude	46.50	47.30	46.40

The blue curves are the fragility curves as obtained by the binary outcome regression. The purple curves show the product of the probability density functions $h(a_{g,max})$ and the fragility curves $P(F|a_{g,max})$, i.e. the integrand of equation (4.1). These curves, which for better illustration are normalized to one, show how the occurrence probabilities are distributed over the intensity range. Evidently, the relevant frequency range is very wide, for all locations and damage mechanisms.

Of particular interest is the lower tail of the fragility curves, i.e. their left end, which indicates the probabilities of limit exceedance in case of earthquakes with minor intensities. Although these probabilities are very small, potentially, they might contribute considerably to the overall probability according to equation (4.1) since the probability density values of the related small ground motion intensities are very high (see red curves). Also, it is known that the lognormal distribution used for the fragility curves is no appropriate distribution function for extremely small probabilities [Office of Nuclear Regulatory Research, 1983]. Hence, it might be necessary to use an advanced MCS sampling technique that is able to estimate these very small probabilities with reasonable effort [Bucher, 2009b, Gasser and Bucher, 2018, Au and Beck, 2001], as it has been proposed in [Au and Beck, 2003].

However, according to this research, it seems that such a procedure is not necessary, in general. In fig. 4.27, the areas underneath the purple ("integrand") curves are shaded up to the intensities where the respective fragility curves reach probabilities of 5%. This means, the areas shaded in purple indicate the contribution of the small exceedance probabilities to the total exceedance probability in 50 years (which according to equation (4.1) is the total area below the purple curves). Evidently, these contributions are very small, for all locations and damage mechanisms.

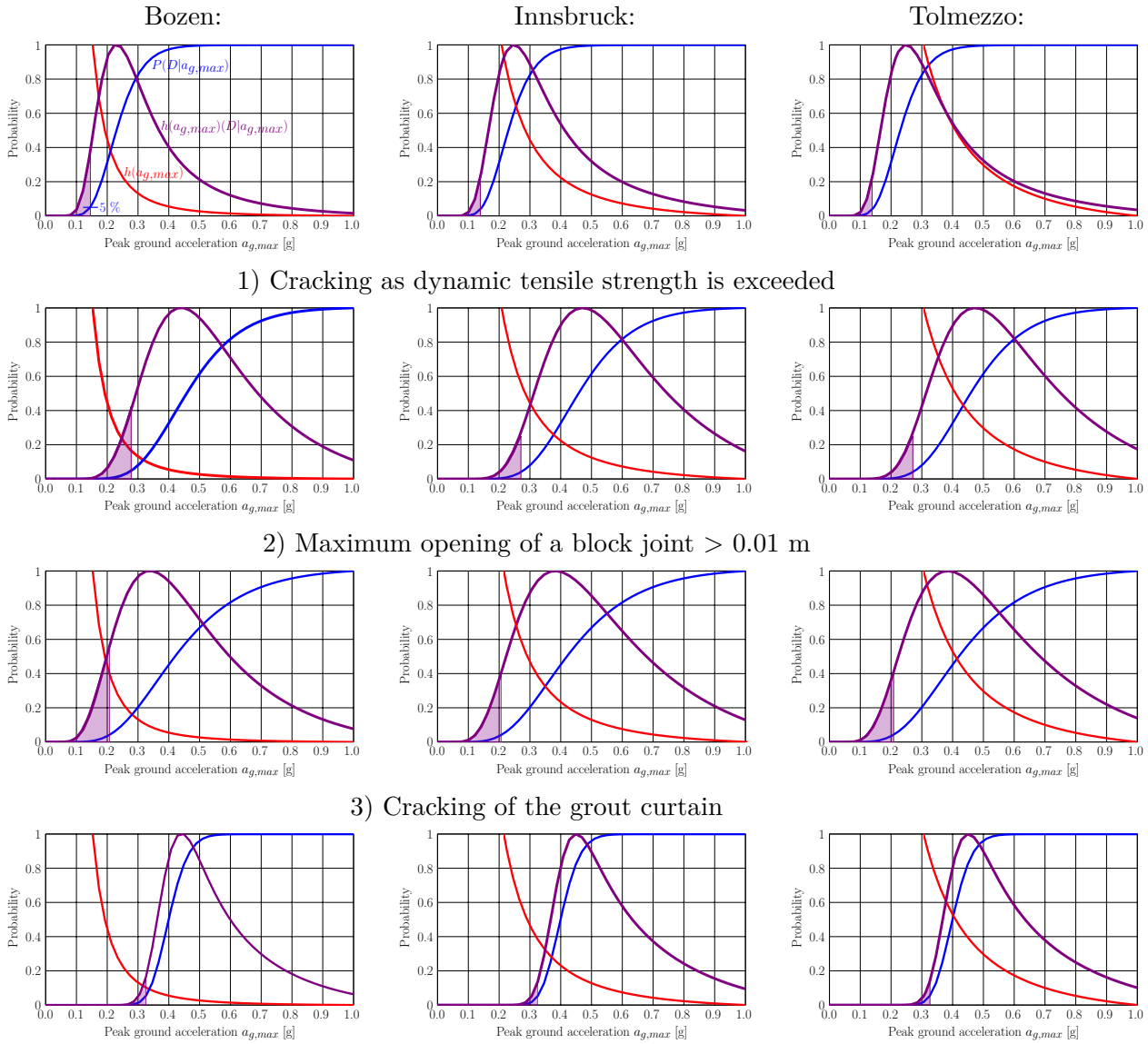

Fig. 4.27: Local probability density functions of PGA, $h(a_{g,max})$, fragility curves $P(D|a_{g,max})$ and their products $h(a_{g,max})P(D|a_{g,max})$

This implies that there is no need to employ a more sophisticated estimation of the tails of the fragility curves.

Table 4.3 shows the occurrence probabilities referred to the four damage mechanisms and the three locations considered, for a period of 50 years. Additionally, the values obtained from the approach conceptually shown in fig. 4.26 are indicated in brackets.

Tab. 4.3: Occurrence probabilities in a period of 50 years

	Bozen	Innsbruck	Tolmezzo
Damage mechanism 1)	0.0387 (0.0291)	0.1353 (0.1061)	0.3151 (0.2520)
Damage mechanism 2)	0.0122 (0.0030)	0.0501 (0.0166)	0.1206 (0.0450)
Damage mechanism 3)	0.0084 (0.0037)	0.0376 (0.0203)	0.0909 (0.0549)
Damage mechanism 4)	0.0099 (0.0084)	0.0449 (0.0398)	0.1070 (0.1048)

The simplified approach according to fig. 4.26 yields satisfying estimates for damage mechanism 4) and acceptable estimates for damage mechanism 1). However, this is certainly not the case for damage mechanisms 2) and 3). At least for damage mechanism 2), this might be explained by the "special" constellation of the corresponding EDP results, which not only are scattered more and more as PGA increases, but are also confined in a very narrow zone between the minimum possible value (0.00 m) and the respective limit value (0.01m) in the PGA range of interest.

However, in general, it should be emphasized that this method can never claim mathematical rigour such as the probability estimate according to equation (4.1), which rests on the total probability theorem. Especially, it completely ignores the dispersion of results, which naturally is a key aspect in any probabilistic analysis.

Anyway the author is also very sceptical about any approach attempting to take account of the dispersion of results at a single intensity level ("single-stripe analysis") with the aim of estimating damage or failure probabilities. These concerns are motivated by two outcomes of this research:

1. The intensity ranges which contribute significantly to the exceedance probabilities (see purple curves in fig. 4.27) depend on the specific location and damage mechanism. Obviously, they are basically unknown prior to identification of the site-specific seismic hazard and construction of the respective fragility curve. However, it should be noticed that the "crucial" intensity ranges are consistently very wide.

2. The dispersion of the outcomes depends very much on the intensity level, see fig. 4.21. Moreover, how the dispersion increases as the intensity increases depends on the specific damage mechanism (or, in general, on the specific problem).

So at least for the (somehow "special") case of an arch dam, it seems that a "*probabilistic*" seismic analysis for a single intensity level cannot be justified.

However, the author does not at all reject seismic analyses for single intensities in general. Given the great difficulties of estimating damage probabilities - as has been demonstrated in this thesis -, it is of course an option to evaluate a structure for a target earthquake intensity. Specifically, the "Operating basis earthquake" (OBE) would be used for damage assessment and the "Safety evaluation earthquake" (SEE), also called "Maximum credible earthquake" (MCE) - would be used for failure assessment [ICOLD, 2010]; naturally, these denotations refer to acceptable risks and to site-specific intensities. This approach is the *deterministic* counterpart to the methods presented above, comparable to an ordinary (static) situation where an engineer designs a structure "for the worst case". Needless to say that this simpler approach is primarily an option for practitioners who want to avoid the difficult fragility curve generation. A further advantage of this approach is that the analyst can inspect the finite element simulation results directly, instead of relying on

(a number of) summarized outcomes of MCS. However, as opposed to the static case where the loads (and responses) are quite well known and the (small) uncertainties may be accounted for by safety factors, in the seismic case, loads and responses are characterized by high variability.

4.10 Summary and conclusions

A general aim of this study was to learn about the challenges of performing a stochastic seismic analysis of a sophisticated finite element model. It was found that the evaluation of a high number of random samples is needed. Consequently, the computational cost of a (rigorous) stochastic analysis is very high.

The main difficulty for the analyst, however, is to set up a proper model and, especially, to identify the essential limit states. This is particularly true for the definition of the ultimate limit state, i.e. failure due to exceedance of material strength, in the present case. While in a deterministic analysis, one can apply her/his best engineering judgement by taking a closer look at the results and evaluate them comprehensively, a probabilistic evaluation generally, in the end, has to rely on automized numerical results. Hence, a realistic modelling of the structure is necessary, including especially an appropriate material model. It was found that the plastic-damage model is able to represent the behaviour of concrete under dynamic excitation and that abortion of simulation may be used as an indicator for ultimate capacity in a MCS.

In particular, the seismic behaviour of an arch dam was studied by means of a nonlinear model including fluid-structure-foundation interaction. Next to the ultimate limit state, four damage mechanisms were identified und respective limit states were defined. Seismic fragility curves have been generated for all five limit states.

The representation of the outcomes of seismic time history analyses as scatter plots of different response values versus the intensity has shown that seismic behaviour strongly depends on the specific ground motion time history. Especially for strong earthquakes, which cause nonlinear behaviour of the structure, the variance in the response values for similar intensities is very high, implying that the responses are highly subjected to randomness.

As a consequence, if one chooses to design a structure according to a target intensity level, it is strongly recommended to perform a number of simulations with different ground motion time histories. They can either be recorded ground motions scaled to the target intensity or artificial ground motions, as used for this work. In any case, by performing several simulation runs (maybe seven), it is rather unlikely to encounter a situation where a structure is fallaciously considered safe only because the chosen time history - though matching the target intensity level - does not cause exceedances of limit values which *usually* will be exceeded at that intensity level.

However, it is clear that this method widely used in engineering practice eventually yields just a small sample out of a strongly scattering result population. A rigorous approach necessitates the construction of fragility curves for the relevant damage (and failure) mechanisms. In general, this requires several MCS estimates which cover the range of conceivable intensities adequately. This is a very time consuming procedure since for one such estimate approximately 100 simulation runs are necessary; for small estimation values, in principle, even considerably more.

One simulation run needs about eight hours on a single-core 1.8 GHz processor. If one MCS estimate is based on 100 runs and a fragility curve is based on twelve such estimates, 1200 runs are needed for a fragility curve. This would result in 9600 hours of computation, whereby parallelization is possible, of course.

However, it has been shown that the number of simulation runs can be reduced considerably (to be exact to 100 in total) by changing the sampling such that the ground motion intensity is increased each time and by adopting more elaborate approaches for processing of results.

In the first approach, the fragility curves were obtained by fitting a lognormal distribution function to binary data points indicating *no damage* or *damage*. The results obtained by this technique were remarkably close to the reference results.

In the second approach, a cloud analysis was performed where the fragility curves were derived based on the exact outcomes of the simulation runs and their variances. Admittedly, the result quality was initially below the author's expectations. However, if the regression of the data points is performed carefully, also this approach yields adequate results. The author believes that the capabilities of cloud analysis are much higher for (standard) buildings where positive (and non-zero) continuous response quantities are studied, e.g. maximum inter-storey drift ratio.

Finally, the fragility curves were combined with site-specific PGA probability density functions. The primary aim was to learn about the contributions of the different intensity levels to the overall exceedance probability. It was found that, for a representative number of examples, the contribution of frequently occurring moderate earthquakes is very small. Hence, it can be concluded that closer examinations regarding minor or moderate earthquakes are not necessary.

Moreover, it has been shown that there is no "way in between" the simplified approach of deterministically analysing the structure's behaviour at a target intensity level, and calculating fragility curves, i.e., determining threshold exceedance probabilities for all intensity levels. In other words, MCS for a single intensity level (so called single-stripe analysis) is incorrect because it neglects the behaviour at all other intensity levels, and especially the corresponding result dispersions.

Chapter 5

Concluding remarks

The results of the studies on the estimation of small failure probabilities as well as on the seismic safety of an arch dam have already been summarized in the corresponding chapters. Thus, here, some general conclusions regarding probabilistic seismic safety are provided.

In principle, studies on seismic safety seem predestinated for involving probabilistic methods. This is because:

- Response variability due to different ground motion time histories is very high. Hence, in principle, these uncertainties should be considered, rather than relying on deterministic results.
- The uncertainty about a (specific) ground motion time history is of aleatoric type. This means that the only way to deal with this uncertainty is to include it in the calculations since it is impossible to reduce or eliminate it. This is in contrast to epistemic uncertainties (e.g. about strength or damping values) where one may still aim at gaining better informations about the quantities by more testing.

However, the (state of the art) framework of probabilistic analysis - as has been outlined in chapter 2 and further developed in chapter 3 - is hardly applicable to seismic analyses in its conventional form. This is because:

- The stochastic representation of a seismic signal is much more difficult than of an uncertain static system - which may be described by a multidimensional PDF for the random variables and a limit state (equation). This is due to the fact that a seismic signal is a random *process* characterized by many parameters such as intensity, frequency content, and duration. To represent the seismicity of a specific site, the analyst can either employ (scaled) recorded ground motions or artificial ground motions. In neither strategy, advanced sampling techniques such as low-discrepancy sampling are applicable.

  Furthermore, the need to implement a random process as well as the desire to simulate the structural behaviour as realistically as possible (including nonlinearities and failure) render a failure probability estimate method relying on design point detection impractical. The design point is the most probable configuration of the random parameters leading to failure.

- A further peculiarity of seismic analyses arises due to the fact that safety estimates result from a superposition of seismic hazard and respective damage/failure probabilities. More specifically, one has to integrate these quantities over all conceivable seismic intensity levels. In this work it has been shown that seismic safety is not a matter of *small* probabilities (as many other reliability problems). Furthermore, it has been demonstrated that any attempt to perform a (more economical) stochastic analysis using a single intensity level is pointless.

According to this study, a saving in computation time may not be gained by advanced sampling of the input parameters, but rather by advanced result processing. Two methods have been presented and tested which allow damage/failure probability estimates based on 100 simulation runs.

Besides, the elaboration of a sophisticated model of an arch dam has shown that the seismic behaviour of special structures may be simulated by modern software. In particular, the gradual deterioration of the concrete may be represented by implementing a suitable material model.

The assessment of the seismic safety of a structure requires the preparation of an appropriate (finite element) model. This necessitates, however, that the analyst comprehends the *essential* physical processes, in particular the seismic excitation and the load bearing characteristics. Furthermore, the engineer must be able to identify realistic damage and failure mechanisms. This is not only the case in a probabilistic analysis, as presented in this work, but rather also when conventional methods are employed such as deterministic time history analysis for a target return period, or response spectrum analysis.

Further research should regard proper modelling of the earthquake input mechanism, the focus being on two aspects:

- Capturing radiation damping realistically. The associated difficulties have been outlined in subsection 4.3.3. A Monte-Carlo-based seismic analysis requires the deconvolution procedure being automized. Hence, it must be implemented in the finite element software package.
- Consideration of spatially varying ground motions. Numerous studies have shown that ground motions time histories are not equal at different points of the foundation-structure interface in case of structures having extensions of several hundreds of meters. Of course, this depends strongly on the shape of the foundation, the ground conditions, and also on the specific seismic excitation. Hence, consequences on the response of the structure may only be described reasonably in a probabilistic sense. Thus, calculations need to be based on Monte-Carlo simulation.

List of Figures

List of Tables

Bibliography

[Abaqus, 2014a] Abaqus (2014a). *Abaqus 6.14 Online Documentation*. Dassault Systèmes.

[Abaqus, 2014b] Abaqus (2014b). *Abaqus Example Problems Guide*. Dassault Systèmes.

[Adam, 2001] Adam, C. (2001). Dynamics of elastic–plastic shear frames with secondary structures: shake table and numerical studies. *Earthquake Engineering & Structural Dynamics*, 30(2):257–277.

[Adam and Jäger, 2012] Adam, C. and Jäger, C. (2012). Seismic collapse capacity of basic inelastic structures vulnerable to the p-delta effect. *Earthquake Engineering & Structural Dynamics*, 41(4):775–793.

[Adam et al., 2017] Adam, C., Kampenhuber, D., and Ibarra, L. F. (2017). Optimal intensity measure based on spectral acceleration for p-delta vulnerable deteriorating frame structures in the collapse limit state. *Bulletin of Earthquake Engineering*, 15(10):4349–4373.

[Alfarah et al., 2017] Alfarah, B., López-Almansa, F., and Oller, S. (2017). New methodology for calculating damage variables evolution in plastic damage model for rc structures. *Engineering Structures*, 132:70 – 86.

[Au and Beck, 2001] Au, S. and Beck, J. (2001). Estimation of small failure probability in high dimensions by subset simulation. *Probabilistic Engineering Mechanics*, 16:263–277.

[Au and Beck, 2003] Au, S. K. and Beck, J. L. (2003). Subset simulation and its application to seismic risk based on dynamic analysis. *Journal of Engineering Mechanics*, 129(8):901–917.

[Baker and Cornell, 2005] Baker, J. W. and Cornell, A. C. (2005). A vector-valued ground motion intensity measure consisting of spectral acceleration and epsilon. *Earthquake Engineering & Structural Dynamics*, 34(10):1193–1217.

[Bamer, 2014] Bamer, F. (2014). *New model order reduction strategies in earthquake engineering and structural dynamics*. PhD thesis, TU Wien.

[Barone et al., 2014] Barone, G., Frangopol, D. M., and Soliman, M. (2014). Optimization of life-cycle maintenance of deteriorating bridges with respect to expected annual system failure rate and expected cumulative cost. *Journal of Structural Engineering*, 140(2).

[Barroso and Winterstein, 2002] Barroso, L. R. and Winterstein, S. (2002). Probabilistic seismic demand analysis of controlled steel moment-resisting frame structures. *Earthquake Engineering & Structural Dynamics*, 31(12):2049–2066.

[Bažant and Oh, 1983] Bažant, Z. P. and Oh, B. H. (1983). Crack band theory for fracture of concrete. *Matériaux et Construction*, 16(3):155–177.

[Bernier et al., 2016] Bernier, C., Monteiro, R., and Paultre, P. (2016). Using the conditional spectrum method for improved fragility assessment of concrete gravity dams in eastern canada. *Earthquake Spectra*, 32(3):1449–1468.

[Bhattacharjee and Léger, 1993] Bhattacharjee, S. S. and Léger, P. (1993). Seismic cracking and energy dissipation in concrete gravity dams. *Earthquake Engineering & Structural Dynamics*, 22(11):991–1007.

[Biondini and Frangopol, 2016] Biondini, F. and Frangopol, D. M. (2016). Life-cycle performance of deteriorating structural systems under uncertainty: Review. *Journal of Structural Engineering*, 2016(9).

[Bratley and Fox, 1988] Bratley, P. and Fox, B. (1988). Algorithm 659: Implementing sobol's quasirandom sequences generator. *ACM Transactions on Mathematical Software*, 14(1):88–100.

[Breitung, 1984] Breitung, K. (1984). Asymptotic approximations for multinormal integrals. *Journal of Engineering Mechanics*, 110(3):357–366.

[Bucher, 2009a] Bucher, C. (2009a). Asymptotic sampling for high-dimensional reliability analysis. *Probabilistic Engineering Mechanics*, 24:504–510.

[Bucher, 2009b] Bucher, C. (2009b). *Computational analysis of randomness in structural mechanics*. Structures and Infrastructures Book Series, Vol. 3. Taylor & Francis, London.

[Bucher, 2013] Bucher, C. (2013). Solving the first passage problem using asymptotic sampling. In Novak, D. and Vorechovsky, M., editors, *Proceedings of the 11th International Probabilistic Workshop*, pages 21–29, Brno. LITERA.

[Bucher, 2015] Bucher, C. (2015). Application of asymptotic sampling to structural reliability problems. In *Proceedings of the 1st International Conference on Uncertainty Quantification in Computational Sciences and Engineering. Crete Island, Greece.*

[Bucher, 2018] Bucher, C. (2018). Metamodels of optimal quality for stochastic structural optimization. *Probabilistic Engineering Mechanics*, 54:131 – 137. ISM 2016.

[Bucher and Bourgund, 1990] Bucher, C. and Bourgund, U. (1990). A fast and efficient response surface approach for structural reliability problems. *Structural Safety*, 7(1):57 – 66.

[Bucher and Frangopol, 2006] Bucher, C. and Frangopol, D. M. (2006). Optimization of lifetime maintenance strategies for deteriorating structures considering probabilities of violating safety, condition, and cost thresholds. *Probabilistic Engineering Mechanics*, 21(1):1 – 8.

[Bucher and Most, 2008] Bucher, C. and Most, T. (2008). A comparison of approximate response functions in structural reliability analysis. *Probabilistic Engineering Mechanics*, 23(2):154 – 163. 5th International Conference on Computational Stochastic Mechanics.

[Bucher and Wolff, 2013] Bucher, C. and Wolff, S. (2013). slangtng - scriptable software for stochastic structural analysis. In DerKiureghian, A. and Hajian, A., editors, *Reliability and Optimization of Structural Systems*, pages 49–56. American university of Armenia Press.

[Caflisch et al., 1997] Caflisch, R. E., Morokoff, W., and Owen, A. (1997). Valuation of mortgage backed securities using brownian bridges to reduce effective dimension. *Journal of Computational finance*, 1(1):27–46.

[Carballo and Cornell, 2000] Carballo, J. E. and Cornell, C. A. (2000). Probabililistic seismic demand analysis. Technical report, Stanford University.

[Cervera et al., 1996] Cervera, M., Oliver, J., and Manzoli, O. (1996). A rate-dependent isotropic damage model for the seismic analysis of concrete dams. *Earthquake Engineering & Structural Dynamics*, 25(9):987–1010.

[Chopra, 1992] Chopra, A. K. (1992). Earthquake analysis, design and safety evaluation of concrete arch dams. In *Proc. Tenth World Conference on Earthquake Engineering*, volume 11, pages 6763–6772.

[Chopra, 2012a] Chopra, A. K. (2012a). *Dynamics of Structures*. Pearson Education.

[Chopra, 2012b] Chopra, A. K. (2012b). Earthquake analysis of arch dams: Factors to be considered. *Journal of Structural Engineering*, 138(2):205–214.

[Chopra and Chakrabarti, 1972] Chopra, A. K. and Chakrabarti, P. (1972). The earthquake experience at koyna dam and stresses in concrete gravity dams. *Earthquake Engineering & Structural Dynamics*, 1(2):151–164.

[Chopra and Chakrabarti, 1973] Chopra, A. K. and Chakrabarti, P. (1973). The koyna earthquake and the damage to koyna dam. *Bulletin of the Seismological Society of America*, 63(2):381.

[Clough, 1980] Clough, R. (1980). Non-linear mechnisms in the seismic response of arch dams. In *Proceedings of the international research conference on earthquake engineering*, pages 669–84. Skopje, Yugoslavia.

[Clough and Penzien, 1993] Clough, R. and Penzien, J. (1993). *Dynamics of Structures*. Civil Engineering Series. McGraw-Hill.

[Cornell et al., 2002] Cornell, C. A., Jalayer, F., Hamburger, R. O., and Foutch, D. A. (2002). Probabilistic basis for 2000 sac federal emergency management agency steel moment frame guidelines. *Journal of Structural Engineering*, 128(4):526–533.

[Cornell and Krawinkler, 2000] Cornell, C. A. and Krawinkler, H. (2000). Progress and challenges in seismic performance assessment. https://apps.peer.berkeley.edu/news/2000spring/performance.html.

[Dai and Wang, 2004] Dai, H. and Wang, W. (2004). Application of low-frequency sampling method in structural reliability. *Probabilistic Engineering Mechanics*, 19:425–436.

[de Angelis et al., 2015] de Angelis, M., Patelli, E., and Beer, M. (2015). Advanced line sampling for efficient robust reliability analysis. *Structural Safety*, 52:170–182.

[de Araújo and Awruch, 1998] de Araújo, J. and Awruch, A. M. (1998). Probabilistic finite element analysis of concrete gravity dams. *Advances in Engineering Software*, 29(2):97 – 104.

[Deierlein et al., 2003] Deierlein, G. G., Krawinkler, H., and Cornell, C. A. (2003). A framework for performance-based earthquake engineering. In *2003 Pacific Conference on Earthquake Engineering*.

[Ditlevsen and Madsen, 2007] Ditlevsen, O. and Madsen, H. (2007). Reliability methods. *Structural Reliability Methods*, Internet edition 2.3.7.

[Dolen et al., 2003] Dolen, T. P., Scott, G. A., von Fay, K. F., and Hamilton, B. (2003). Effects of concrete deterioration on safety of dams. Technical report, Dam Safety Office.

[EFEHR, 2017] EFEHR (2017). European facilities for earthquake hazard and risk: Hazard curves. http://www.efehr.org/en/hazard-data-access/hazard-curves/.

[EN1990, 2013] EN1990 (2013). *Eurocode 0: Basis of structural design.* Austrian standards institute, 2013-03-15 edition.

[EN1992, 2015] EN1992 (2015). *Eurocode 2: Design of concrete structures - Part 1-1: General ruels and rules for buildings.* Austrian standards institute, 2015-02-15 edition.

[EN1998, 2017] EN1998 (2017). *Eurocode 8: Design of structures for earthquake resistance - Part 1: General rules, seismic action and rules for buildings - National specifications concerning ÖNORM EN 1998-1 and national comments (Austria).* Austrian standards institute, 2017-07-01 edition.

[Fang and Wang, 1994] Fang, K. and Wang, Y. (1994). *Number-theoretic methods in statistics.* Chapman & Hall, London.

[Feenstra, 1993] Feenstra, P. H. (1993). *Computational Aspects of Biaxial Stress in Plain and Reinforced Concrete.* PhD thesis, Delft University of Technology.

[Feix and Walkner, 2010] Feix, J. and Walkner, R. (2010). Betonbau 1, lecture notes. Universität Innsbruck.

[fib, 2012] fib (2012). Model code 2010. Technical report, The International Federation for Structural Concrete (fib), Lausanne, Switzerland.

[Frangopol and Maute, 2003] Frangopol, D. M. and Maute, K. (2003). Life-cycle reliability-based optimization of civil and aerospace structures. *Computers Structures*, 81(7):397 – 410.

[Frangopol and Soliman, 2016] Frangopol, D. M. and Soliman, M. (2016). Life-cycle of structural systems: recent achievements and future directions. *Structure and Infrastructure Engineering*, 12(1):1–20.

[Gasser and Bucher, 2017a] Gasser, C. and Bucher, C. (2017a). High-dimensional reliability analysis with asymptotic sampling using regression surface. In C. Bucher, B. Ellingwood, D. F., editor, *Proceedings of the 12th International Conference on Structural Safety and Reliability.* TU Verlag, Vienna, Austria.

[Gasser and Bucher, 2017b] Gasser, C. and Bucher, C. (2017b). Seismic safety assessment by an enhanced monte carlo method. In *Proceedings of the 2nd International Conference on Uncertainty Quantification in Computational Sciences and Engineering. Rhodes Island, Greece.*

[Gasser and Bucher, 2018] Gasser, C. and Bucher, C. (2018). An optimized strategy for using asymptotic sampling for reliability analysis. *Structural Safety*, 71:33 – 40.

[Gasser et al., 2019a] Gasser, C., Bucher, C., and Goldgruber, M. (2019a). Some remarks on monte carlo based probabilistic seismic demand analysis using the example of an arch dam. *Journal of Engineering Mechanics.* (submitted for publication).

[Gasser et al., 2019b] Gasser, C., Goldgruber, M., and Bucher, C. (2019b). Seismic fragility curves of an arch dam with special regard to ultimate limit state. *ASCE-ASME Journal of Risk and Uncertainty in Engineering Systems: Part B. Mechanical Engineering.* (revised manuscript submitted for publication).

[Ghanaat et al., 2012] Ghanaat, Y., Patev, R. C., and Chudgar, A. K. (2012). Seismic fragility analysis of concrete gravity dams. In *Proceeding of the 15th WCEE*. Lisbon, Portugal.

[Ghrib and Tinawi, 1995] Ghrib, F. and Tinawi, R. (1995). An application of damage mechanics for seismic analysis of concrete gravity dams. *Earthquake Engineering & Structural Dynamics*, 24(2):157–173.

[Goldgruber, 2015] Goldgruber, M. (2015). *Nonlinear seismic modelling of concrete dams*. PhD thesis, TU Graz, Austria.

[Gollwitzer and Rackwitz, 1988] Gollwitzer, R. and Rackwitz, R. (1988). An efficient numerical solution to the multinormal integral. *Probabilistic Engineering Mechanics*, 3(2):98–101.

[Hall, 1998] Hall, J. F. (1998). Efficient non-linear seismic analysis of arch dams. *Earthquake Engineering & Structural Dynamics*, 27(12):1425–1444.

[Halton, 1960] Halton, J. (1960). On the efficiency of certain quasi-random sequences of points in evaluating multi-dimensional integrals. *Numer Math*, 2:84–90.

[Hariri-Ardebili and Kianoush, 2014] Hariri-Ardebili, M. A. and Kianoush, M. R. (2014). Integrative seismic safety evaluation of a high concrete arch dam. *Soil Dynamics and Earthquake Engineering*, 67:85 – 101.

[Hariri-Ardebili and Saouma, 2014] Hariri-Ardebili, M. A. and Saouma, V. (2014). Quantitative failure metric for gravity dams. *Earthquake Engineering & Structural Dynamics*, 44(3):461–480.

[Hariri-Ardebili and Saouma, 2016a] Hariri-Ardebili, M. A. and Saouma, V. E. (2016a). Collapse fragility curves for concrete dams: Comprehensive study. *Journal of Structural Engineering*, 142(10):04016075.

[Hariri-Ardebili and Saouma, 2016b] Hariri-Ardebili, M. A. and Saouma, V. E. (2016b). Probabilistic seismic demand model and optimal intensity measure for concrete dams. *Structural Safety*, 59:67 – 85.

[Hariri-Ardebili and Saouma, 2016c] Hariri-Ardebili, M. A. and Saouma, V. E. (2016c). Seismic fragility analysis of concrete dams: A state-of-the-art review. *Engineering Structures*, 128:374 – 399.

[Hariri-Ardebili et al., 2016] Hariri-Ardebili, M. A., Saouma, V. E., and Porter, K. A. (2016). Quantification of seismic potential failure modes in concrete dams. *Earthquake Engineering & Structural Dynamics*, 45(6):979–997. eqe.2697.

[Hasofer and Lind, 1974] Hasofer, A. M. and Lind, N. C. (1974). Exact and invariant second-moment code format. *Journal of the Engineering Mechanics Division (ASCE)*, 100:111–121.

[Hillerborg et al., 1976] Hillerborg, A., Modéer, M., and Petersson, P.-E. (1976). Analysis of crack formation and crack growth in concrete by means of fracture mechanics and finite elements. *Cement and Concrete Research*, 6(6):773 – 781.

[Hofstetter and Mang, 1995] Hofstetter, G. and Mang, H. (1995). *Computational Mechanics of Reinforced Concrete Structures*. Vieweg+Teubner Verlag.

[Hong and Hickernell, 2003] Hong, H.-S. and Hickernell, F. (2003). algorithm 823: Implementing scrambled digital sequences. *ACM Transactions on Mathematical Software*, 29(2):95–109.

[ICOLD, 2010] ICOLD (2010). Selecting seismic parameters for large dams guidelines. Technical report, International Commission on Large Dams, Bulletin 72.

[Jalayer, 2003] Jalayer, F. (2003). *Direct Probabilistic Seismic Analysis: Implementing Non-Linear Dynamic Assessments.* PhD thesis, Stanford University.

[Jalayer et al., 2007] Jalayer, F., Franchin, P., and Pinto, P. E. (2007). A scalar damage measure for seismic reliability analysis of rc frames. *Earthquake Engineering & Structural Dynamics*, 36(13):2059–2079.

[Ju et al., 2015] Ju, M., Guoyan, Z., Longjun, D., Guanghui, C., and Chuxuan, Z. (2015). A comparison of mine seismic discriminators based on features of source parameters to waveform characteristics. *Shock and Vibration*, 2015:10.

[Kisliakov, 1997] Kisliakov, D. (1997). Seismic risk analysis of concrete gravity dams-problems and solutions. In *Proc. Int. Conf. Hydropower*, volume 97.

[Kiureghian and Ditlevsen, 2009] Kiureghian, A. D. and Ditlevsen, O. (2009). Aleatory or epistemic? does it matter? *Structural Safety*, 31(2):105 – 112. Risk Acceptance and Risk Communication.

[Kolymbas, 2011] Kolymbas, D. (2011). *Geotechnik - Bodenmechanik, Grundbau und Tunnelbau.* Springer.

[Krätzig and Pölling, 2004] Krätzig, W. B. and Pölling, R. (2004). An elasto-plastic damage model for reinforced concrete with minimum number of material parameters. *Computers & Structures*, 82(15):1201 – 1215.

[Krawinkler, 2005] Krawinkler, H. (2005). Van nuys hotel building testbed report: exercising seismic performance assessment. peer report. Technical report, PEER.

[Kucherenko et al., 2011] Kucherenko, S., Feil, B., Shah, N., and Mauntz, W. (2011). The identification of model effective dimensions using global sensitivity analysis. *Reliability Engineering and System Safety*, 96:440–449.

[Lee and Fenves, 1998a] Lee, J. and Fenves, G. L. (1998a). A plastic-damage concrete model for earthquake analysis of dams. *Earthquake Engineering & Structural Dynamics*, 27(9):937–956.

[Lee and Fenves, 1998b] Lee, J. and Fenves, G. L. (1998b). Plastic-damage model for cyclic loading of concrete structures. *J. Eng. Mech.*, 124(8):892–900.

[Liu and Der Kiureghian, 1986] Liu, P.-L. and Der Kiureghian, A. (1986). Multivariate distribution models with prescribed marginals and covariances. *Probabilistic Engineering Mechanics*, 1(2):105–112.

[Løkke and Chopra, 2018] Løkke, A. and Chopra, A. K. (2018). Direct finite element method for nonlinear earthquake analysis of 3-dimensional semi-unbounded dam–water–foundation rock systems. *Earthquake Engineering & Structural Dynamics*, 47(5):1309–1328.

[Lubliner et al., 1989] Lubliner, J., Oliver, J., Oller, S., and Oñate, E. (1989). A plastic-damage model for concrete. *International Journal of Solids and Structures*, 25(3):299 – 326.

[Lysmer and Kuhlemeyer, 1969] Lysmer, J. and Kuhlemeyer, R. (1969). Finite dynamic model for infinite media. *Journal of the Engineering Mechanics Division (ASCE)*, 95:859–878.

[Nataf, 1962] Nataf, A. (1962). Détermination des distributions de probabilités dont des marges sont données. *Comptes Rendus de l'Académie des Sciences*, 225:42–43.

[Office of Nuclear Regulatory Research, 1983] Office of Nuclear Regulatory Research (1983). *PRA procedures guide: A guide to the performance of probabilistic risk assessment for nuclear power plants*.

[Olsson et al., 2003] Olsson, A., Sandberg, G., and Dahlblom, O. (2003). On latin hypercube sampling for structural reliability analysis. *Structural Safety*, 25(1):47–68.

[Padgett et al., 2008] Padgett, J. E., Nielson, B. G., and DesRoches, R. (2008). Selection of optimal intensity measures in probabilistic seismic demand models of highway bridge portfolios. *Earthquake Engineering & Structural Dynamics*, 37(5):711–725.

[Papaioannou et al., 2015] Papaioannou, I., Betz, W., Zwirglmaier, K., and Straub, D. (2015). Mcmc algorithms for subset simulation. *Probabilistic Engineering Mechanics*, 41:89 – 103.

[Penner et al., 2017] Penner, O., Bergmann, B., Razavi-Darbar, S., Queen, D., Léger, P., Boivin, Y., and Leclerc, M. (2017). Non-linear time domain analysis of ruskin dam in ls-dyna including reservoir-foundation-structure interaction. In *Proceedings of the 37th Annual USSD Conference*.

[Porter, 2003] Porter, K. A. (2003). An overview of peer's performance-based earthquake engineering. In *ICASP9*. Civil Engineering Risk and Reliability Association (CERRA), San Francisco.

[Pradlwarter et al., 2007] Pradlwarter, H., Schuëller, G., Koutsourelakis, P., and Charmpis, D. (2007). Application of line sampling simulation method to reliability benchmark problems. *Structural Safety*, pages 208–221.

[Ramamoorthy et al., 2006] Ramamoorthy, S. K., Gardoni, P., and Bracci, J. M. (2006). Probabilistic demand models and fragility curves for reinforced concrete frames. *Journal of Structural Engineering*, 132(10):1563–1572.

[Saouma et al., 2011] Saouma, V., Miura, F., Lebon, G., and Yagome, Y. (2011). A simplified 3d model for soil-structure interaction with radiation damping and free field input. *Bulletin of Earthquake Engineering*, 9(5):1387.

[Schneider, 1997] Schneider, J. (1997). *Introduction to Safety and Reliability of Structures*. IABSE.

[Schuëller and Pradlwarter, 2007] Schuëller, G. and Pradlwarter, H. (2007). Benchmark study on reliability estimation in higher dimensions of structural systems - an overview. *Structural Safety*, 33(4-5):305–316.

[Schuëller et al., 2004] Schuëller, G., Pradlwarter, H., and Koutsourelakis, P. (2004). A critical appraisal of reliability estimation procedures for high dimensions. *Probabilistic Engineering Mechanics*, 19(4):463 – 474.

[Shinozuka et al., 2000] Shinozuka, M., Feng, M. Q., Lee, J., and Naganuma, T. (2000). Statistical analysis of fragility curves. *Journal of Engineering Mechanics*, 126(12):1224–1231.

[Shome, 1999] Shome, N. (1999). *Probabilistic seismic demand analysis of nonlinear structures*. PhD thesis, Stanford University.

[Sobol and Asotsky, 2003] Sobol, I. M. and Asotsky, D. I. (2003). One more experiment on estimating high-dimensional integrals by quasi-monte carlo methods. *Mathematics and Computers in Simulation*, 62:255–263.

[Strauss et al., 2008] Strauss, A., Frangopol, D. M., and Kim, S. (2008). Use of monitoring extreme data for the performance prediction of structures: Bayesian updating. *Engineering Structures*, 30(12):3654 – 3666.

[Sudret et al., 2005] Sudret, B., Defaux, G., and Pendola, M. (2005). Time-variant finite element reliability analysis – application to the durability of cooling towers. *Structural Safety*, 27(2):93 – 112.

[Sudret et al., 2017] Sudret, B., Mai, C., and Konakli, K. (2017). Assessment of the log-normality assumption of seismic fragility curves using non-parametric representations. https://hal.archives-ouvertes.fr/hal-01432508.

[Tekie and Ellingwood, 2003] Tekie, P. B. and Ellingwood, B. R. (2003). Seismic fragility assessment of concrete gravity dams. *Earthquake Engineering & Structural Dynamics*, 32(14):2221–2240.

[Vanderplaats and Moses, 1973] Vanderplaats, G. N. and Moses, F. (1973). Structural optimization by methods of feasible directions. *Computers and Structures*, 3:739–755.

[Varbanov et al., 2012] Varbanov, G., Kostov, M., Andonov, A., Apostolov, K., and Iliev, A. (2012). Seismic risk assessment of large dams. In *Proceedings of the 15th WCEE*. Lisbon, Portugal.

[Wang et al., 2013] Wang, J., Jin, F., and Zhang, C. (2013). Chapter 17 - seismic safety of arch dams with aging effects11science china technological sciences 2011; 54: 522–30. © science china press and springer. In Zhang, C., Jin, F., Wang, J., and Xu, Y., editors, *Seismic Safety Evaluation of Concrete Dams*, pages 387 – 406. Butterworth-Heinemann.

[Wang and Chopra, 2010] Wang, J.-T. and Chopra, A. K. (2010). Linear analysis of concrete arch dams including dam–water–foundation rock interaction considering spatially varying ground motions. *Earthquake Engineering & Structural Dynamics*, 39(7):731–750.

[Wang et al., 2018] Wang, J.-T., Zhang, M.-X., Jin, A.-Y., and Zhang, C.-H. (2018). Seismic fragility of arch dams based on damage analysis. *Soil Dynamics and Earthquake Engineering*, 109:58 – 68.

[Wang and Hichernell, 2000] Wang, X. and Hichernell, F. (2000). Randomized halton sequences. *Math Comput*, 32(7-8):887–899.

[Wittke, 2014] Wittke, W. (2014). *Rock Mechanics: Theory and Applications with Case Histories*. Springer Berlin Heidelberg.

[Zhang et al., 2013] Zhang, C., Jin, F., Wang, J., and Xu, Y. (2013). *Seismic Safety Evaluation of Concrete Dams: A Nonlinear Behavioral Approach*. Butterworth Heinemann.

[Zhang et al., 2009] Zhang, C., Pan, J., and Wang, J. (2009). Influence of seismic input mechanisms and radiation damping on arch dam response. *Soil Dynamics and Earthquake Engineering*, 29(9):1282 – 1293.

[Ziegler, 1998] Ziegler, F. (1998). *Mechanics of Solids and Fluids*. Springer.

[Zilch and Zehetmaier, 2006] Zilch, K. and Zehetmaier, G. (2006). *Bemessung im konstruktiven Betonbau*. Springer.